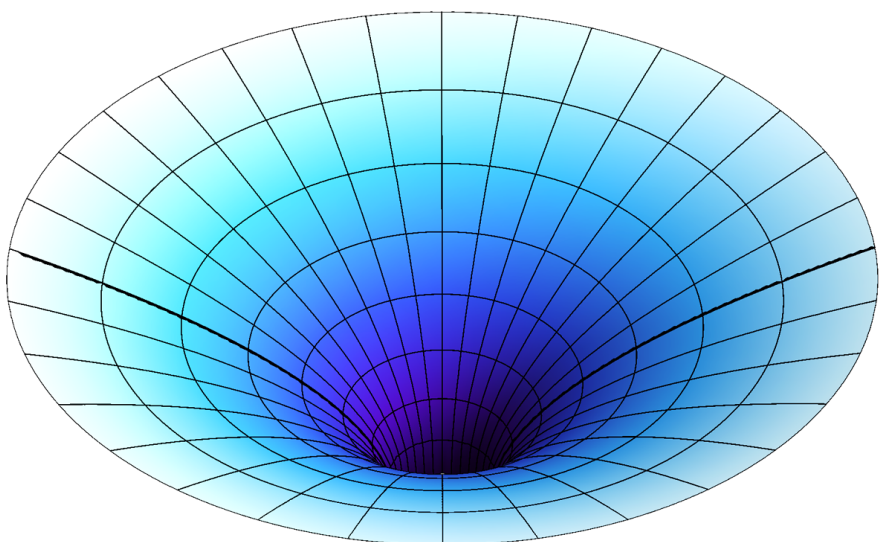


A DYNAMICAL SYSTEMS APPROACH TO KERR GEODESICS

PABLO GALINDO



A journey into the freefall movement around rotating black holes

Miguel Sanchez Caja and Marc Mars Lloret

Facultad de Ciencias

Universidad de Granada



Ars est celare artem

ORIGINALITY DECLARATION

D. _____, of legal age, with NIF _____ born in _____
EXHIBITS:

That assumes the originality of this work understood according to the GUIDELINES OF THE UNIVERSITY OF GRANADA FOR THE DEVELOPMENT OF THE COURSE **TRABAJO DE FIN DE MÁSTER** BELONGING TO ITS MASTER'S DEGREE, approved by the Governing Council of March 4, 2013 and published in the N 69 BOUGR March 11, 2013.

Witness whereof,

In Granada, on ____ __, 20__.

Signed: _____

A B S T R A C T

The Kerr spacetime is a fundamental topic in General Relativity and astrophysics since it is known that almost every collapsing object will behave as the Kerr black hole. The motion of test particles in this spacetime is crucial in astrophysics because a lot of interesting astrophysical objects are black holes. In this work we present a method that makes particularly easy to understand the characteristics of the motion of particles in some important regions of the Kerr spacetime. Concretely, we will analyze the geodesic flow by reducing widely the problem to a simple two-dimensional phase portrait, valid even in regions beyond the event horizon. In addition, we will study some of the most popular features of Kerr black holes by direct representation of the geodesics obtained by numerical integration.

CONTENTS

Acronyms	xi
i INTRODUCTION	1
1 INTRODUCTION, CONTEXT AND AIMS	3
ii DEVELOPMENT AND RESULTS	9
2 THE KERR SPACETIME	11
2.1 The Kerr metric in Boyer-Lindquist coordinates	11
2.2 Symmetries	12
2.3 The curvature	13
2.4 Singularities and horizons	14
2.5 ZAMOS	15
2.6 The ergosphere	17
2.7 The Penrose process	21
3 THE KERR-SCHILD COORDINATE SYSTEM	23
3.1 Metric in Eddington-Finkelstain coordinates	23
3.2 Metric in Kerr-Schild form	25
3.2.1 Displaying the metric in Kerr-Schild coordinates	25
3.2.2 Surface embedding into Kerr-Schild coordinates	28
3.3 Conserved quantities in Kerr-Schild coordinates	31
3.3.1 Killing vectors	31
3.3.2 Killing tensors	32
4 MAXIMAL EXTENSION	35
4.1 Ring identification	35
4.2 Kerr-Schild patches	40
4.3 Causality violations	42
5 AXIS OF SYMMETRY	45
5.1 Hamiltonian equations of the geodesics	45
5.2 Variation ranges and causal structure	48
5.3 Phase space and dynamic equations	52
5.3.1 Null geodesics	53
5.3.2 Timelike geodesics	54
5.4 Lower energy orbit	66
6 THE EQUATORIAL PLANE: THE INNER DISK	69
6.1 Hamiltonian equations of the geodesics	69
6.2 Variation ranges and causal structure	70
6.3 Stability of the inner disk	72
6.4 A glimpse at the geodesics outside the inner disk	73
7 NUMERICAL RESOLUTION OF THE GEODESICS	77
iii CONCLUSIONS AND COMMENTS	87
8 CONCLUSIONS	89

iv APPENDIX	91
A KILLING VECTORS AND KILLING TENSORS	93
A.1 Properties of Killing vectors	93
A.2 Killing vectors and Lagrangian symmetries	93
A.3 Killing vectors and first integrals	94
A.4 Noether currents and Killing vectors	94
A.5 Killing Tensors	95
A.6 Killing algebra	95

ACRONYMS

BL	Boyer-Lindquist. 11 , 13–15 , 19 , 21 , 23 , 25 , 28 , 29 , 31 , 32 , 35 , 40 , 42 , 45 , 62 , 69 , 77 , 79 , 83
EF	Eddington-Finkelstein. 23–27 , 29 , 31 , 35
KS	Kerr-Schild. 23 , 25–27 , 29 , 31–33 , 35 , 37 , 40–42 , 45–47 , 51–54 , 56 , 58 , 62 , 63 , 69 , 72 , 74 , 76
MAE	Maximal Analytic Extension. 35 , 36 , 39–41 , 45 , 54 , 61
PC	Penrose-Carter. 41 , 51 , 52 , 56 , 58
RN	Reissner-Nordström. 4 , 5 , 11 , 15 , 18
SW	Schwarzschild. 4 , 5 , 11 , 12 , 15 , 17 , 18 , 33 , 40 , 61 , 62 , 67 , 70 , 76
ZAMO	Zero Angular Momentum Observer. 16 , 17 , 21 , 85

Part I
INTRODUCTION

INTRODUCTION, CONTEXT AND AIMS

Along this work, we are going to perform a deep study of the geodesic movement of free fall particles in the Kerr spacetime. The Kerr spacetime describes what is known as a rotating black hole. Some examples of popular black holes are the supermassive black holes located at the center of the active galaxies, or the intermediate mass black holes, which are the bridge between stellar mass black holes and supermassive black holes, and its existence is still a mystery. Using the solution to the motion of test particles we can explain many purely relativistic effects such as the precession of the perihelion of Mercury and the deflection of light rays as they pass close to a massive object. Thus, the motion of test particles in the Kerr spacetime conforms not only a way to understand more thoroughly relativistic phenomena but also determines important information for the detection and prediction of relevant astrophysical objects as pulsars (which are highly magnetized rotating neutron star that emits a beam of electromagnetic radiation) and quasars. Therefore, the understanding and the study of motion around Kerr black holes helps us to understand their nature in more detail. Solutions to the motion of particles in this spacetime are commonly difficult to understand and categorize and there are entire books dedicated to this task. There are a lot of definitions of what a black hole is. The physical definition of a black hole is "a region of spacetime from which gravity prevents anything, including light, from escaping". The mathematically accurate version of this definition is more technical and involves the existence of a *spacetime singularity*, which is a region

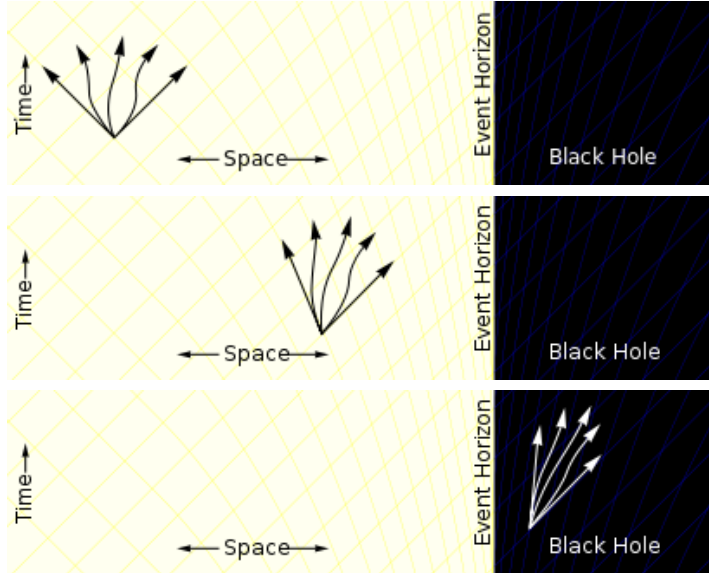


Figure 1: The figure shows how particles can move in any direction outside the event horizon but they can only move inwards the black hole once the event horizon is crossed.

of the spacetime where the movement of the particles that reaches this area cannot be extended, and an *event horizon*, which is a surface that has the property to prevent the particles that cross this region to go back. We can understand this behavior with the use of the Minkowsky diagrams, that are plots in which the time coordinate is represented in the vertical axis and the space coordinate is represented in the horizontal axis. In these diagrams the trajectories of the photons are straight lines sloping at 45 degrees. As photons (null particles onwards) are the limit behavior of mass particles (timelike particles onwards), the last ones must remain inside the cone defined by the straight lines at 45 degrees. This is known as the "light cone" and can be used to study the regions of the spacetime that are accessible to physical particles (causal particles onwards). As we can see in fig. 1, the light cones outside the event horizon allow causal particles to move in any direction, but closer to the horizon the spacetime starts to deform. There are more allowed movements going towards the horizon than moving away. Inside the event horizon causal particles are not allowed to escape from this region, as the spacetime is so bended that the only allowed behavior is moving towards the black hole.

The black holes can be categorized in virtue of the "no hair theorem", which stipulates that these entities can be described with three properties: Mass, electromagnetic charge and angular momentum. With this information in mind, the black holes are named as

	Non-rotating ($L = 0$)	Rotating ($L \neq 0$)
Uncharged ($Q = 0$)	Schwarzschild	Kerr
Charged ($Q \neq 0$)	Reissner Nordström	Kerr-Newman

The complexity order is

$$\text{Schwarzschild} \rightarrow \text{Reissner Nordström} \rightarrow \text{Kerr} \rightarrow \text{Kerr-Newman}.$$

As general relativity states, freefall particles in the spacetime must move along causal (timelike or lightlike) *geodesics*, and therefore in order to understand the paths of these particles we must obtain and analyze the geodesics trajectories of the spacetime. In the **Schwarzschild (SW)** spacetime, the geodesic flow is well understood but its study still provides new and interesting results [1, 10, 7]. In the **Reissner-Nordström (RN)** spacetime, the geodesic flow is much more complicated due to the fact that the spacetime structure is more complex and some features of the geodesics are still being analyzed nowadays [7]. The study of the Kerr spacetime is even more complex than in the **RN** spacetime and the geodesic flow is very difficult to understand and analyze. Indeed, there are very intricate technical books dedicated to this topic [11] that do not even provide a general (either quantitatively or qualitatively) description for all possible geodesics. Due to its complexity, the Kerr metric is still an important research field because it is known that the spacetime described by every collapsing astrophysical object approaches the Kerr spacetime asymptotically, and therefore almost every black hole in the universe is a Kerr black hole (except those which also have charge, but as the charge is very low for common astrophysical objects). It is interesting to note that while the **SW** and **RN** geometries can be used to describe the exterior

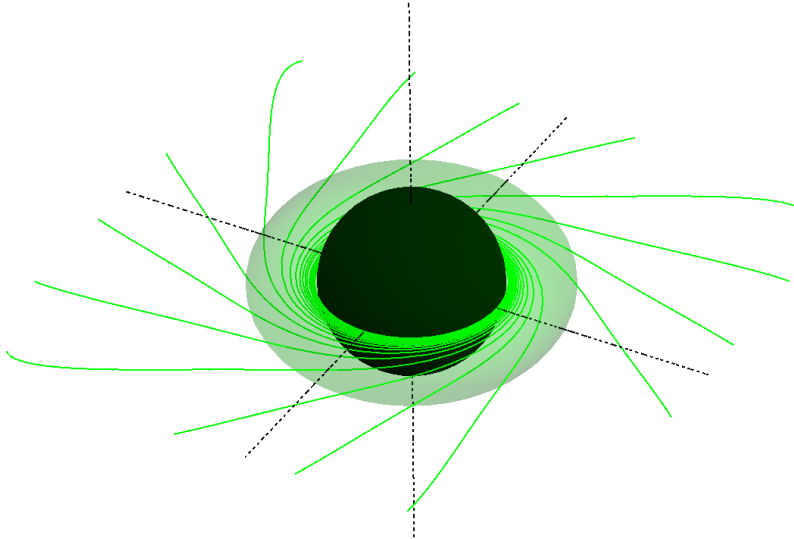


Figure 2: Trajectories with zero angular momentum in the Kerr spacetime.

of a spherically symmetric object in virtue of the Birkhoff theorem [2], the Kerr geometry only describes a black hole. For example, it is known that while the spacetime singularities in the [SW](#) and [RN](#) geometries are single points (that for mathematical reasons are not in the spacetime), the Kerr singularity is a topological ring. Also, one of the most popular features in the Kerr geometry is the *frame dragging*. This phenomenon consists in the Kerr black hole dragging the fabric of spacetime itself in its movement and therefore, it also drags the trajectory of the physical particles moving in its presence. This effect can be so relevant, that there are some regions in the black hole known as *ergoregions* where all the particles are forced to rotate in the same direction as the black hole does. Indeed, trajectories with zero angular momentum (that in the [SW](#) and [RN](#) spacetimes correspond to straight lines) are not straight lines but curved trajectories that spin co-rotating with the black hole as is depicted in fig. 2. All the possible behaviors are depicted in fig. 3 where we can see how trajectories attempting to enter the ergoregion contra-rotating with respect to the black hole, are forced to spin in the same direction of the black hole. Also, particles with zero angular momentum are still moving in a co-rotating movement as well as particles with positive angular momentum. As also happens in the [SW](#) and [RN](#) geometries, particles with enough angular momentum can move in circular orbits around the Kerr black hole.

But there are features of the Kerr black holes even stranger than the frame dragging. The Kerr black hole has what is known as a Einstein - Rosen bridge or more typically as a *wormhole*, which is a topological feature of the spacetime that connects two different regions (called sometimes "universes" in the literature) of the spacetime. In this case, the wormhole (which is located at the center of the ring singularity) leads to the *negative space*, a region of the spacetime in which gravity is repulsive. In this space there also causal violations, i.e. there exist trajectories allowed to physical particles that lead to time travel. As the wormhole is inside the event horizon, these trajectories cannot be seen from

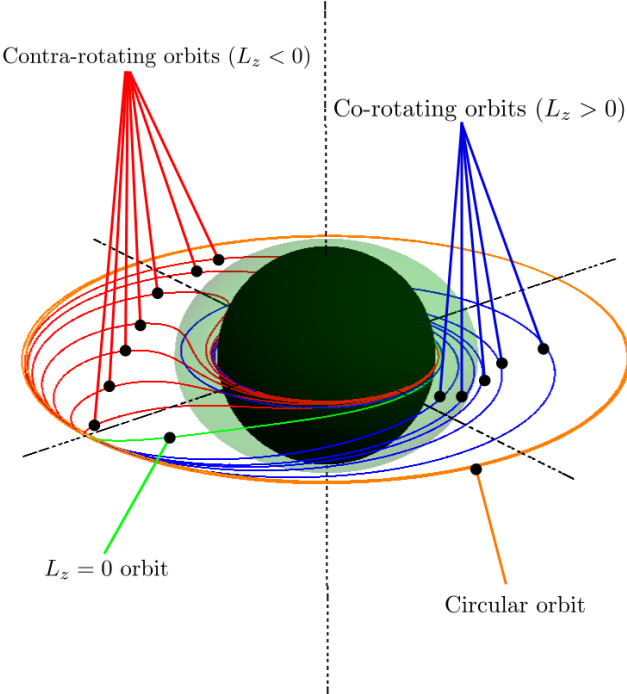


Figure 3: Behavior of timelike particles near a Kerr black hole. The black hole is rotating anticlockwise. The black region correspond to the event horizon while the green one correspond to the ergoregion. The orbits drawn red are retrograde geodesic that are spin-reversed by the black hole, the blue paths are direct geodesics, the orange curve is a circular orbit while the green one is the $L_z = 0$ geodesic.

outside the black hole. Thus, possible causality violations are "protected" by the event horizon. The maximal analytic extension of the Kerr black hole (which is the whole spacetime described by the Kerr metric) is even more complex and reveals that the Kerr black hole has an infinite amount of asymptotically flat regions and an infinite amount of wormholes that connects them. These wormholes are different from the wormholes that connect with the negative space.

As we can see, the structure of the spacetime is very complex and therefore, the description of the movement of physical particles in the Kerr geometry is very difficult to understand. The aim of this work is present a method that allows us to analyze the full motion of the particles in some regions of interest in the spacetime. Our main focus will be the use of dynamical systems, which have proven to be a powerful tool in the study and description of physical systems, as demonstrated by theoretical mechanics. The combination of General Relativity and dynamical systems is a very novel approach to the problem [12, 1, 7] which describes certain known results from a completely new perspective. The two regions in which we are interested are the axis of symmetry and the equatorial plane. The axis of symmetry is a very important region because it contains the easiest way to travel to the negative space. The description of the geodesic flow in the axis of symmetry is a very difficult topic with the standard methods because a complete study of the geodesic flow involves the movement in an infinite amount of asymptotically flat regions and negative spaces. This is the reason why the current analysis of the geodesic flow in the axis is very difficult to understand

and why it had remained incomplete. In this work, we achieve to describe the whole geodesic flow in the axis of symmetry by the use of a dynamical system technique that projects all the different trajectories into one two-dimensional phase portrait. This is a great simplification of this problem. The other region in which we are interested is in the equatorial plane, because it contains the ring singularity of the Kerr spacetime and the disk inside this singular ring, which is the wormhole that connects to the negative space. The analysis of the trajectories in the axis and in the equatorial plane is essential because allows us to understand some very important characteristics of the black holes as the jets or accretion disks. What is known as the Penrose process conforms a mechanism that allows us to understand the powerful jets that quasars and rotating black holes emit. This process involves expelled particles that gain energy while the black hole loses it, decreasing its own rotation. This is still one of many viable competing models for quasar jets.

It's important to warn that the Kerr metric describes an *eternal black hole*, which has existed forever and therefore does not come from a collapsing astrophysical object. It is known that the Kerr black holes produced by the gravitational collapse probably will not have the infinite wormhole structure, as these wormholes are unstable and will collapse under small perturbations. However, the wormhole that leads to negative space is stable and probably will survive the gravitational collapse.

This work is organized as follows: In chapter 2 we present a brief but concise description of the Kerr spacetime and its main features. As we will see in this chapter we will need a new coordinate system that allow us to describe the geodesic flow in the whole spacetime without having to worry about horizons or wormholes. In chapter 3 we define the new coordinate system and we express all the quantities of interest in this new coordinates. Also, we show how the Kerr spacetime is described in the new coordinates and the main features of the important surfaces. In chapter 4 perform a rigorous analysis of the topological identification describing the wormhole that lead to the negative space and we also describe how the new coordinates are very useful studying the movement in maximal extension, which is also examined in detail. In chapter 5 we performed a comprehensive study of the geodesic flow along the axis of symmetry in terms of dynamical systems, with particular attention to the causal structure and the stability of the motion along the axis. After that, a similar study about the equatorial plane is performed in chapter 6 with special emphasis in the disk inside the singular ring and its stability. Finally in chapter 7 we display some interesting geodesic defined along the whole Kerr spacetime obtained by a numerical integration software developed for this work. Some useful information that completes the understanding of this work can be found in appendix A.

Part II
DEVELOPMENT AND RESULTS

2

THE KERR SPACETIME

Throughout all the work we will use natural units, so we will set the speed of light ($c = 1$) and the universal gravitation constant ($G_N = 1$). Notice that in this unit system the dimension of space and the dimension of time are equivalent. Also, the Penrose index notation will be used (the contravariant or covariant character of the tensors is described by the number of super-indexes and sub-indexes respectively). In this chapter we are going to display some interesting and basic features of the Kerr-Spacetime. All this features are well known and can be found with much more detail in the first Chapter of [11]. Despite this, we believe it is interesting to make a brief illustrative trip through the behaviors of the Kerr black hole as well as the features of the causal observers moving in the Kerr geometry in a suitable way for any reader with a basic knowledge of differential geometry and general relativity. As any other black hole, the Kerr black hole has an event horizon that prevents that any observer that cross this surface can go back and therefore “protects” the singularity. But in the Kerr spacetime the structure of the horizons (there is more than one) is more complicated than in the SW geometry or the RN geometry because in this case there is also a region called *ergosurface*, in which particles cannot remain static, neither can rotate in the opposite direction of the black hole rotation, i.e. in this region the only allowed movement is to move co-rotating with the black hole. Also, as we will see, the Kerr true singularity cannot be understood in the standard coordinates (which are called Boyer-Lindquist (BL) coordinates) and we will have to express the metric in another coordinate system to unveil the true nature of this singularity.

2.1 THE KERR METRIC IN BOYER-LINDQUIST COORDINATES

The explicit form of the metric in BL coordinates is

$$ds^2 = -d\bar{t}^2 + \Sigma \left(\frac{dr^2}{\Delta} + d\theta^2 \right) + (r^2 + a^2) \sin^2(\theta) d\bar{\phi}^2 + \frac{2Mr}{\Sigma} (a \sin^2(\theta) d\bar{\phi} - d\bar{t})^2$$

where

$$\Delta(r) = r^2 - 2Mr + a^2 \tag{1}$$

$$\Sigma(r, \theta) = r^2 + a^2 \cos^2 \theta \tag{2}$$

The BL coordinates are form by the tetrad $\{\bar{t}, r, \theta, \phi\}$ which takes values on $\bar{t} \in \mathbb{R}$, $r \in \mathbb{R}^+$, $\{\theta, \phi\} \in S^1$. The Kerr metric depends on two parameters, M and a . If we compare the metric with the far field metric generated by an isolated object we can deduce that these parameters are respectively the mass and the angular momentum per unit of mass of the black hole, both measured at the

infinity. Some properties of the Kerr black hole arise from the properties of the metric:

1. The Kerr metric is stationary, which means that the metric it does not depend explicitly on the coordinate \bar{t} that yields the (asymptotic) time..
2. The Kerr metric is axisymmetric, which means that the metric does not depend on the ϕ coordinate.
3. The Kerr metric is not static because it is not invariant under the time reversal transformation $\bar{t} \rightarrow -\bar{t}$
4. The Kerr metric is invariant under the transformation

$$\bar{t} \rightarrow -\bar{t} \tag{3}$$

$$\phi \rightarrow -\phi \tag{4}$$

this can be interpreted as the time reversal of the Kerr metric produces a black hole that is rotating in the opposite direction.

5. Is asymptotically flat, which means that in the limit $r \rightarrow \infty$ the Kerr metric becomes the Minkowsky metric in spherical coordinates.
6. In the limit $a \rightarrow 0$ the Kerr metric becomes the [SW](#) metric in Droste coordinates.
7. In the limit $M \rightarrow 0$ (but $a \neq 0$) the Kerr metric becomes isometric to the Minkowsky spacetime in spherical coordinates.

2.2 SYMMETRIES

As we notice before, the Kerr metric has two important symmetries because its stationary and axisymmetric. Therefore, the Kerr metric admits two Killing vector fields (to know more about Killing vectors, see appendix A on page 93)

$$\xi_1 = \partial_t \quad \xi_2 = \partial_\phi. \tag{5}$$

If we name u^α to the geodesics tangent vector, there exist two conserved quantities associated with this Killing vectors:

$$-E = u^\alpha \xi_{1\alpha} \quad L_z = u^\alpha \xi_{2\alpha} \tag{6}$$

In the case of timelike geodesic these conserved quantities can be interpreted as the energy per unit of mass of the particle measured at the infinity and the angular momentum per unit of mass measured at the infinity. In the case of null geodesics this interpretation can be maintained if we parametrize the geodesic flow with the affine parameter of the geodesic. In the following, this convention will be maintained.

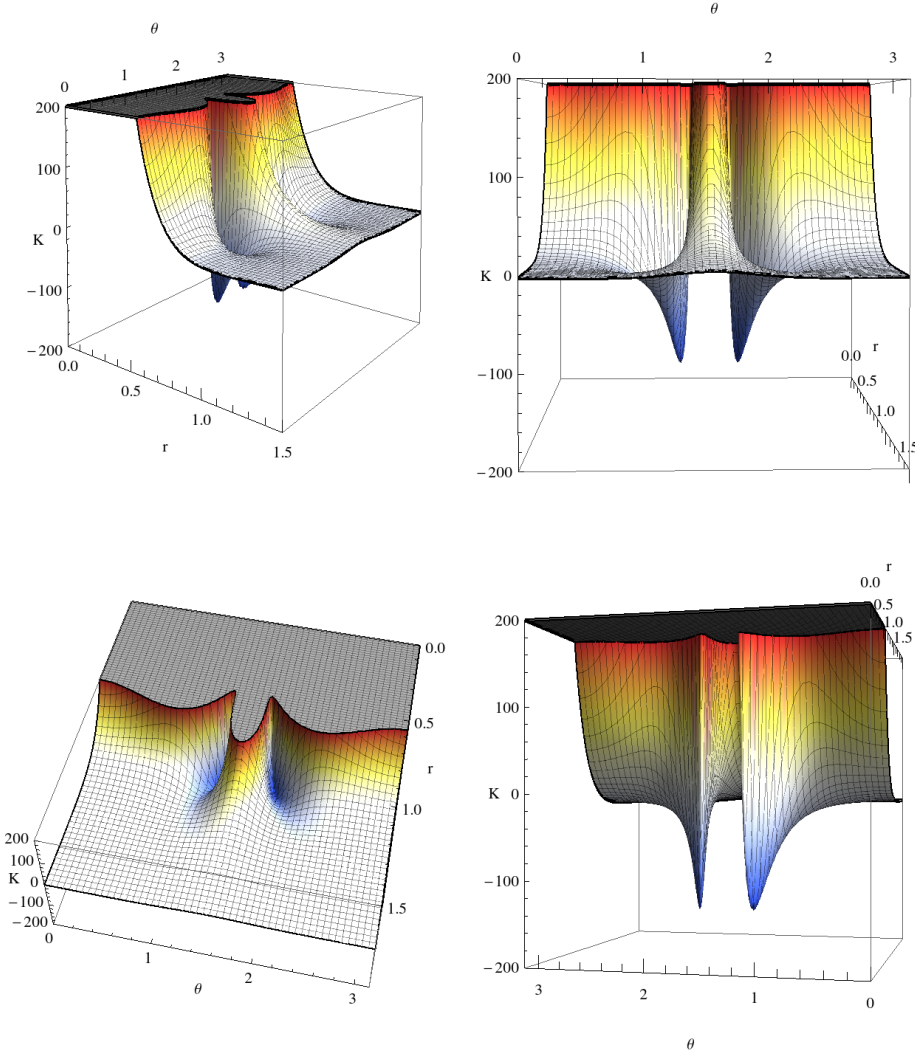


Figure 4: The figure shows the variation of the Kretschmann invariant as a function of the variables r and θ of the BL coordinates. The grey region indicates the cut-off of the surface which continues to higher values. $M = 1$ and $a = 0.9$ has been chosen for illustrative purposes.

2.3 THE CURVATURE

The curvature scalar is usually defined by the Riemann scalar

$$R = Ric_{\alpha}^{\alpha} \quad (7)$$

where $Ric_{\alpha\beta} = R_{\alpha\gamma\beta}^{\gamma}$ and $R_{\beta\gamma\delta}^{\alpha}$ is the Riemann tensor. However the scalar R vanishes because the Kerr solution corresponds to a solution of the vacuum Einstein equations. The Einstein equations without cosmological constant are

$$Ric_{\alpha\beta} - \frac{1}{2}g_{\alpha\beta}R = T_{\alpha\beta} \quad (8)$$

where $T_{\alpha\beta}$ is the Energy-Stress tensor. Taking the trace of the equations we get

$$-R = T \quad (9)$$

where $T = T^\alpha_\alpha$. As for the vacuum Einstein field equations we have that $T_{\alpha\beta} = 0$ then $R = 0$ and therefore the curvature scalar does not give any information of the spacetime curvature. But we can construct other invariant quantities with the Riemann tensor. One of the most important ones is the invariant $K = R_{\alpha\beta\gamma\delta}R^{\alpha\beta\gamma\delta}$, which is known as the Kretschmann invariant. As any other invariant, its properties does not depend of the choice of the coordinate system. A direct computation of the Kretschmann invariant in BL coordinates gives

$$K = R_{\alpha\beta\gamma\delta}R^{\alpha\beta\gamma\delta} = \frac{8(6M^2(-a^6\cos^6(\theta) + 15a^4\cos^4(\theta) - 15a^2r^4\cos^2(\theta) + r^6))}{(a^2\cos^2(\theta) + r^2)^6} \quad (10)$$

The variation of K as a function of r and θ is depicted in fig. 4. Notice that there exist regions with negative curvature, which means that in this region the Riemann tensor is fundamentally timelike, which can only happen in Lorenzian manifolds. We see that the curvature becomes infinite iff

$$a^2\cos^2(\theta) + r^2 = 0 \rightarrow r = 0 \quad \text{and} \quad \theta = \frac{\pi}{2}, \quad (11)$$

which is the only true spacetime singularity.

2.4 SINGULARITIES AND HORIZONS

The Kerr metric has some interesting properties that concern spacetime singularities. Some of these singularities are not really there, as they are which is known as *Coordinate singularities*, that are points where the expression of the metric element becomes singular but due to a bad election of the coordinate system. Although this may seem only a problem of the coordinate system, these singularities are much more interesting, because they reveal some interesting causal properties of the Kerr spacetime. We can see that the Kerr metric is singular when

$$\Delta = 0, \quad (12)$$

$$\Sigma = 0. \quad (13)$$

We will name these equations *singularity equations*. The singularities of the first equation (namely $r = r_\pm$) correspond to a pair of *coordinate singularities* as the computation of the Kretschmann invariant $R_{\alpha\beta\gamma\delta}R^{\alpha\beta\gamma\delta}$ (where R is the Riemann tensor) suggests that these points are not truly spacetime singularities and we call them *horizons*. On the other hand the singularity of the second equation is really a spacetime singularity as we have seen in the last section.

The coordinate singularities given by $\Delta = 0$ are located at

$$r = r_\pm = M \pm \sqrt{M^2 - a^2} \quad (14)$$

When $a^2 < M^2$ the two solutions of the singularity equation exist but when $a^2 = M^2$ they become one solution as $r_+ = r_- = M$. For values of the angular momentum of the black hole that fulfill $a^2 > M^2$ there is no real solution to the singularity equation and therefore no horizons exist. In this situation the

Kerr solution does not describe a black hole, as the spacetime singularity is not covered by any event horizon, which will lead to paradoxes. This is the reason that all astrophysical processes are believed to lead to black holes with $a^2 \leq M^2$. When $|a| = |M|$ the Kerr spacetime is called *extremal black hole* and for values of a and M such that $|a| > |M|$ the black hole is called *superextreme black hole*. Let us consider now the normal 1-form to the constant- r hypersurfaces which is given in [BL](#) coordinates as

$$n_\alpha = (0, 1, 0, 0) \quad (15)$$

By the use of the Kerr metric we can evaluate its norm as

$$n^\alpha n_\alpha = n^\alpha n^\beta g_{\alpha\beta} = \frac{\Delta}{\Sigma}. \quad (16)$$

We can see that on the horizons ($r = r_\pm$) $n^\alpha n_\alpha = 0$ which reveal that they are null hypersurfaces, and this is because they are called horizons. The two horizons separate the structure of the spacetime in three regions

1. The region in which $r > r_+$. In this region the constant- r surfaces have timelike causal character and as in the limit $r \rightarrow \infty$ the metric becomes the Minkowsky metric, we say that this is the exterior of the black hole.
2. The region in which $r_- < r < r_+$ the constant- r surfaces have spacelike causal character. A deeper analysis of the causal structure tell us that an object that falls through $r = r_+$ can only continue falling until it reaches $r = r_-$. This is the reason we call $r = r_+$ the event horizon.
3. The region in which $r < r_-$ the constant- r surfaces are timelike again and this is the region that contains the spacetime singularity.

Notice that in the range $a^2 \geq M^2$ the second region does not exist and when $a^2 > M^2$ the 1st and 3rd regions are causally connected because there is no horizon that prevent this behavior.

Notice that the spacetime singularity is located at $r = 0$ and $\theta = \frac{\pi}{2}$ (but no at $r = 0$ and $\theta \neq \frac{\pi}{2}$). This relation has no meaning in spherical-like coordinates (the [BL](#) coordinates). We need another coordinate system to reveal the true shape and properties of the spacetime singularity. In the next chapter, we will see that in another well-behaved coordinate system, the Kerr singularity happens to be a ring that increases it radius with the value of a , being a single point when $a = 0$.

2.5 ZAMOS

We are going to study one of the most popular Kerr features, that is the frame dragging. Remember that a Newtonian observer in a axisymmetric potential (or even an observer in the [SW](#) or [RN](#) geometries) in freefall has a radial trajectory if $L_z = 0$. This is because the radial velocity is proportional to the angular momentum L_z . To study what happens in the Kerr spacetime, let us consider an observer with zero angular momentum. In virtue of eq. (6) we can write

$$L_z = u_{\bar{\phi}} = 0 \quad (17)$$

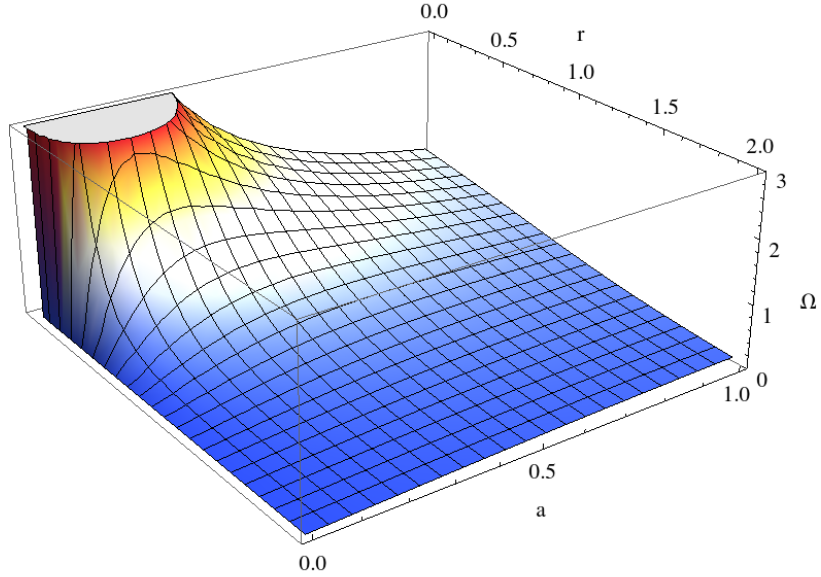


Figure 5: The figure shows the ZAMO angular velocity Ω in the equatorial plane ($\theta = \frac{\pi}{2}$). The color is proportional to the value of Ω (that is in the vertical axis also) and it is only for improve the visualization.

In the literature, this observer is commonly known as [Zero Angular Momentum Observer \(ZAMO\)](#). Notice that the contravariant component of the velocity is

$$u^{\bar{\phi}} = g^{\bar{\phi}\bar{t}} u_{\bar{t}} \neq 0 \quad (18)$$

and therefore the [ZAMO](#) can, in principle, have radial component in the tangent vector and therefore its trajectory will not be a radial movement. From eq. (17) we can write

$$u_{\bar{\phi}} = g_{\bar{\phi}\bar{\phi}} u^{\bar{\phi}} + g_{\bar{\phi}\bar{t}} u^{\bar{t}} = 0 \quad (19)$$

and therefore the angular velocity of the [ZAMO](#) is given by

$$\Omega = \frac{u^{\bar{\phi}}}{u^{\bar{t}}} = -\frac{g_{\bar{\phi}\bar{t}}}{g_{\bar{\phi}\bar{\phi}}} = \frac{2Mar}{(r^2 + a^2)^2 - a^2 \Delta \sin^2 \theta}. \quad (20)$$

The fig. 5 shows the behavior of this function in the equatorial plane (the behavior is similar for other values of θ). Notice that as the denominator is always positive then

$$\text{sign}(\Omega) = \text{sign}(Ma) \quad (21)$$

and therefore the [ZAMO](#) rotates in the same direction as the black hole. We conclude two important results:

- Observers with zero angular momentum cannot move in radial movements (straight lines).

- An observer which approaches a Kerr black hole with zero angular momentum is dragged by the gravitational force of the black hole and the only movement allowed is rotate in the same direction as the black hole.

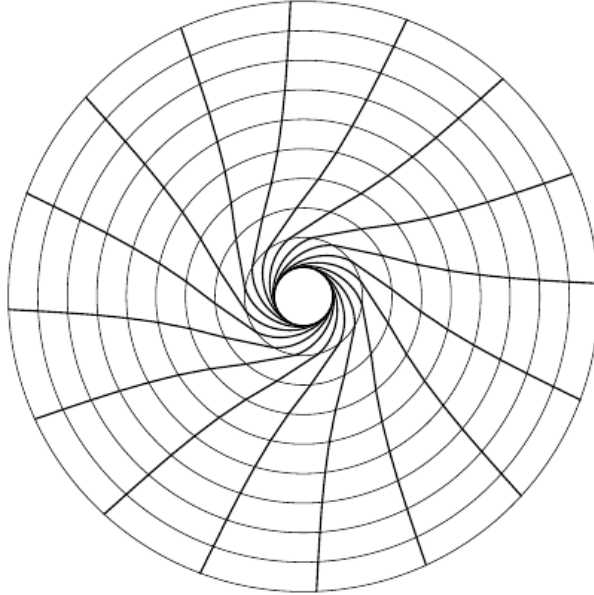


Figure 6: Frame dragging in the Kerr spacetime.

The effect of the frame dragging over the **ZAMOs** can be visualized in fig. 6, where we can see how the trajectories with $L_z = 0$ (that are straight lines in the infinity as $\lim_{r \rightarrow \infty} \Omega = 0$) are dragged by the Kerr black hole. We will see that the frame dragging is even more strong and complex than that and has a very important role in what is known as the ergoregions.

2.6 THE ERGOSPHERE

In the **SW** geometry it is known that the Killing vector $\partial_{\bar{t}}$ is timelike outside the event horizon (remember that in the **SW** geometry there is only one horizon), null over the horizon and spacelike inside the horizon. That is why it is said that inside the horizon the coordinate \bar{t} measures space while the coordinate r measures time. As the **SW** singularity is located at $r = 0$ and as inside the horizon r measures time, it is said that the **SW** singularity is not a place but a time: *The singularity is not there but it is tomorrow*. This can be easily understood if you think that tomorrow the universe reachable by you is supposed to disintegrate and disappear. This is what "hitting" the **SW** singularity is not a "place", it is everywhere in the future. However, in the Kerr spacetime the singularity is located at $r = 0$, and in this region r is a spacelike coordinate and therefore the singularity is really a "place", not a moment in time. In the Kerr geometry, the points where the Killing vector changes its spacetime causal character (timelike, null or spacelike) do not match with the singularities (coordinate singularities) of

the metric. As the causal character of the Killing vector is given by $g(\partial\bar{t}, \partial\bar{t}) = g_{tt}$ we can see where the component g_{tt} changes its sign. We write

$$g_{tt} = -1 + \frac{2Mr}{\Sigma} = \frac{r^2 - 2Mr + a^2 \cos^2 \theta}{\Sigma} = 0. \quad (22)$$

This equation has two solutions

$$r_{E\pm} = M \pm \sqrt{M^2 - a^2 \cos^2 \theta}. \quad (23)$$

These two solutions are known as the *ergosurfaces* and also as the *infinity redshift surfaces*. The reason of the second name is that if we think in a light source located on a point p_s that emits a light pulse with frequency ν_s it will be observed with frequency

$$\nu_{\text{obs}} = \sqrt{\frac{g_{tt}(p_s)}{g_{tt}(p_{\text{obs}})}} \nu_s \quad (24)$$

(where ν_{obs} is the frequency measured by an observator located at the point p_{obs}) and therefore the observed frequency is $\nu_{\text{obs}} = 0$ if the light pulse is emitted from $p_s = r_{E\pm}$ because $g_{tt}(r_{E\pm}) = 0$. Let us call $\mathcal{I} = [r_{E-}, r_{E+}]$, the interval between the two ergosurfaces. Notice that the two horizons are always in this interval ($r_{\pm} \in \mathcal{I}$) as

$$r_- \leq r_{E-} \leq r_{E+} \leq r_+. \quad (25)$$

In fig. 7, a schematic image of the horizon and ergosurfaces is displayed. Given these results, we have have that $g_{tt} < 0$ iff $r \notin \mathcal{I}$ and $g_{tt} > 0$ iff $r \in \mathcal{I}$. Therefore, there is a region between the outer horizon and the outer ergosurface where $g_{tt} > 0$ (this does not happen in the **SW** spacetime). This region is known as the *ergoregion* and $r = r_{E+}$ is called *ergosphere*. Its very important that the ergoregion exists outside the outer horizon, because this fact allows a geodesic that comes from the asymptotically flat region enter the ergoregion and escape to the asymptotically flat region again (without being trapped by the black hole as the geodesic does not cross the even horizon). As $g_{tt} > 0$ in this region, the Killing vector becomes spacelike. Some strange features happen in this region. First of all, as the conserved quantity of the ∂_t Killing vector is $u^\alpha \xi_{1\alpha} = -E$ and as ξ_1 is spacelike, E can be negative as well. Negative energies are only allowed inside the horizon in the **SW** geometry, as in the **RN** geometry (that is the **SW** spacetime with charge in the source of the gravitational field). The main strange feature is that there is no stationary observers allowed in the ergoregion. An stationary observer is an observer which does not see the metric change in its motion. For example, a observer in ∂_t , which is an observer that does not change the coordinates $\{r, \theta, \phi\}$ (and therefore its tangent vector must be proportional to ∂_t) is an example of a stationary observer. As stationary observers does not see the metric change in its motion, and we know that the metric does not change along the trajectories of the Killing vectors, the tangent vector to the geodesic of the stationary observer must be a Killing vector, i.e. a linear combination of the independent Killing vector fields in eq. (5). As the observers in the spacetime must move along causal timelike curves ($u^\alpha u_\alpha = -1$,

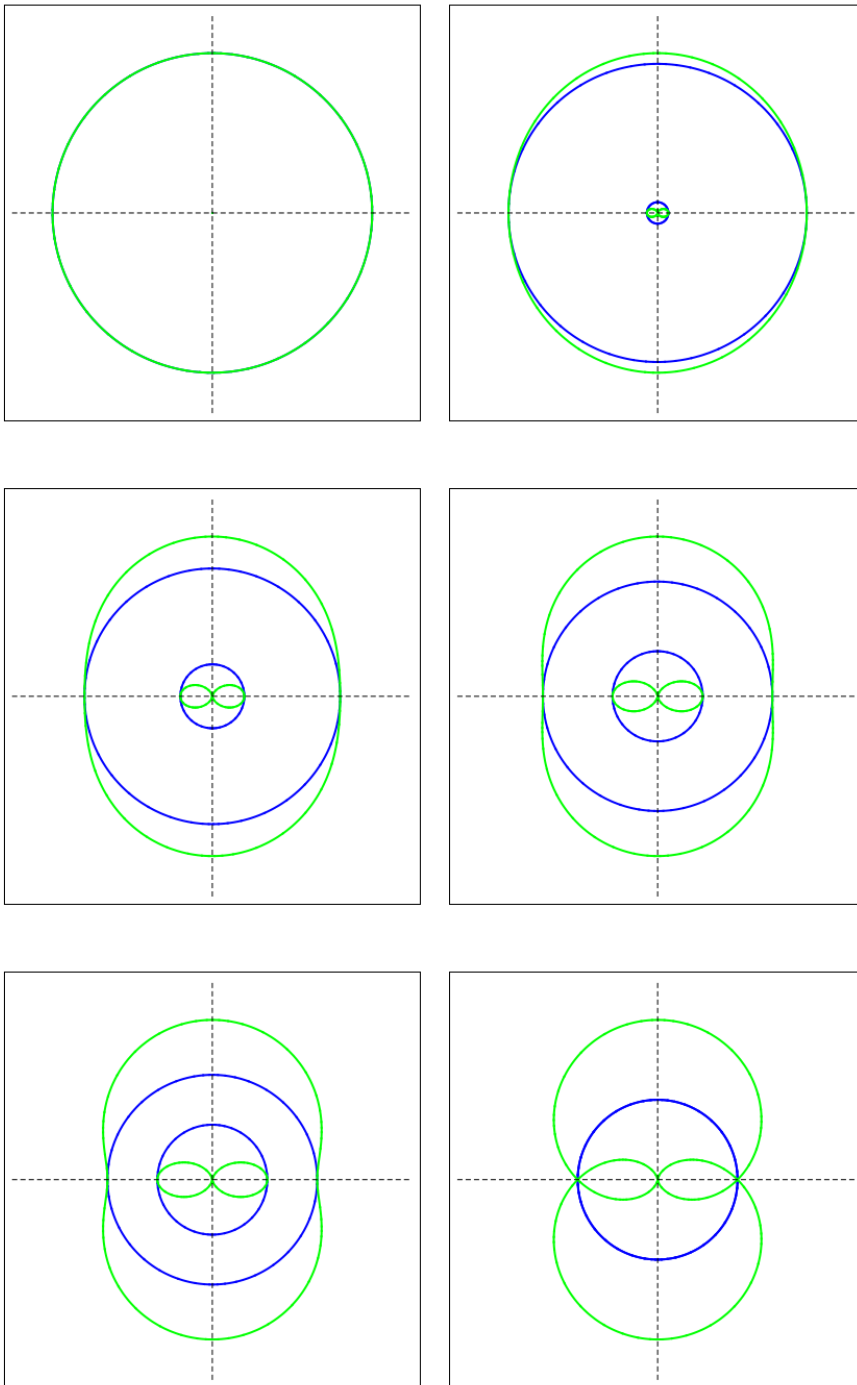


Figure 7: Schematic location of the horizons, ergosurfaces, and curvature singularity in the side view of the Kerr Spacetime in BL coordinates as a function of the parameter a . The images correspond to (from left to right and from top to bottom) $a = 0, a = 0.5, a = 0.8, a = 0.9, a = 0.95, a = 1$. The green surfaces are the outer and inner ergosurfaces and the blue curves represent the inner and outer horizon. Notice that the singularity is at the center of the image ($r = 0$, $\theta = \frac{\pi}{2}$). For simplicity $M = 1$ is chosen.

where u^α is the tangent vector to the trajectory) we can see that observers in ∂_t (those whose tangent vector is proportional to ∂_t) are not allowed in the ergoregion because in this region ∂_t is spacelike and therefore only stationary observers whose tangent vector is a linear combination of the two Killing vectors are allowed. To understand what this means we are going to compute the unitary tangent vector of a general stationary observer as

$$u^\alpha = \frac{\partial_t + \omega \partial_\phi}{|\partial_t + \omega \partial_\phi|} = (u^t, 0, 0, u^\phi) = u^t(1, 0, 0, \omega), \quad (26)$$

where we have defined ω as

$$\omega = \frac{d\phi}{dt} = \frac{u^\phi}{u^t}, \quad (27)$$

to be the constant angular velocity of the observer. As we see, the trajectory of the observer has constant r and θ coordinates and can only move along a circle with angular velocity ω . Observer's tangent vectors must fulfill

$$u^\alpha u_\alpha = (u^t)^2 (g_{tt} + 2\omega g_{t\phi} + \omega^2 g_{\phi\phi}) = -1 \rightarrow g_{tt} + 2\omega g_{t\phi} + \omega^2 g_{\phi\phi} < 0. \quad (28)$$

To understand this equation, let us solve

$$g_{tt} + 2\omega g_{t\phi} + \omega^2 g_{\phi\phi} = 0. \quad (29)$$

The solutions of this equation are

$$\omega_\pm = \frac{-g_{t\phi} \pm \sqrt{g_{t\phi}^2 - g_{tt}g_{\phi\phi}}}{g_{\phi\phi}}. \quad (30)$$

Notice that the discriminant of the equation is $g_{t\phi}^2 - g_{tt}g_{\phi\phi} = \Delta \sin^2 \theta$ and therefore this equation has no real solutions for $\Delta < 0$ which implies $r_- < r < r_+$. This has the meaning that no stationary observers are allowed when $r_- < r < r_+$. Outside the outer horizon $r > r_+$ we have that $\Delta > 0$ and the inequality eq. (28) is satisfied when

$$\omega_- < \omega < \omega_+. \quad (31)$$

As we have that in the ergosphere ($r = r_{E+}$) $\omega_-(r = r_{E+}) = 0$ as $g_{tt} = 0$ in this surface, then for $r \geq r_{E+}$ we will have $\omega_- \leq 0$ and the stationary observer can spin contra-rotating with the black hole ($\omega < 0$) or co-rotating with the black hole ($\omega > 0$). For $r_+ < r < r_{E+}$ we have that $\omega_- > 0$ and therefore the observer can only rotate co-rotating with the black hole. This can be summarized as

1. There is no stationary observer in the region $r_- < r < r_+$.
2. When a particle is in the ergoregion ($r_+ < r < r_{E+}$, it can only move spinning co-rotating with the black hole and it cannot remain static (constant $\{r, \phi, \theta\}$ at the same time).
3. Outside the ergoregion ($r \geq r_{E+}$) particles can move co-rotating or contra-rotating and observers in ∂_t are allowed.

Notice that as only photons (null causal curves) are allowed to move in the outer horizon ($r = r_+$) and in this region $\omega_- = \omega_+$, then the only angular velocity of a null stationary observer is $\omega = \omega_{\pm} = \frac{2Mar_+}{(r_+^2 + a^2)^2} = \frac{a}{r_+^2 + a^2} = \Omega$, which is also the **ZAMO** angular velocity. As this angular velocity is constant we can say that the black hole *rotates rigidly*. This is because the angular velocity of the only curves that can remain in $r = r_+$ (that are null causal geodesic with its tangent vector given by $u^\alpha = (u^t, 0, 0, u^\phi)$ with $u^\alpha u_\alpha = 0$) does not depend on the value of any coordinate.

2.7 THE PENROSE PROCESS

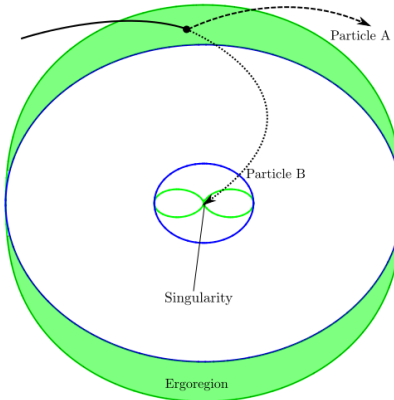


Figure 8: The figure shows the Penrose process in **BL** coordinates. The green curves represent the inner and outer ergosphere and while the blue ones are the outer and inner horizons. Remember that in this coordinate system the singularity is located at $r = 0$. For illustrative purposes $a = 0.8$ and $M = 1$ is chosen.

The ergosphere has another very interesting feature: The Penrose process. As we have seen, the energies in the ergosphere can be negative ($E < 0$) as the Killing is spacelike in this region. Let us consider a particle that follows a geodesic that comes from the asymptotically flat region and then enters the ergosphere. Under some specific circumstances circumstances can decay into two particles A and B between the ergosphere and the outer horizon (this region is called ergoregion). The decay can be done in such a way that the particle B falls into the singularity, passing through the outer horizon, the inner horizon and the inner ergosphere and the particle B escapes to the asymptotically flat region. If the ingoing particle has energy E and the two particles have energies E_A and E_B respectively, the global energy conservation allow us to write

$$E = E_A + E_B, \quad (32)$$

$$E_{\text{Kerr initial}} + E = E_{\text{Kerr final}} + E_A. \quad (33)$$

Particle B, crossing the event horizon, has a negative energy because within the ergosphere, the Killing vector ∂_t is spacelike and negative energies are allowed (remember that $g(\partial_t, u^\alpha) = -E$, where $-E < 0$ in the ergoregion). Then, as the

total energy is conserved, the black hole absorbs a negative energy. The particle A that goes to infinity will gain that amount of energy because of the energy conservation $E_A > E$. Notice that as this process occurs at $r > r_+$ the particle A can return to the asymptotically flat region with more energy and therefore this act like a "generator", because we sent a particle with energy E and we have gained a particle with energy $E_A > E$. The global result is that the Kerr black hole decelerates its rotation since it has absorbed negative energy. Blandford and Znajek (1977) suggested that the Penrose process could be a characteristic feature of Kerr black holes surrounded by a accretion disk containing a strong magnetic field. If this magnetic fields penetrates the ergoregion, then it could be a realistic source of electrons and positrons (created in pairs) which could start the Penrose process. This scenario involves that one of the particles end up with negative energy and falls into the black hole, while the other escapes to the asymptotically flat region. This second particle might form the characteristic energetic jets of charged particles that are known to be emitted from Kerr black holes, especially in quasars. By this process, quasar jets are powered by the energy that they extract from the Kerr black hole.

3

THE KERR-SCHILD COORDINATE SYSTEM

The Kerr metric defined originally in [BL](#) coordinates [3] has multiple singular points. These singular points in the metric are associated only to the election of the coordinate system and are not true spacetime singularities. The existence of this kind of "coordinate singularities" prevent us to obtain continuous geodesic equations when crossing the horizons that this false singular points define. To get rid of this problem, we will transform the metric from [BL](#) coordinates to another coordinate system called [Kerr-Schild \(KS\)](#) coordinate system in which the metric has only the true spacetime singularity located at $r = 0$ (in [BL](#) coordinates). In addition, the new coordinate system will reveal some hidden features in the Kerr spacetime that there are only clear when the metric is expressed in this way. This will allow us to analyze some of the geodesic movements that can only be correctly analyzed in this system, wherein the true form of singularity is revealed. To achieve this coordinate transform we will need to perform a previous transform into the [Eddington-Finkelstein \(EF\)](#) coordinate system in order to finally express the metric in [KS](#) coordinates.

3.1 METRIC IN EDDINGTON-FINKENSTAIN COORDINATES

In this section we are going to transform the Kerr metric from [BL](#) coordinates into [EF](#) keeping the sign of the future causal vector that defines this coordinates.

Lemma 1. *The Kerr metric defined on [BL](#) coordinates*

$$ds^2 = -d\bar{t}^2 + \Sigma \left(\frac{dr^2}{\Delta} + d\theta^2 \right) + (r^2 + a^2) \sin^2(\theta) d\bar{\phi}^2 + \frac{2Mr}{\Sigma} (a \sin^2(\theta) d\bar{\phi} - d\bar{t})^2$$

once expressed in [EF](#) coordinates takes the form

$$ds^2 = -dt^2 + dr^2 + \Sigma d\theta^2 + (r^2 + a^2) \sin^2(\theta) d\phi^2 + 2\sigma a \sin^2(\theta) dr d\phi + \frac{2Mr}{\Sigma} (-\sigma dt + dr - \sigma a \sin^2(\theta) d\phi)^2,$$

Proof. We start with the expression of the metric in [BL](#) coordinates

$$ds^2 = -d\bar{t}^2 + \Sigma \left(\frac{dr^2}{\Delta} + d\theta^2 \right) + (r^2 + a^2) \sin^2(\theta) d\bar{\phi}^2 \quad (34)$$

$$+ \frac{2Mr}{\Sigma} (a \sin^2(\theta) d\bar{\phi} - d\bar{t})^2 \quad (35)$$

where $\Delta = r^2 - 2Mr + a^2$ and $\Sigma = r^2 + a^2 \cos^2(\theta)$. The [EF](#) coordinates are defined to be the coordinate system adapted to the geodesic of the null vectors

$$l^\mu = \left(\frac{d\bar{t}}{d\tau}, \frac{dr}{d\tau}, \frac{d\theta}{d\tau}, \frac{d\bar{\phi}}{d\tau} \right) = \left(\frac{r^2 + a^2}{\Delta}, \sigma, 0, \frac{a}{\Delta} \right), \quad (36)$$

where $\sigma = 1$ correspond to the outgoing coordinate system and $\sigma = -1$ correspond to the ingoing coordinate system. Let us parametrize the geodesic in terms of r as

$$\frac{d\bar{t}}{dr} = \sigma \frac{r^2 + a^2}{\Delta} \quad \frac{d\bar{\phi}}{dr} = \sigma \frac{a}{\Delta}. \quad (37)$$

We want these geodesics to be coordinate lines of our new system; thus, one of our coordinates is r , while the others are quantities which are constant along each geodesic belonging to the family. One of these is θ ; the remaining two coordinates are given by

$$v \equiv \bar{t} - \sigma T(r), \quad (38)$$

$$\phi \equiv \bar{\phi} - \sigma \Phi(r), \quad (39)$$

where $\Phi(r)$ and $T(r)$ are chosen to fulfill

$$\frac{dT}{dr} = \frac{r^2 + a^2}{\Delta}, \quad (40)$$

$$\frac{d\Phi}{dr} = \frac{a}{\Delta}. \quad (41)$$

Therefore, along this family of geodesics we have that

$$\frac{dv}{dr} = \frac{d\phi}{dr} = 0, \quad (42)$$

and the tangent vector in this new coordinate system is simply $l^\mu = (0, \sigma, 0, 0)$. We can now compute the metric tensor in [EF](#) coordinate system. We have that

$$dv = d\bar{t} - \sigma \frac{r^2 + a^2}{\Delta} dr, \quad (43)$$

$$d\phi = d\bar{\phi} - \sigma \frac{a}{\Delta}. \quad (44)$$

$$(45)$$

Then, we can compute the following relations

$$\begin{aligned} -dt^2 &= -dv^2 - \frac{(r^2 + a^2)^2}{\Delta^2} dr^2 \\ &\quad - \sigma 2 \frac{r^2 + a^2}{\Delta} dv dr, \end{aligned} \quad (46)$$

$$\begin{aligned} (r^2 + a^2) \sin^2(\theta) d\bar{\phi}^2 &= (r^2 + a^2) \sin^2(\theta) d\phi^2 \\ &\quad + (r^2 + a^2) \frac{a^2}{\Delta^2} \sin^2(\theta) dr^2 \\ &\quad + \sigma 2(r^2 + a^2) \sin^2(\theta) \frac{a}{\Delta} dr d\phi, \end{aligned} \quad (47)$$

$$\begin{aligned} \frac{2Mr}{\Sigma} (dt - a \sin^2(\theta) d\bar{\phi})^2 &= \frac{2Mr}{\Sigma} dv^2 + \frac{2Mr}{\Sigma} a^2 \sin^2(\theta) d\phi^2 \\ &\quad + \frac{2Mr\Sigma}{\Delta^2} dr^2 - \frac{4aMr\sigma \sin^2(\theta)}{\Delta} dr d\phi \\ &\quad - \frac{4aMr \sin^2(\theta)}{\Sigma} dv d\phi \\ &\quad + \frac{4Mr\sigma}{\Delta} dr dv. \end{aligned} \quad (48)$$

Collecting terms in $dr, dv, d\phi, d\theta$ we can rewrite the metric tensor as

$$\begin{aligned} ds^2 = & - \left(1 - \frac{2Mr}{\Sigma} \right) dv^2 - 2\sigma dv dr + \Sigma d\theta^2 \\ & + \frac{(r^2 + a^2)^2 - \Delta a^2 \sin^2(\theta)}{\Sigma} \sin^2(\theta) d\phi^2 \\ & + 2\sigma a \sin^2(\theta) dr d\bar{\phi} - \frac{4mra}{\Sigma} \sin^2(\theta) dv d\phi \end{aligned} \quad (49)$$

Which can be rearrange into

$$\begin{aligned} ds^2 = & -dv^2 - 2\sigma dv dr + \Sigma d\theta^2 + (r^2 + a^2) \sin^2(\theta) d\phi^2 \\ & + 2\sigma a \sin^2(\theta) dr d\phi + \frac{2Mr}{\Sigma} (-dv + a \sin^2(\theta) d\phi)^2. \end{aligned} \quad (50)$$

We can now define a explicit time coordinate (which we will name t but does not coincide with the time coordinate of [BL](#) coordinates)

$$t \equiv v + \sigma r \quad (51)$$

so that the metric becomes

$$\begin{aligned} ds^2 = & -dt^2 + dr^2 + \Sigma d\theta^2 + (r^2 + a^2) \sin^2(\theta) d\phi^2 + 2\sigma a \sin^2(\theta) dr d\phi \\ & + \frac{2Mr}{\Sigma} (-dt + \sigma dr + a \sin^2(\theta) d\phi)^2, \end{aligned} \quad (52)$$

Which is equivalent to

$$\begin{aligned} ds^2 = & -dt^2 + dr^2 + \Sigma d\theta^2 + (r^2 + a^2) \sin^2(\theta) d\phi^2 + 2\sigma a \sin^2(\theta) dr d\phi \\ & + \frac{2Mr}{\Sigma} (-\sigma dt + dr + \sigma a \sin^2(\theta) d\phi)^2, \end{aligned} \quad (53)$$

■

3.2 METRIC IN KERR-SCHILD FORM

Now that we have the Kerr metric expressed in [EF](#) for both time orientations (encoded in the sign of σ), we are ready to transform the metric into its final form in [KS](#) coordinates. once we have the metric in this coordinates we will proceed to analyze the features that are only revealed in this coordinate system.

3.2.1 Displaying the metric in Kerr-Schild coordinates

Lemma 2. *The Kerr metric defined on [BL](#) coordinates*

$$\begin{aligned} ds^2 = & -d\bar{t}^2 + \Sigma \left(\frac{dr^2}{\Delta} + d\theta^2 \right) + (r^2 + a^2) \sin^2(\theta) d\bar{\phi}^2 \\ & + \frac{2Mr}{\Sigma} (a \sin^2(\theta) d\bar{\phi} - d\bar{t})^2 \end{aligned}$$

once expressed in [KS](#) coordinates takes the form

$$g = \eta + hK \otimes K,$$

where η is the Minkowsky metric and

$$f = \frac{2Mr^3}{r^4 + a^2z^2},$$

$$K = -\sigma dt + \frac{r(xdx + ydy)}{r^2 + a^2} + \frac{a(xdy - ydx)}{r^2 + a^2} + \frac{zdz}{r}.$$

Proof. By the use of lemma 1 we can start with the expression of the metric in **EF** coordinates. The goal is transform the metric

$$ds^2 = -dt^2 + dr^2 + \Sigma d\theta^2 + (r^2 + a^2) \sin^2(\theta) d\phi^2 + 2\sigma a \sin^2(\theta) dr d\phi \\ + \frac{2Mr}{\Sigma} (-\sigma dt + dr + \sigma a \sin^2(\theta) d\phi)^2, \quad (54)$$

into **KS** coordinates. The **KS** [9] coordinates (T, x, y, z) are defined by

$$x = \sqrt{r^2 + a^2} \sin(\theta) \cos\left(\sigma\phi - \arctan\frac{a}{r}\right), \quad (55)$$

$$y = \sqrt{r^2 + a^2} \sin(\theta) \sin\left(\sigma\phi - \arctan\frac{a}{r}\right), \quad (56)$$

$$z = r \cos\theta. \quad (57)$$

From defining $\beta = \arctan \frac{a}{r}$ we have

$$r^2 \sin \beta^2 = a^2 \cos \beta^2, \quad (58)$$

thus

$$r^2 = (r^2 + a^2) \cos \beta^2, \quad (59)$$

$$a^2 = (r^2 + a^2) \sin \beta^2. \quad (60)$$

We can rewrite eqs. (55) and (56) as

$$x = \sqrt{r^2 + a^2} \sin \theta (\cos \beta \cos(\sigma\phi) + \sin \beta \sin(\sigma\phi)), \quad (61)$$

$$y = \sqrt{r^2 + a^2} \sin \theta (\cos \beta \sin(\sigma\phi) - \sin \beta \cos(\sigma\phi)), \quad (62)$$

$$x = r \cos \theta, \quad (63)$$

and substituting eqs. (59) and (60) into this relations it follows that

$$x = \sin \theta (r \cos(\sigma\phi) + a \sin(\sigma\phi)), \quad (64)$$

$$y = \sin \theta (r \sin(\sigma\phi) - a \cos(\sigma\phi)), \quad (65)$$

$$z = r \cos \theta. \quad (66)$$

Differentiating this relations we obtain that

$$dx = d\theta \cos(\theta) (a \sin(\sigma\phi) + r \cos(\sigma\phi)) + dr \sin(\theta) \cos(\sigma\phi) \\ + d\phi \sin(\theta) (a \sigma \cos(\sigma\phi) - r \sigma \sin(\sigma\phi)) \quad (67)$$

$$dy = d\phi \sin(\theta) (a \sigma \sin(\sigma\phi) + r \sigma \cos(\sigma\phi)) + dr \sin(\theta) \sin(\sigma\phi) \\ + d\theta \cos(\theta) (r \sin(\sigma\phi) - a \cos(\sigma\phi)) \quad (68)$$

$$dz = dr \cos(\theta) - d\theta r \sin(\theta) \quad (69)$$

We can relate the Minkowsky metric in **KS** coordinates with the **EF** coordinates as

$$\begin{aligned} dx^2 + dy^2 + dz^2 - dt^2 &= dr^2 + (r^2 + a^2 \cos^2(\theta))d\theta^2 \\ &\quad + (r^2 + a^2) \sin^2(\theta)d\phi^2 + 2\sigma \sin^2(\theta)adr d\phi - dt^2. \end{aligned} \quad (70)$$

Comparing this with the metric eq. (53) we realize that the Kerr metric can be written as

$$\begin{aligned} dx^2 + dy^2 + dz^2 - dt^2 &+ \frac{2Mr}{r^2 + \cos^2(\theta)}(-\sigma dt + dr + \sigma a \sin^2(\theta)d\phi)^2 \\ &= dx^2 + dy^2 + dz^2 - dt^2 + \frac{2Mr^3}{r^4 + a^2 z^2}(-\sigma dt + dr + \sigma a \sin^2(\theta)d\phi)^2 \end{aligned} \quad (71)$$

To complete the coordinate transformation we have to express the one-form $K = -\sigma dt + dr + \sigma a \sin^2(\theta)d\phi$ into Kerr-Schild coordinates. To achieve that we will prove that

$$-\sigma dt + dr + \sigma a \sin^2(\theta)d\phi = dt + \frac{r(xdx + ydy)}{r^2 + a^2} + \frac{a(xdy - ydx)}{r^2 + a^2} + \frac{zdz}{r}. \quad (72)$$

We start expressing first eqs. (67) to (69) as

$$dx = \frac{\cos(\theta)}{\sin(\theta)}xd\theta + \sin(\theta)\cos(\sigma\phi)dr - \sigma yd\phi, \quad (73)$$

$$dy = \frac{\cos(\theta)}{\sin(\theta)}yd\theta + \sin(\theta)\sin(\sigma\phi)dr + \sigma xd\phi, \quad (74)$$

$$dz = -r \sin(\theta)d\theta + \cos(\theta)dr. \quad (75)$$

From this relations we have

$$\begin{aligned} xdx + ydy &= \frac{\cos(\theta)}{\sin(\theta)}(x^2 + y^2)d\theta + \sin(\theta)(x\cos(\sigma\phi) + y\sin(\sigma\phi))dr \\ &= \sin(\theta)\cos(\theta)(r^2 + a^2)d\theta + \sin^2(\theta)rdr, \end{aligned} \quad (76)$$

$$\begin{aligned} xdy - ydx &= \sigma(x^2 + y^2)d\phi - \sin(\theta)(y\cos(\sigma\phi) - x\sin(\sigma\phi))dr \\ &= \sigma(r^2 + a^2)\sin^2(\theta)d\phi + \sin^2(\theta)adr, \end{aligned} \quad (77)$$

$$zdz = -r^2 \sin(\theta)\cos(\theta)d\theta + r\cos^2(\theta)dr. \quad (78)$$

then

$$\begin{aligned} &\frac{r(xdx + ydy)}{r^2 + a^2} + \frac{a(xdy - ydx)}{r^2 + a^2} + \frac{zdz}{r} \\ &= (r \sin(\theta)\cos(\theta)d\theta + \frac{r^2}{r^2 + a^2}\sin^2(\theta)dr) \\ &\quad + (\sigma a \sin^2(\theta)d\phi + \frac{a^2}{r^2 + a^2}\sin^2(\theta)dr) \\ &\quad + (-r \sin(\theta)\cos(\theta)d\theta + \cos^2(\theta)dr) \\ &= dr + \sigma a \sin^2(\theta). \end{aligned} \quad (79)$$

Therefore, the Kerr metric in **KS** coordinates can be written as

$$g = \eta + hK \otimes K, \quad (80)$$

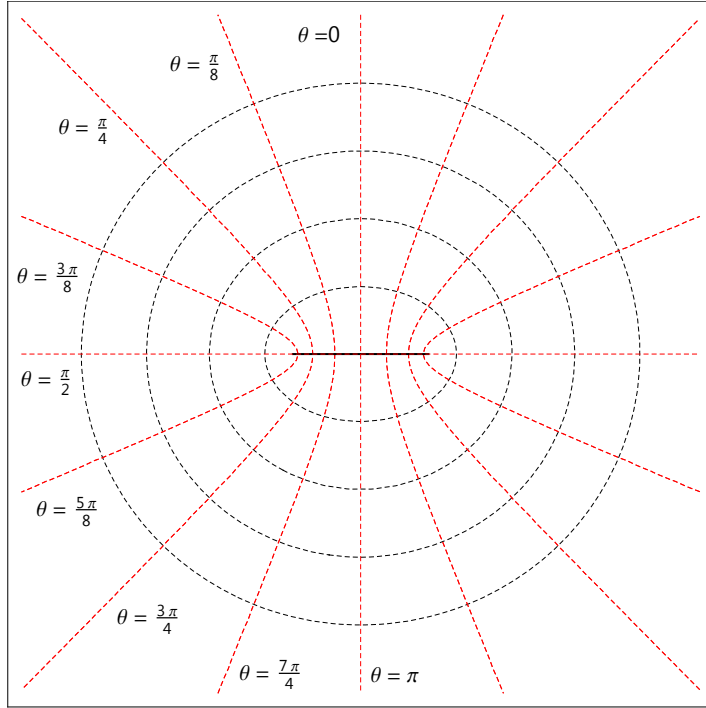


Figure 9: Surfaces with constant r (black ellipsoids) and constant θ (red half - hyperboloids) in the Kerr spacetime.

where η is the Minkowsky metric and

$$f = \frac{2Mr^3}{r^4 + a^2z^2},$$

$$K = -\sigma dt + \frac{r(xdx + ydy)}{r^2 + a^2} + \frac{a(xdy - ydx)}{r^2 + a^2} + \frac{zdz}{r}.$$

■

3.2.2 Surface embedding into Kerr-Schild coordinates

We are now able to see how the different surfaces are embedded in the Kerr-Schild version of the Kerr spacetime. Let's start with the BL-constant-coordinate surfaces. Notice that from eqs. (64) to (66) it follows that

$$x^2 + y^2 = (a^2 + r^2) \sin^2(\theta), \quad (81)$$

$$z^2 = r^2 \cos^2(\theta), \quad (82)$$

thus

$$1 = \frac{x^2 + y^2}{r^2 + a^2} + \frac{z^2}{r^2}, \quad (83)$$

$$1 = \frac{x^2 + y^2}{a^2 \sin^2(\theta)} - \frac{z^2}{a^2 \cos^2(\theta)}. \quad (84)$$

The first equation serves as implicit definition of the function $r = r(x, y, z)$ and tell us that the surfaces with constant r are ellipsoids while the second equation shows that the surfaces with constant θ are half-hyperboloids. This surfaces are displayed in fig. 9 on page 28. A helpful diagram of the horizons and singularities can be found in figs. 10 and 11 on this page and on the next page. Now that we

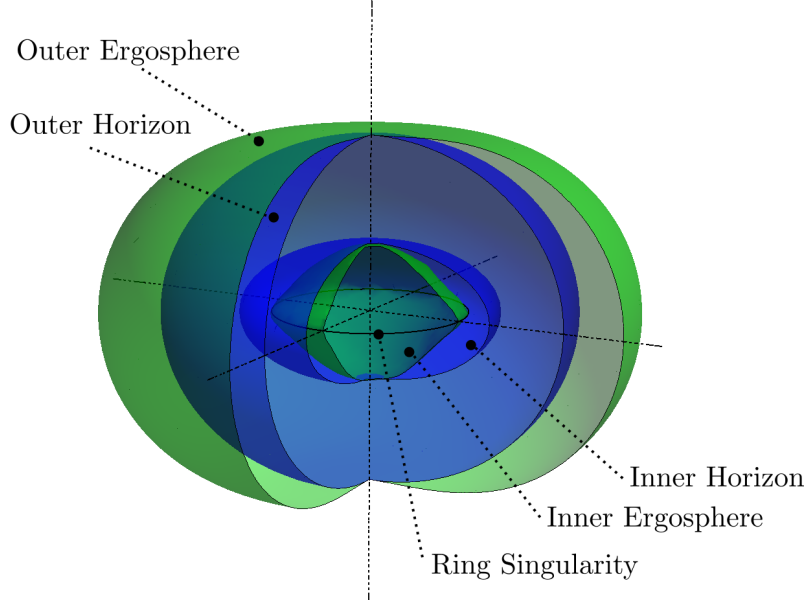


Figure 10: Schematic location of the horizons, ergosurfaces, and curvature singularity in the Kerr spacetime. For simplicity $M = 1$ and $a = 0.9$ is chosen.

know how the **BL**-constant-coordinate surfaces look like in the **KS** version of the Kerr spacetime, we will proceed to analyze the singularity surfaces. Notice that the metric 80 is only singular at $x^2 + y^2 = a^2$ and therefore all the remaining singularities that we find in **BL** coordinates or **EF** coordinates are gone. The remaining singularity is the *True* spacetime singularity and once embedded in the **KS** version of the Kerr spacetime the ring shape is revealed. Transforming the solutions to the singularity equations ($\Delta = r^2 - 2Mr + a^2 = 0$ and $\Sigma = r^2 + a^2 \cos^2(\theta) = 0$), which gives the horizons and the spacetime singularity, and the solution to the points where g_{tt} changes sign ($g_{tt} = -1 + \frac{2Mr}{\Sigma} = 0$), which gives the ergosurfaces, to **KS** coordinates we realize that the horizons and singularities of the Kerr metric in **KS** coordinates are

1. Spacetime singularity at $x^2 + y^2 = a^2$ and $z = 0$,
2. Event horizon at $r_+ = M + \sqrt{m^2 - a^2}$,
3. Cauchy horizon at $r_- = M - \sqrt{m^2 - a^2}$,
4. Outer Ergosurface at $r_E^+ = M + \sqrt{M^2 - a^2 \frac{z^2}{r^2}}$,
5. Inner Ergosurface at $r_E^- = M - \sqrt{M^2 - a^2 \frac{z^2}{r^2}}$.

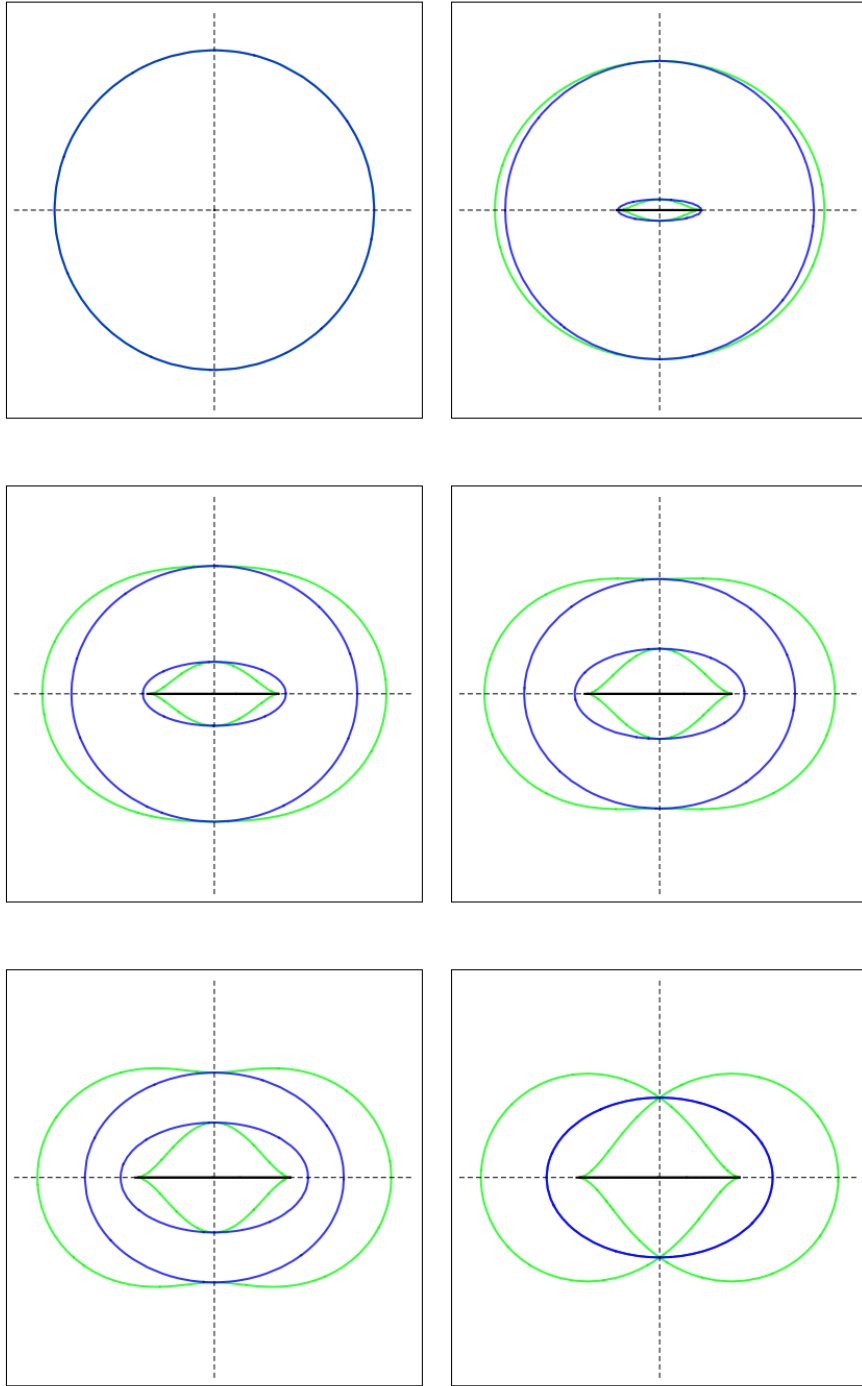


Figure 11: Schematic location of the horizons, ergosurfaces, and curvature singularity in the side view of the Kerr-Schild Spacetime as a function of the parameter a . The images correspond to (from left to right and from top to bottom) $a = 0, a = 0.5, a = 0.8, a = 0.9, a = 0.95, a = 1$. The green surfaces are the outer and inner ergosurfaces and the blue curves represent the inner and outer horizon. The ring singularity is represented as the black curve while the black dashed curves are the z and y Kerr-Schild axes. For simplicity $M = 1$ is chosen.

Notice that a closer look at eqs. (55) and (56) reveals the **BL** coordinates $\{r, \phi, \theta\}$ behave like spherical coordinates for large values of r , which means that if we analyze the Kerr black hole far away from its center, we will tend to see the Minkowsky spacetime. When this happens we say that the metric is *asymptotically flat*, i.e. the curvature in the infinity vanishes. The **KS** coordinates also reveal the true nature of the Kerr singularity, despite the spacetime singularity is at $r = 0$ and $\theta = \frac{\pi}{2}$ (in **BL** coordinates), in **KS** coordinates this reads $x^2 + y^2 = a^2$ and $z = 0$, which is a ring in the **KS** version of the Kerr spacetime. The **KS** coordinates also reveal what is called *the inside of the ring* which is the region $x^2 + y^2 < a^2$ and $z = 0$. We will discuss in the next chapters the role of this inner disk in the Kerr spacetime as well as the geodesic movement in it.

3.3 CONSERVED QUANTITIES IN KERR-SCHILD COORDINATES

Now that we understand the metric and the bifurcation surfaces (horizons) in **KS** coordinates, we have to obtain the conserved quantities in **KS** coordinates. These conserved quantities comes from the existence of two Killing vectors (associated to the temporal invariance and the axisymmetric invariance) and one Killing tensor. Useful information about Killing vectors and Killing tensor can be found in appendix A on page 93. To obtain the conserved quantities in the new coordinates we must get first the Killing vectors and tensors in the **KS** coordinates.

3.3.1 Killing vectors

Lemma 3. *The Killing vectors of the Kerr metric in **KS** coordinates are:*

$$\xi_1 = \partial_t \tag{85}$$

$$\xi_2 = \sigma(x\partial_y - y\partial_x) \tag{86}$$

Proof. As the metric eq. (80) does not depend on the time coordinate t then ∂_t is a Killing vector. To obtain the second Killing vector, is easy to notice that the metric in **EF** coordinates (eq. (53)) does not depend on the coordinate ϕ and therefore ∂_ϕ is a Killing vector. We only need to transform this vector into the new coordinates using the relation between **KS** coordinates and **EF** coordinates of eqs. (64) and (65), The final killing vectors are

$$\begin{aligned} \partial_\phi &= \frac{\partial x}{\partial \phi} \partial_x + \frac{\partial y}{\partial \phi} \partial_y, \\ &= \sin(\theta)(a\sigma \cos(\sigma\phi) - r\sigma \sin(\sigma\phi))\partial_x + \sin(\theta)(a\sigma \sin(\sigma\phi) + r\sigma \cos(\sigma\phi))\partial_y \\ &= \sigma(x\partial_y - y\partial_x), \end{aligned}$$

as claimed . ■

By the use of this lemma the conserved quantities defined by this Killing vectors are:

$$-E = g(\partial_t, u) \tag{87}$$

$$\sigma L_z = g(x\partial_y - y\partial_x, u) \tag{88}$$

where u is the geodesic tangent vector.

3.3.2 Killing tensors

The third constant of motion was first noticed by Brandon Carter [5, 4] and in his original work, it comes from a separability constant in the Hamilton-Jacobi equations once the metric is written in BL coordinates. This third constant of motion is written in BL coordinates as

$$\mathcal{C} = (aE - \sigma L_z)^2 + p_\theta^2 + \cos^2(\theta) \left(a^2(M^2 - E^2) + \left(\frac{L_z}{\sin(\theta)} \right)^2 \right). \quad (89)$$

where L_z is the total angular momentum. To clarify the genesis of this third constant of motion we are going to derive it from a generalized Killing tensor.

Lemma 4. *The conserved quantity given by the Carter's Killing tensor in KS coordinates is*

$$\begin{aligned} \mathcal{C} = & (\sigma L_z + aE)^2 + \left(\frac{z}{r}(xp_x + yp_y) + \sqrt{r^2 - z^2}p_z \right)^2 \\ & + \frac{z^2}{r^2} \left(a^2(M^2 - E^2) \right) + \frac{L_z^2 z^2}{r^2 - z^2} \end{aligned} \quad (90)$$

Proof. The generalized Killing equation for Killing tensor is

$$\nabla_{(\alpha} T_{\beta\gamma)} = 0, \quad (91)$$

where (\dots) denotes symmetrization in the indexes. Is useful to use what is known as the Killing-Yano tensor, which is in some sense the “square root” of a Killing tensor and it is defined to fulfill

$$T_{\alpha\beta} = F_{\alpha\gamma} F_\beta^\gamma, \quad (92)$$

and by this definition $F_{[\alpha\gamma]} = 0$ (where $[\dots]$ denotes antisymmetrization in the indexes). Inserting this equation into the definition of the Killing tensor we get that the Killing-Yano tensor must satisfy that

$$\nabla_{(\gamma} F_{\alpha)\beta} = 0. \quad (93)$$

Conversely, if we find a tensor $F_{\alpha\beta}$ that satisfy eq. (93) we can compute the associated Killing tensor using eq. (92). In [6] one can find the only independent solution of eq. (93) for the Kerr metric in KS coordinates given by

$$F_{\alpha\beta} = \begin{pmatrix} 0 & 0 & 0 & -\sigma a \\ 0 & 0 & z & -y \\ 0 & -z & 0 & x \\ \sigma a & y & -x & 0 \end{pmatrix} \quad (94)$$

$$F^{\alpha\beta} = \begin{pmatrix} 0 & 0 & 0 & \sigma a \\ 0 & 0 & z & -y \\ 0 & -z & 0 & x \\ -\sigma a & y & -x & 0 \end{pmatrix} \quad (95)$$

the quantity $T_{\alpha\beta} = F_{\alpha\gamma}F_{\beta}^{\gamma}$ has never been computed in this coordinate system (as far as we know) because the metric has a complicated expression in **KS** coordinates. However, a direct computation using the algebraic manipulation software *Mathematica* gives us the full conserved quantity given by:

$$\begin{aligned}\mathcal{C} &= F_{\alpha\gamma}F_{\beta}^{\gamma}u^{\alpha}u^{\beta} = (\sigma L_z + aE)^2 + \left(\frac{z}{r}(xp_x + yp_y) + \sqrt{r^2 - z^2}p_z\right)^2 \\ &\quad + \frac{z^2}{r^2} \left(a^2(M^2 - E^2)\right) + \frac{L_z^2 z^2}{r^2 - z^2}\end{aligned}\tag{96}$$

where $p_{\alpha} = g(\partial_{\alpha}, u)$. ■

Notice that for the **SW** limit ($a \rightarrow 0$) the conserved quantity becomes

$$\begin{aligned}\mathcal{C} &= p_x^2(y^2 + z^2) - 2p_yy(p_{xx} + p_zz) - 2p_xp_zxz + p_y^2(x^2 + z^2) + p_z^2(x^2 + y^2) \\ &= (p_yx - p_xy)^2 + (p_zx - p_xy)^2 + (p_yx - p_zy)^2 = L_z^2 + L_y^2 + L_z^2 = \vec{L}^2,\end{aligned}$$

while for the equatorial plane $z = 0$ it becomes

$$\mathcal{C} = (aE - \sigma L_z)^2.\tag{97}$$

In both cases the Carter's constant is not a independent conserved quantity, which we could expect because for the equatorial plane we cannot have three constants of motion because in two dimensions three constants of motion leads to constant trajectories and in the **SW** case the Carter constant follows from the Killing tensor $K = \xi_1 \otimes \xi_1 + \xi_2 \otimes \xi_2 + \xi_3 \otimes \xi_3$ (where ξ_i are the three Killing vectors of S_2).

4

MAXIMAL EXTENSION

Now that we have the Kerr metric in [KS](#) coordinates we are going to analyze the [Maximal Analytic Extension \(MAE\)](#) of the Kerr spacetime. The [MAE](#) of a spacetime is based on the idea of atlas of an inextensible analytic manifold. We could say that [BL](#) coordinates are a patch that only covers a limited region of the whole manifold that the Kerr spacetime is. Expressing the Kerr metric in the [KS](#) coordinates reveal that this system covers the whole manifold and acts as full atlas for it. As we see in this section, this atlas is formed by a countably infinite number of copies of two basic patches that are joined together indefinitely. To develop the [MAE](#) of the Kerr spacetime, geodesic completeness must be analyzed (see [11]). As the [MAE](#) in [EF](#) coordinates is well known [4, 11] and exceeds this work, in this chapter we are only going to study how this known [MAE](#) is described in [KS](#) coordinates and how the basic patches are assembled to construct it.

4.1 RING IDENTIFICATION

It was first noticed by Brandon Carter [4] that the Kerr spacetime can be extended beyond the previous description. This extension takes its origin in the fact that the Kerr metric in [BL](#) coordinates is no singular at $r = 0$ and therefore the variation range of this coordinate (initially $r \in (0, \infty)$) can be extended to $r \in (-\infty, \infty)$. This is due to the fact that the singularity is not a point but a ring. This identification is very easy to perform in [KS](#) coordinates. First of all notice that if we restrict the values of the function $r = r(x, y, z) \in (0, \infty)$, then a geodesic that is defined along the z axis ($x = y = 0$) starting from the positive branch ($z > 0$) will reach the disk inside the singular ring (located at $z = 0, x^2 + y^2 < a^2$) with no problems because the inner disk is not singular, but there is still problems. For the $z > 0$ axis the definition of the function r that follows from eq. (83) (with positive sign) is $r(x, y, z) = z$ and when the geodesic reaches the inner disk and passes through it, the definition of the function r must change to $r(x, y, z) = -z$ as now $z < 0$ and the function r must remain positive. This change of sign in the function r leads to a discontinuous definition as well as to discontinuous curvature invariants (like $R^{\alpha\beta\gamma\delta}R_{\alpha\beta\gamma\delta}$ (where $R^\alpha_{\beta\gamma\delta}$ is the Riemann tensor)). To remove this singularity we must extend the variation range of the function r to $r(x, y, z) \in (-\infty, \infty)$ which leads to a identification between two copies of the Kerr spacetime.

Proposition 5. *The Kerr spacetime once the function $r(x, y, z)$ is extended to $r \in (-\infty, \infty)$ is foliated by the leafs*

$$\mathcal{M} = \frac{\mathbb{R}_+^3 \cup \mathbb{R}_-^3}{\sim} \quad (98)$$

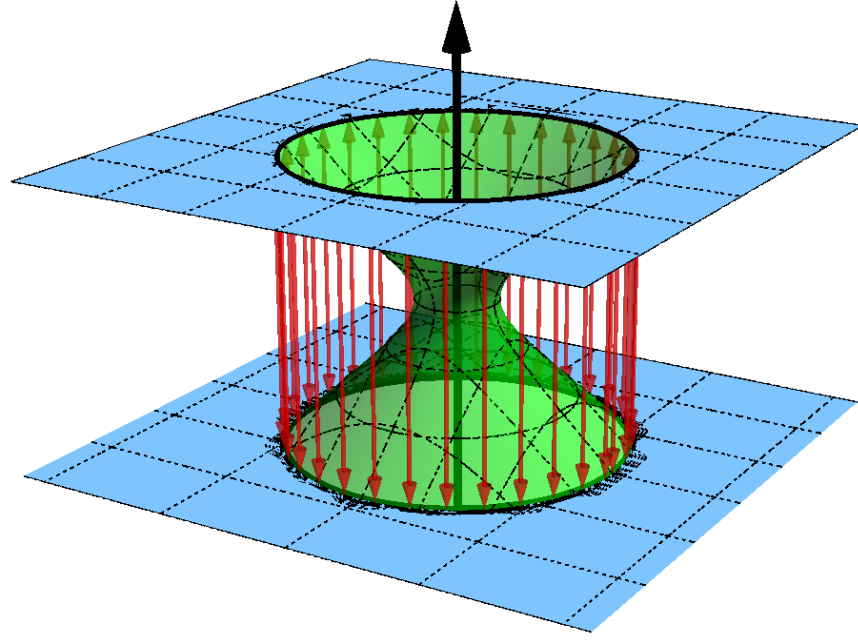


Figure 12: Pictoric image showing the identification process between the $x^2 + y^2 < a^2$ disks. The red arrows indicate that the two disk are glued together (not the rings) and there is no “space” between the two planes in this representation. The blue planes represent the $z = 0$ planes in the $r > 0$ and $r < 0$ spaces. The green surface only serves to show the wormhole product of the identification but as the two disks are glued together, this surface does not exist in reality. Notice that in this representation the space between the two planes does not exist and therefore there is only displayed the $z > 0$ semi-space of the upper copy of \mathbb{R}^3 and the $z < 0$ semi-space of the lower copy of \mathbb{R}^3 . The other semi-space are not in the picture as we would need another one to display them. We remark that as the green surface does not exist, topological properties cannot be derived from it. Moreover, the topology of the identification is trivial.

where in each leaf the time coordinate has a different value (which defines the foliation), \mathcal{M} denotes the final MAE manifold, \mathbb{R}_+^3 and \mathbb{R}_-^3 denotes two copies of \mathbb{R}^3 and \sim is the equivalence relation given by

$$\begin{aligned} p_1 &= (x_1, y_1, z_1) \in \mathbb{R}_+^3, \\ p_2 &= (x_2, y_2, z_2) \in \mathbb{R}_-^3, \\ p_1 \sim p_2 &\longleftrightarrow \{x_1 = x_2, y_1 = y_2, z_1 = z_2 = 0, x_i^2 + y_i^2 < a^2\} \end{aligned} \quad (99)$$

The tangent planes are identified in the following way

$$v_1 \in T_p \mathbb{R}_+^3, \quad p \in x_1^2 + y_1^2 < a^2, z = 0 \quad (100)$$

$$v_2 \in T_p \mathbb{R}_-^3, \quad p \in x_1^2 + y_1^2 < a^2, z = 0 \quad (101)$$

$$v_1 \sim v_2 \longleftrightarrow v_1^\alpha = v_2^\alpha. \quad (102)$$

The function $r(x, y, z)$ after de identification takes the form

$$r(x, y, z) = \lambda \frac{\sqrt{\sqrt{(a^2 - x^2 - y^2 - z^2)^2 + 4a^2z^2} - a^2 + x^2 + y^2 + z^2}}{\sqrt{2}} \quad (103)$$

$$(104)$$

with $\lambda = 1$ for \mathbb{R}_+^3 and $\lambda = -1$ for \mathbb{R}_-^3 .

Proof. The implicit definition of the function r in **KS** coordinates given by eq. (83) reads

$$r^2 (a^2 + r^2) = z^2 (a^2 + r^2) + r^2 (x^2 + y^2). \quad (105)$$

This equation have four solutions, two of them always real and the other two always imaginary (they are complex conjugate). The two real solutions are

$$r(x, y, z) = \sqrt{\sqrt{(a^2 - x^2 - y^2 - z^2)^2 + 4a^2z^2} - a^2 + x^2 + y^2 + z^2} \quad (106)$$

$$r(x, y, z) = -\sqrt{\sqrt{(a^2 - x^2 - y^2 - z^2)^2 + 4a^2z^2} - a^2 + x^2 + y^2 + z^2} \quad (107)$$

This is the reason that for each set of **KS** coordinates there are two different values of $r(x, y, z)$. Therefore we have two different copies of the Kerr space-time described by the metric eq. (80) with different sign in the definition of the function $r(x, y, z)$. Let's name this copies \mathbb{R}_+^3 and \mathbb{R}_-^3 . When we perform the similarity relation given by

$$\begin{aligned} p_1 &= (x_1, y_1, z_1) \in \mathbb{R}_+^3, \\ p_2 &= (x_2, y_2, z_2) \in \mathbb{R}_-^3, \\ p_1 \sim p_2 &\longleftrightarrow \{x_1 = x_2, y_1 = y_2, z_1 = z_2 = 0, x_i^2 + y_i^2 < a^2\} \end{aligned} \quad (108)$$

we are constructing a topological manifold product of gluing the two disks together. In order to construct a differential manifold, we must say how we identify the tangent planes. They are under the following similarity relation:

$$v_1 \in T_p \mathbb{R}_+^3, \quad p \in x_1^2 + y_1^2 < a^2, z = 0 \quad (109)$$

$$v_2 \in T_p \mathbb{R}_-^3, \quad p \in x_1^2 + y_1^2 < a^2, z = 0 \quad (110)$$

$$v_1 \sim v_2 \longleftrightarrow v_1^\alpha = v_2^\alpha. \quad (111)$$

Under this identification of the disks and the tangent planes, we are finally identifying the top the disk $x_1^2 + y_1^2 < a^2, z_1 = 0$ with the bottom of the disk $x_2^2 + y_2^2 < a^2, z_2 = 0$ and vice versa as is displayed in figs. 12 and 13 on page 36 and on the following page. After the identification is complete, the definition of the function $r(x, y, z)$ becomes

$$r(x, y, z) = \lambda \frac{\sqrt{\sqrt{(a^2 - x^2 - y^2 - z^2)^2 + 4a^2z^2} - a^2 + x^2 + y^2 + z^2}}{\sqrt{2}} \quad (112)$$

$$(113)$$

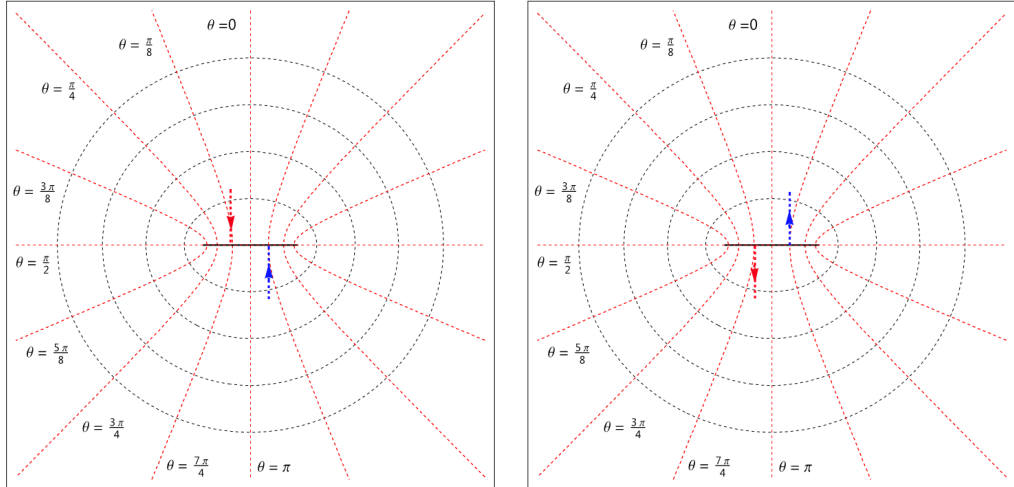


Figure 13: Side view of the spaces \mathbb{R}^3_+ (left image) and \mathbb{R}^3_- (right image). The red dotted lines represent the surfaces with $\theta = \text{const.}$ while the black dotted lines represent the $r = \text{const.}$ surfaces. The singular ring is the thick black line in the middle. The arrows show how the identification works: A geodesic that follows the red arrow in the left image emerges in the right image following the red arrow and equivalently for the blue arrow. Once in the right image the situation becomes the same as it started. Note that a geodesic following one arrow can surround the ring and pass through the disk as the other arrow. As the green surface does not exist, the topological implications of its shape are nonexistent, as the identification has trivial topology.

with $\lambda = 1$ for \mathbb{R}^3_+ and $\lambda = -1$ for \mathbb{R}^3_- . As the function r becomes $r(x, y, z) = 0$ at the disk, we have a continuous and at least C^2 definition and therefore the curvature scalars are continuous. We must proof that this definition for the function $r(x, y, z)$ is also analytic. To achieve this, write for points near the inner disk ($x^2 + y^2 < a^2$ and $z \sim 0$)

$$r(x, y, z) = z\sqrt{f(x, y, z)} \quad (114)$$

where $f(x, y, z) : \mathbb{R}^3 \rightarrow \mathbb{R}^+$ is a everywhere positive function. Under this ansatz we can rewrite eq. (105) as

$$f(x, y, z) \left(z^2 f(x, y, z) + a^2 - x^2 - y^2 - z^2 \right) - a^2 = 0 \quad (115)$$

which leads to

$$f(x, y, z) = \frac{\pm\sqrt{(-a^2 + x^2 + y^2 + z^2)^2 + 4a^2z^2} - a^2 + x^2 + y^2 + z^2}{2z^2} \quad (116)$$

to obtain a positive function we must chose the $+$ in the square root. This function satisfies that

$$\lim_{z \rightarrow 0} f(x, y, z) = \frac{-a^2}{-a^2 + x^2 + y^2} \quad (117)$$

The function $f(x, y, z)$ is a analytic function because it is the result of composing analytic functions. As the function z under the identification is continuous and analytic, we conclude that the function $r(x, y, z)$ is continuous because is the product of analytic functions. This is also because

$$\lim_{z \rightarrow 0} z \sqrt{f(x, y, z)}|_{x^2 + y^2 < a^2} = 0 \quad (118)$$

As now the manifold is formed under a identification that leads to continuous and smooth functions and curvature scalars, we have removed the “singularity” across the disk. Of course, this corresponds only to the spatial part of the Kerr spacetime, i.e each foil of the whole foliation, where each foil has a different value of the time coordinate t . \blacksquare

With this identification of the inner disk, a geodesic that falls through the $z > 0$ branch of the z -axis with $r > 0$ (\mathbb{R}_+^3 copy), reach the top of the inner disk at $x^2 + y^2 < a^2, z = 0$ and emerges on the bottom of the inner disk of the space with $r < 0$ (\mathbb{R}_-^3 copy). At this point, the geodesic can go to the asymptotically flat limit $r \rightarrow -\infty$. Is important to note that in the \mathbb{R}_-^3 copy, there are no horizons as the singularity equation $\Delta(r) = 0$ only gives positive solutions for the horizons.

As the geodesics are not necessarily defined on the z -axis, to fully understand this part of the Kerr MAE, we must think in the spacetime as two complete and independent copies of \mathbb{R}^3 . Imagine that in the two copies there is a disk inside the singular ring. If the identification is not yet done, if we travel across this disk nothing happens, i.e. if a geodesic goes from under the disk it will emerge above the disk and vice versa. This is obvious because we are only passing through a disk in a “regular space”. Imagine now that after the identification is done, the behavior of the geodesic is the same (in the sense that if you pass through the disk from underneath you will emerge from the top and if you go across the disk from the top you will emerge from the bottom) but when you pass across the disk, you emerge in another space (another copy of \mathbb{R}^3) in the same way (top to bottom and bottom to top). Each copy is complete in the sense that have everything that the other copy have. Therefore, there are two different z -axis (one in each copy), two different singular rings (but only one disk because the identification is between the disks and no between the singular rings), two different asymptotically flat ends of the spacetime... The only thing that is not analogous between the two copies is that in \mathbb{R}_-^3 there is no horizons and the only singular surface is the singular ring, as was noticed previously.

Notice also that the MAE of a geodesic that is imposed to move along the z -axis is formed by two disjoint parts. This is because if we consider a geodesic falling along the z -axis with $z > 0$ in \mathbb{R}_+ when it reaches the inner disk, it emerges in \mathbb{R}_- with $z < 0$. As the geodesic is imposed to move along the axis, it cannot surround the ring and access the $z > 0$ branch of \mathbb{R}_- so this geodesic is forced to move in the space $\mathcal{Z}_1 = \mathbb{R}_+|_{z>0} \cup \mathbb{R}_-|_{z<0}$. Similarly a geodesic that falls along the z -axis with $z < 0$ is forced to move in the space $\mathcal{Z}_2 = \mathbb{R}_+|_{z<0} \cup \mathbb{R}_-|_{z>0}$. Indeed, the definition of the function $r(x, y, z)$ for a geodesic that falls along the z -axis ($x = y = 0$) becomes

$$r(z, 0, 0) = \lambda z \quad (119)$$

with $\lambda = 1$ for the space \mathcal{Z}_1 and $\lambda = -1$ for the space \mathcal{Z}_2 .

4.2 KERR-SCHILD PATCHES

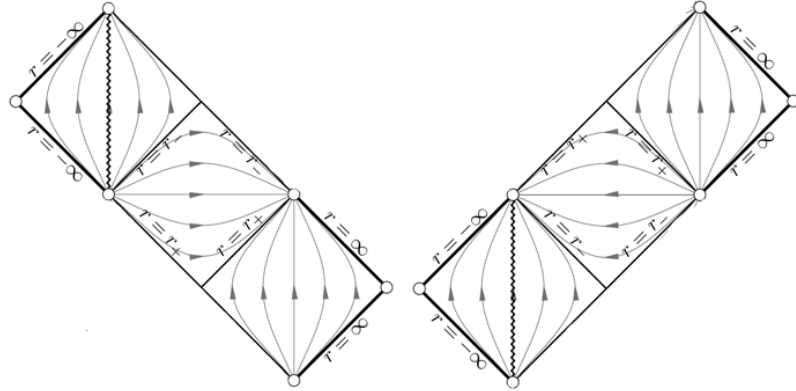


Figure 14: The figure on the left shows the ingoing Kerr-Schild patch ($\sigma = -1$) while the figure on the right shows the outgoing Kerr-Schild patch ($\sigma = 1$).

Actually the **MAE** of the Kerr spacetime is much larger than the ring identification. We are going to study which part of the known maximal extension of the spacetime is covered by each **KS** patch and how they are assembled. To do this we must know how the **KS** time coordinate is related to the **BL** time coordinate. From eqs. (43) and (51) on page 24 and on page 25 we can relate the **KS** coordinate t to the **BL** analogue \bar{t} :

$$d\bar{t} = dt + \sigma \left(\frac{r^2 + a^2}{\Delta} - 1 \right). \quad (120)$$

A direct integration for constant- t trajectories gives

$$\bar{t}(r) = M\sigma \left(\log \left(a^2 - 2Mr + r^2 \right) + \frac{2M \tan^{-1} \left(\frac{r-M}{\sqrt{(a-M)(a+M)}} \right)}{\sqrt{(a-M)(a+M)}} \right). \quad (121)$$

The outer horizon is located at $r_+ = M + \sqrt{(M^2 - a^2)}$ and we can evaluate the function $\bar{t}(r)$ as it reaches the outer horizon, which gives that

$$\lim_{r \rightarrow r_+} \bar{t}(r)|_{t=const.} = -\sigma\infty, \quad (122)$$

$$\lim_{r \rightarrow \infty} \bar{t}(r)|_{t=const.} = \sigma\infty. \quad (123)$$

Therefore the Kerr-Schild patch with $\sigma = -1$ approaches $r \rightarrow r_+$ with $\bar{t} \rightarrow \infty$ and comes from $r = \infty$ in the past ($\bar{t} = -\infty$) and the Kerr-Schild patch with $\sigma = 1$ approaches $r = \infty$ with $\bar{t} \rightarrow \infty$ and comes from $r \rightarrow r_+$ in the past ($\bar{t} = -\infty$). We will assign (as is usually done in the **SW** case) the denomination *Black hole* to the **KS** patch with $\sigma = -1$ and *White hole* to the **KS** patch with

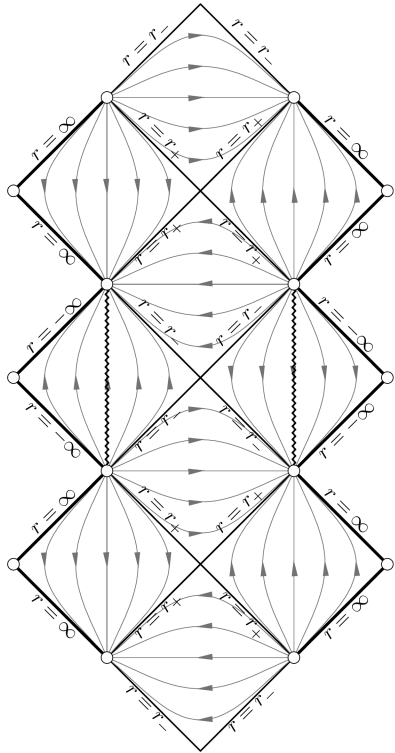
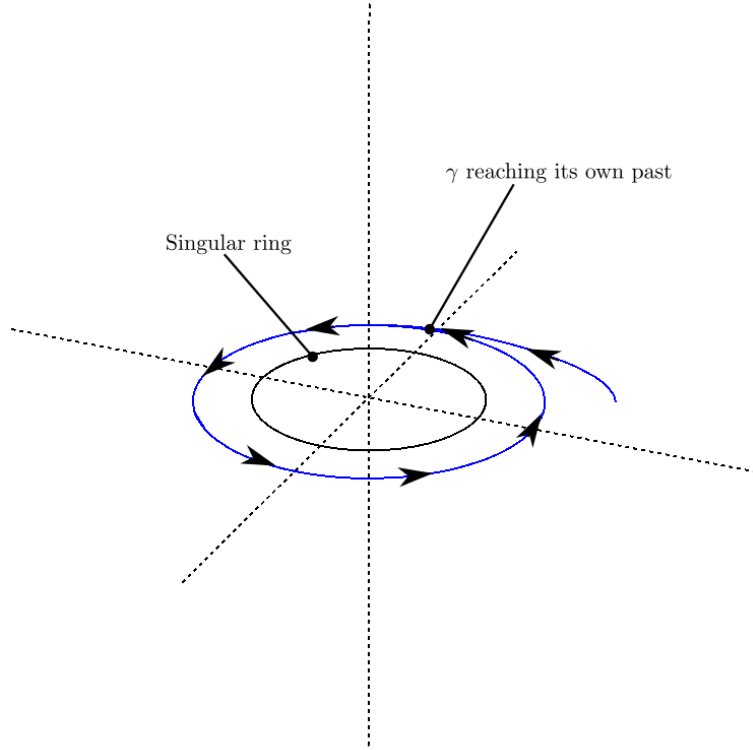


Figure 15: Penrose-Carter (PC) diagram of the Kerr spacetime along the axis of symmetry for simplicity. The PC diagrams are conformal compactifications of the spacetime that help to understand the causal structure of the whole manifold. The diagram is constructed to maintain the light cones as straight lines at $\frac{\pi}{2}$ rad. For more information and resources to understand PC diagrams see [11, 8].

$\sigma = 1$. Of course, in KS coordinates, the geodesic flow does not stop at r_+ and can be extended over r_- until reaches $r = 0$ for both values of σ . This two patches can be glued together an indefinitely number of times, allowing the geodesic flow to pass over r_+ and r_- as many times as needed. A in-depth study of the geodesic completeness (see chapter 3 of [11]) reveal that the basic structure of the maximal extension is in reality formed by four basic patches (two of them isometric to the other two) as one can visualize in the Penrose carter diagram of fig. 15. The two basic patches of the left are isometric to the two basic patches of the right (these two basic patches are the ones that we have studied), and this group is glued together and infinite number of times conforming the Penrose Carter diagram. The whole MAE of the Kerr spacetime is not globally hyperbolic and also, if we can connect two points in the spacetime with a causal curve is not necessary true that there is a geodesic that connect this two points. Despite the MAE is not globally hyperbolic, the two KS patches are globally hyperbolic and therefore it is true that if we find a causal curve connecting two points, exists a geodesic that connect the same points. This is quite useful to think in the different geodesic trajectories that we are going to describe in the next chapters. As a geodesic can be extended across the PC diagram, it can

Figure 16: The curve γ as it reaches its own past.

travel infinitely across the **KS** regions and escape to one of the asymptotically flat regions in $r = \infty$, end in the ring singularity or even pass through one of the inner disks (one of the infinite disk in the middle of the singular rings) and cross to one of the \mathbb{R}^3_- copy of the spacetime. As we can see, the geodesic behavior in the whole spacetime is very complicated even if we restrict the movement to the z -axis. But as we will see in the next chapters, we are going to develop a method that allows us to describe all the complicate geodesic trajectories in one simple and 2D phase space where all possible geodesics will be displayed.

4.3 CAUSALITY VIOLATIONS

We have seen that in the region \mathbb{R}^3_- the value of the coordinate r is bounded in the interval $[-\infty, 0]$. We are going to see that this lead to causality violations. This causality violations are closed causal curves that can correspond to physical observers (timelike curves with $u^\alpha u_\alpha < 0$, where u^α is the tangent vector), which lead to time travel as the curve reach his own past for finite value of the proper time. This is easier to show in **BL** coordinates. Let us consider a timelike curve γ consisting a circle in the equatorial plane outside the singular ring in the space \mathbb{R}^3_- . This curve is defined as

$$\gamma \equiv \{\bar{t} = \text{const.}, \theta = \frac{\pi}{2}, 0 \leq \bar{\phi} \leq 2\pi, r < 0\}. \quad (124)$$

This curve can be the curve of an observer which stats in \mathbb{R}^3_+ , crosses the two horizons, pass through the inner disk and goes around the equatorial plane just outside the singular ring. The norm of the tangent vector is

$$\begin{aligned} u^\alpha u_\alpha &= \frac{1}{r^2} \left((r^2 + a^2)^2 - a^2(r^2 + a^2 - 2Mr) \right) \\ &= \frac{1}{r^2} (r^4 + r^2a^2 + 2Mra^2) = r^2 + a^2 + \frac{2Ma^2}{r} \end{aligned}$$

If we set $|r| \ll a, M$ (which we can do because the ring singularity is at $r = 0$) we will have that $r^2 + a^2 + \frac{2Ma^2}{r} < 0$ and the curve is a timelike curve that correspond to a physical observer. As the curve is a closed curve because is a ring, the curve reach itself in its own past. In any case, this is not a physical problem, as the space \mathbb{R}^3_- is beyond the even horizon and then cannot be observed (at least as long as we do not fall inside the black hole).

5

AXIS OF SYMMETRY

As we now fully understand how the **KS** patches are assembled in order to construct the whole **MAE** of the Kerr spacetime and we have removed the coordinate singularity of the inner disk by identify the two disk between the two copies of \mathbb{R}^3 we are ready to analyze the geodesic flow in the Kerr spacetime. the geodesic behavior is really complicated in general and, with the exception of the cases that we will develop, more complicated in **KS** coordinates. the geodesic flow is well known outside the outer horizon and is commonly analyzed in **BL** coordinates, but in this coordinate system, as we already know, the geodesic equations cannot be extended over the horizons and therefore the knowledge of the complete behavior is incomplete or discontinuous. This is the advantage of the **KS** coordinates, as they are continuous and regular across the horizons we can analyze without discontinuity problems the whole geodesic flow across the manifold. Indeed, there exist regions of the **MAE** that are not well described by the **BL** coordinates and the geodesic flow in this regions remain unknown or poorly-analyzed. We will start with a simple but complete case of the geodesic flow: the symmetry axis.

5.1 HAMILTONIAN EQUATIONS OF THE GEODESICS

As we discussed in the previous chapter, the geodesic flow for the z -axis in each copy of the basic **KS** patches is formed by two disjoint copies of \mathbb{R} namely \mathcal{Z}_1 and \mathcal{Z}_2 . the definition of each copy (outwards “space”) is

$$\mathcal{Z}_1 \equiv \mathbb{R}_+|_{z>0} \cup \mathbb{R}_-|_{z<0} \quad (125)$$

$$\mathcal{Z}_2 \equiv \mathbb{R}_+|_{z<0} \cup \mathbb{R}_-|_{z>0} \quad (126)$$

the function $r(x, y, z)$ in each copy is defined as (by the use of eq. (112)) is

$$r(0, 0, z) = \lambda z \quad (127)$$

where $\lambda = +1$ for \mathcal{Z}_1 and $\lambda = -1$ for \mathcal{Z}_2 .

In this section, we define the spacetimes on the z -axis as the pair (\mathcal{M}, g) where $\mathcal{M} = \mathcal{Z}_i$ ($i = 1, 2$) and the Kerr metric g in **KS** coordinates restricted to the hypersurface of the z -axis is written as

$$g = \eta + \lambda h K \otimes K = -dt^2 + dz^2 + \lambda \frac{2Mz}{a^2 + z^2} (-\sigma dt + \lambda dz) \otimes (-\sigma dt + \lambda dz) \quad (128)$$

where $\sigma = \pm 1$ indicates in which **KS** patch we are, $h = \frac{2Mz}{a^2 + z^2}$ and $K = (-\sigma dt + \lambda dz)$. We will refer to M indistinctly if $M = \mathcal{Z}_1$ or \mathcal{Z}_2 as all the calculations are dependent of the sign of λ , which tell us in which z -axis we are.

Theorem 6. *The geodesic equations for the Kerr metric restricted to the axis of symmetry in KS coordinates are the solution of*

$$E = (1 - hK_z) \frac{dt}{ds} + h\sigma K_z \frac{dz}{ds}, \quad (129)$$

and the Hamilton equations that are described by the Hamiltonian

$$\hat{H} = \frac{1}{2}\hat{p}_z^2 - \frac{\lambda\mu M z}{a^2 + z^2} \quad (130)$$

where $E = g(\partial_t, u)$ (u is the tangent vector to the geodesic) is a first integral of the system, $H = \frac{1}{2}(E^2 - \mu)$, $\mu = 0$ for null geodesics, $\mu = 1$ for timelike geodesics and s is the affine parameter.

Proof. In any spacetime affinely parametrized geodesics are the solutions of the Hamilton equations of the Hamiltonian

$$H = \frac{1}{2}(g^{-1})^{\alpha\beta} p_\alpha p_\beta \quad (131)$$

defined on the cotangent bundle of \mathcal{M} . The Hamilton equations fix $\mathbf{p} = g(u, \cdot)$ where u is the tangent vector to the geodesic. Using the explicit expression (128) for the metric, this Hamiltonian takes the form

$$H = \frac{1}{2} \left(\eta^{\alpha\beta} p_\alpha p_\beta - h(K^\alpha p_\alpha)^2 \right). \quad (132)$$

Given that ∂_t is a Killing vector, the quantity $E := -\mathbf{p}(\partial_t)$ is conserved along geodesics. Note also that, with this definition,

$$K^\alpha p_\alpha = -\sigma E + K_z p_z, \quad (133)$$

where we have written $\mathbf{p} = \{\hat{p}, p_z\}$.

the Hamiltonian itself is a conserved quantity with the value of $H = -\frac{1}{2}\mu$ where $\mu = 0, \pm 1$ depending on whether the geodesic is timelike ($\mu = 1$), spacelike ($\mu = -1$) or null ($\mu = 0$). Inserting (133) and the conserved quantity E into (132) the following Hamiltonian arises naturally

$$H' := H + \frac{1}{2}E^2 = \frac{1}{2} \left(p_z^2 - h(K_z p_z - \sigma E)^2 \right), \quad (134)$$

which is now defined on the cotangent bundle of \mathbb{R} .

The interest of this Hamiltonian lies in the fact (easy to check) that if a curve $(t(s), z(s))$ is a geodesic in (\mathcal{M}, g) with tangent vector u satisfying $g(u, u) = -\mu$ and conserved quantity $\mathbf{p}(\partial_t) = -E$, then $\{z(s)\}$ is the projection to the base space \mathbb{R} of a solution of the Hamilton equations of (134) satisfying

$$H' = \epsilon := \frac{1}{2} (E^2 - \mu) \quad (135)$$

along the curve and $t(s)$ satisfies the ODE

$$(1 - hK_z) \frac{dt}{ds} + h\sigma K_z \frac{dz}{ds} = E, \quad (136)$$

which is simply the explicit form for $g(u, \partial_t) = -E$ in the **KS** coordinates $\{t, z\}$.

The Hamiltonian of eq. (134) reads once K_z and h are replaced for their expressions

$$H' = \frac{1}{2} \left(p_z^2 - \frac{\lambda(2Mz)}{a^2 + z^2} (\lambda p_z - \sigma E)^2 \right). \quad (137)$$

The Hamilton equations for this Hamiltonian are

$$\frac{M(z^2 - a^2)(-\lambda p_z + E\sigma)^2}{(a^2 + z^2)^2} + p'_z = 0, \quad (138)$$

$$\frac{1}{2} \left(2p_z - \frac{4Mz(-\lambda p_z - E\sigma)}{a^2 + z^2} \right) - z' = 0. \quad (139)$$

We can now resolve the second equation for p_z obtaining

$$p_z = \frac{a^2 z' - 2EM\sigma z + z^2 z'}{a^2 - 2\lambda Mz + z^2}. \quad (140)$$

By the use of this relation we can rewrite the conserved quantity that the Hamiltonian describes as a function of $\{z, z'\}$, this relation reads

$$\frac{1}{2} (E^2 - \mu) = \frac{(a^2 + z^2) z'^2 - \lambda 2E^2 Mz}{2(a^2 + z(-\lambda 2M + z))}. \quad (141)$$

Solving for z'^2 we get

$$z'^2 = E^2 - \mu + \frac{2\lambda\mu Mz}{a^2 + z^2}. \quad (142)$$

We can rearrange this equation to obtain

$$\frac{1}{2}(E^2 - \mu) = \frac{1}{2}z'^2 - \frac{\lambda\mu Mz}{a^2 + z^2}. \quad (143)$$

If we name $\epsilon \equiv \frac{1}{2}(E^2 - \mu)$ to be the Newtonian energy (the total energy minus the rest mass μ) we realize that this equation has the form

$$\epsilon = \frac{1}{2}z'^2 - \frac{\lambda\mu Mz}{a^2 + z^2} = T + V(z), \quad (144)$$

where $t = \frac{1}{2}z'^2$ is the kinetic energy and $V(z) = -\frac{\lambda\mu Mz}{a^2 + z^2}$ is the potential. The solutions of this equation are equivalent to the solutions of the Hamiltonian

$$\hat{H} = \frac{1}{2}\hat{p}_z^2 - \frac{\lambda\mu Mz}{a^2 + z^2}, \quad (145)$$

where $H = \epsilon = \frac{1}{2}(E^2 - \mu)$. This statement lays on the fact that the for a two dimensional Hamiltonian (one dimension for the spatial coordinate and other for the conjugate momenta), the system is always integrable because the Hamiltonian itself is a first integral. This proves the theorem. \blacksquare

Remark 7. It is interesting that the Hamiltonian \hat{H} is independent of σ , so that we will be able to describe the geodesics in (\mathcal{M}, g) both for the case when

\mathbf{K} is future directed (plus sign) or past directed (negative sign). Moreover, the Hamiltonian \hat{H} is a standard Hamiltonian in Newtonian mechanics for a point particle in a potential. This is a substantial simplification over the original problem of solving the geodesic equations in the symmetry axis of the Kerr spacetime, because we can exploit all the information known for trajectories of point particles in Newtonian mechanics under the influence of a potential of the form

$$V(z) = \frac{\lambda\mu M z}{a^2 + z^2} \quad (146)$$

The main consequence of theorem 6 is, thus, that the spatial part of all geodesics in the symmetry axis of the Kerr spacetime turns out to be equivalent to the (much simpler) problem of solving the trajectory of a Newtonian point particle in the potential (eq. (146)). Once the spatial part of the geodesics is solved, the temporal part is dealt with by solving equation (129).

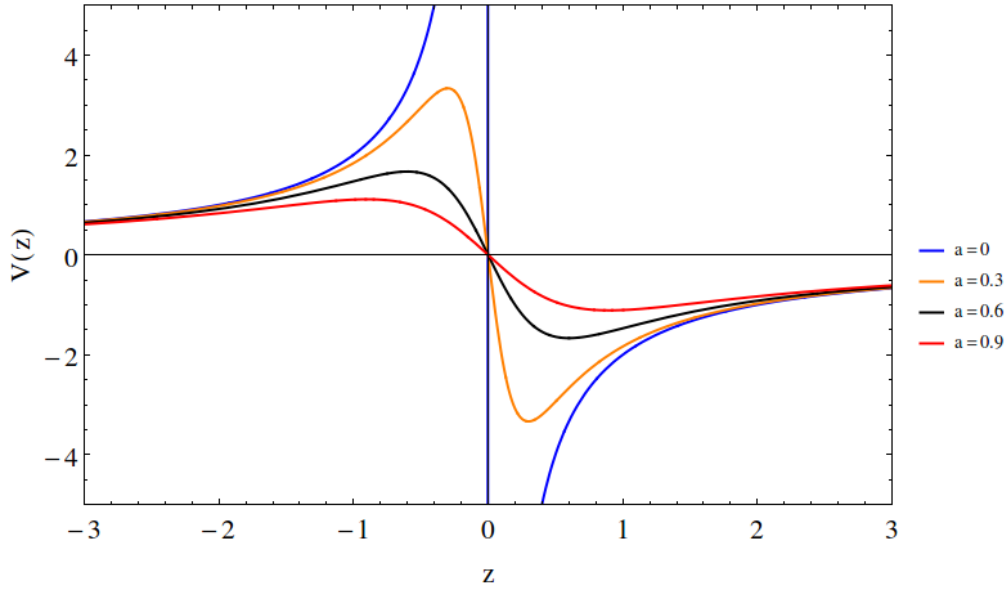


Figure 17: The potential $V(z)$ is displayed for various values of the parameter a . Note that the extremal points become lower as the parameter increases. For simplicity $M = 1$ and $\lambda = 1$ has been chosen. The potential for $\lambda = -1$ is the specular image of this representation using the z -axis as the axis of reflection.

5.2 VARIATION RANGES AND CAUSAL STRUCTURE

Since we are interested in causal and future directed geodesics we need to find the restrictions on the initial data which guarantee this. The following Proposition summarizes the results above and addresses the issue of future directed initial data for both choices of σ .

Before we can start to study the variation ranges, we are going to define a new coordinate in which the metric does not depend if the spacetime is $(\mathcal{M}, g|_{\lambda=1}) = (\mathcal{Z}_1, g|_{\lambda=2})$ or $(\mathcal{M}, g_1) = (\mathcal{Z}_2, g_2)$. Defining

$$\bar{z} = \lambda z \quad (147)$$

the metrics $g|_{\lambda=1}$ and $g|_{\lambda=2}$ become

$$ds^2 = \eta + \lambda h K \otimes K = -dt^2 + dz^2 + \frac{2M\bar{z}}{a^2 + \bar{z}^2}(-\sigma dt + d\bar{z}) \otimes (-\sigma dt + d\bar{z}) \quad (148)$$

The equations of the theorem 6 become

$$E = (1 - h) \frac{dt}{ds} + h\sigma \frac{d\bar{z}}{ds}, \quad (149)$$

and the Hamiltonian is transformed to

$$\hat{H} = \frac{1}{2} \hat{p}_{\bar{z}}^2 - \frac{\mu M \bar{z}}{a^2 + \bar{z}^2} \quad (150)$$

This can be done because the manifolds \mathcal{Z}_1 and Z_2 are diffeomorphic under the transformation $z \rightarrow -z$. By the use of this result, we can analyze more easily the variation ranges which are described in the following proposition.

Proposition 8. *If the time orientation of (\mathcal{M}, g) is chosen so that the null vector $\partial_t + \sigma \partial_{\bar{z}}$ is future directed, then a geodesic with $\mu = 0, 1$ starting at a point (t_0, \bar{z}_0) is future causal if and only if $\dot{\bar{z}}_0$ satisfies (with $h_0 := h(|\bar{z}_0|)$)*

$$\begin{aligned} \text{if } h_0 > 1, \quad & \begin{cases} \sigma \dot{\bar{z}}_0 \in [a_0, \infty) \\ E = \pm \sqrt{\dot{\bar{z}}_0^2 - a_0^2} \end{cases} & \text{if } h_0 < 1, \quad & \begin{cases} \sigma E \in [a_0, \infty) \\ \dot{\bar{z}}_0 = \pm \sqrt{E^2 - a_0^2} \end{cases} \\ \text{if } h_0 = 1, \quad & \begin{cases} \sigma \dot{\bar{z}}_0 \in [0, \infty) \\ E = \sigma \dot{\bar{z}}_0 \end{cases} & \text{with } \dot{\bar{z}}_0 = 0 \implies \mu = 0 \end{aligned}$$

where $a_0(\bar{z}_0, \mu) := \sqrt{|1 - h(\bar{z}_0)|} \mu \geq 0$.

Proof. For the statements on the initial data, let $(t_0, \bar{z}_0 \neq 0)$ be the initial point of the geodesic and $u_0 = (t_0, \dot{\bar{z}}_0)$ the initial velocity, normalized to satisfy $g(u_0, u_0) = -\mu$ ($\mu = 0, 1$) and assumed to be future directed. Recall that the Kerr-Schild vector is $K^\alpha = (\sigma, \cdot)$. the choice of time orientation means that σK^α is future directed. thus, u_0 being future directed is equivalent to $g(u_0, \sigma K|_{s=0}) < 0$ or $u_0 = b\sigma K|_{s=0}$, with $b \geq 0$. to compute $g(u_0, \sigma K|_{s=0})$ observe that $g(\sigma K, \cdot) = -dt + \sigma d\bar{z}$ which implies

$$g(u_0, \sigma K|_{s=0}) = \sigma \dot{\bar{z}}_0 - t_0. \quad (151)$$

On the other hand, the condition $u = b\sigma K|_{s=0}$ ($b \geq 0$) is $(t_0 = b, \dot{\bar{z}}_0 = b\sigma)$ or equivalently $(t_0 = \sigma \dot{\bar{z}}_0 \geq 0)$. the eqs. (136) and (143) evaluated at $s = 0$ read

$$E^2 = \dot{\bar{z}}_0^2 + \text{sign}(1 - h_0)a_0^2, \quad (152)$$

$$E = (1 - h_0)t_0 + h_0\sigma \dot{\bar{z}}_0, \quad (153)$$

where $\text{sign}(1 - h_0)$ takes the values 1, 0, -1 depending on whether $h_0 < 1$, $h_0 = 1$ or $h_0 > 1$ respectively and a_0 is as defined in the statement of the theorem. At points $h_0 \neq 1$, eqs. (152) and (153) imply $g(u_0, u_0) = -\mu$. However, when $h_0 = 1$, eq. (152) is a trivial consequence of eq. (153) and $g(u_0, u_0) = -\mu$ must be imposed additionally. We compute (with $h_0 = 1$)

$$\begin{aligned} -\mu &= g(u_0, u_0) = \eta(u_0, u_0) + h_0 (\mathbf{K}|_{s=0}(u_0))^2 = \\ &= -t_0^2 + \dot{z}_0^2 + g(\sigma K|_{s=0}, u_0)^2 = \\ &= 2\sigma \dot{z}_0 (\sigma \dot{z}_0 - t_0), \end{aligned} \quad (154)$$

where (151) has been used in the last equality.

We can now find the most general u_0 satisfying all these restrictions. the analysis depends on whether $h_0 > 1$, $h_0 < 1$ or $h_0 = 1$. We start with $h_0 \neq 1$. Because of (153), the initial data t_0 can be substituted by the value of E . Moreover,

$$\begin{aligned} (1 - h_0)^2 g(u_0, \sigma K|_{s=0}) &= (1 - h_0) ((+h_0 - 1)t_0 + (1 - h_0)\sigma \dot{z}_0) \\ &= (h_0 - 1)(E - \sigma \dot{z}_0), \end{aligned}$$

where (153) has been again inserted in the last equality. thus, the statement $g(u_0, \sigma K|_{s=0}) < 0$ or $u_0 = b\sigma K|_{s=0}$ with $b \geq 0$ is equivalent to

$$(h_0 - 1)(E - \sigma \dot{z}_0) < 0 \quad \text{or} \quad E = \sigma \dot{z}_0 \geq 0,$$

the second inequality being a consequence of $t_0 = \sigma \dot{z}_0 \geq 0$ and (153). Assume now $h_0 > 1$. the conditions to be imposed are $\{E < \sigma \dot{z}_0 \text{ or } E = \sigma \dot{z}_0 \geq 0\}$, together with $E^2 = \dot{z}_0^2 - a_0^2$ (from equation (152)). the locus of this quadratic equation is a hyperbola with two branches (degenerating to two straight lines when $a_0 = 0$) and with asymptotes $E = \pm \dot{z}_0$. the condition $\{E < \sigma \dot{z}_0 \text{ or } E = \sigma \dot{z}_0 \geq 0\}$ selects precisely the branch satisfying $\sigma \dot{z}_0 \geq a_0$, as claimed in the Proposition. the case $h_0 < 1$ is analogous: the conditions are now $\{E > \sigma \dot{z}_0 \text{ or } E = \sigma \dot{z}_0 \geq 0\}$ together with $E^2 = \dot{z}_0^2 + a_0^2$. the solution to these inequalities is the branch of the hyperbola satisfying $\sigma E \geq a_0$.

For the case $h_0 = 1$, equation (154) reads

$$2\sigma \dot{z}_0 (\sigma \dot{z}_0 - t_0) = -\mu \leq 0. \quad (155)$$

thus, the condition $\{\sigma \dot{z}_0 - t_0 < 0 \text{ or } t_0 = \sigma \dot{z}_0 \geq 0\}$ is equivalent to $\sigma \dot{z}_0 \geq 0$ and zero only if $\mu = 0$. this is because, when $\sigma \dot{z}_0 > 0$, equation (155) can be solved uniquely for t_0 with the solution satisfying $\sigma \dot{z}_0 - t_0 \leq 0$, that is, either $\sigma \dot{z}_0 - t_0 < 0$ or $t_0 = \sigma \dot{z}_0 > 0$. When $\sigma \dot{z}_0 = 0$ then $\mu = 0$ and $t_0 \geq 0$ is arbitrary, so again we satisfy $\{\sigma \dot{z}_0 - t_0 < 0 \text{ or } t_0 = \sigma \dot{z}_0 \geq 0\}$. Finally, the statement $E = \sigma \dot{z}_0$ when $h_0 = 1$ follows directly from (153). ■

Remark 9. Note that when $\mu = 0$ we have $a_0 \equiv 0$ and this Proposition admits the initial data $\dot{r}_0 = 0, E = 0$ irrespectively of the value of h_0 . When $h_0 \neq 1$, this boundary case corresponds to the situation when the initial tangent four-vector vanishes, and hence the geodesic is a trivial curve. This is consistent with the fact that the zero vector is null and future directed. Admitting trivial curves as null future directed geodesics has the advantage that allows one to treat at once the cases $\mu = 0$ and $\mu = 1$.

Corollary 10. *The variation ranges for ϵ are*

$$\begin{cases} \epsilon \in [-\frac{\mu}{2}, \infty) & \text{if } h_0 \geq 1 \\ \epsilon \in [\frac{a_0^2 - \mu}{2}, \infty) & \text{if } h_0 < 1 \end{cases} \quad (156)$$

independently of the sign of σ and of the function $h(\vec{x})$ in the Kerr-Schild metric.

Proof. Immediate from the ranges of variation of E in Proposition 8 and the relation $\epsilon = \frac{1}{2}(E^2 - \mu)$. \blacksquare

This information will be very useful because this will allow us to distinguish and categorize the different curves that will appear in the phase space of the spatial part of the geodesic movement. In the future phase space we will deal with curves that cross multiple time the different horizons and that are traveling through the PC diagram of the z -axis of the Kerr spacetime that is displayed in fig. 18, changing from **KS** patch over and over.

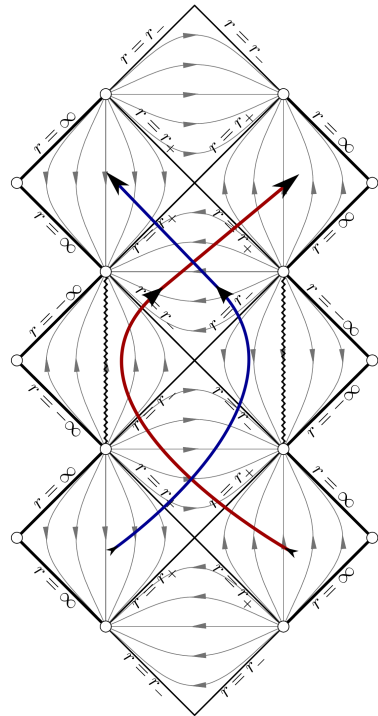


Figure 18: PC diagram of the Kerr spacetime along the axis of symmetry for simplicity.

The red path represents a geodesic that crosses $r = r_+$ twice and changes from the **KS** patch in which $\sigma = 1$ to the patch in which $\sigma = -1$. The blue curve is analogous to the red one but for a geodesic that starts in the isometric region of the left. These isometric regions are disconnected as are remarked in the text. Remember that for the z -axis the coordinate $r = \lambda z = \bar{z}$.

By the use of the proposition 8 we can know that a geodesic that start in the **KS** patch with $\sigma = 1$ (see fig. 14 on page 40 to see the **KS** patches) that crosses the even horizon at $\bar{z} = r_+$ for the first time, cannot cross the same even

horizon at $\bar{z} = r_+$ (in the same **KS** patch) because once crossed this point with $\sigma = -1$ then $\dot{r} = \dot{\bar{z}} < 0$ and therefore as $-\infty < r_- < r_+ < \infty$ the geodesic cannot go back to the asymptotically flat region of the **KS** patch where it stated. In the other hand the same geodesic can continue its journey through $\bar{z} = r_-$ and once crossed this point change to the **KS** patch with $\sigma = +1$ and then cross $\bar{z} = r_-$ again (moving upwards in the **PC** diagram of fig. 18). Once $\bar{z} = r_-$ is crossed in the patch with $\sigma = +1$ the variation ranges in this region imply $\dot{r} = \dot{\bar{z}} > 0$ and therefore the geodesic cannot go back to $\bar{z} = r_-$ but it can cross the even horizon at $\bar{z} = r_+$ in the **KS** patch with $\sigma = +1$ and continue to the asymptotically flat region of the **KS** patch with $\sigma = +1$. This behavior can be summarized in the fact that if a geodesic cross twice $\bar{z} = r_+$ its traveling upwards in the **PC** diagram and therefore changing from one **KS** patch to another. This can be done as many times as needed and the geodesic journey can stop in any of the infinite asymptotically flat regions.

Notice that there is no causal geodesic starting from a left-most quadrant which, after crossing the null hypersurface $\bar{z} = r_+$ then goes across the portion of the null hypersurface at $\bar{z} = r_-$ lying at the left of the diagram (and similarly for geodesics starting at a right-most quadrant). The reason is that the Killing 1-form $dt := g(\partial_t, \cdot)$ (defined on a single **KS** patch) is integrable with orthogonal hypersurfaces foliating the region $r_- < z < r_+$ with timelike leaves. Let us label these leaves by T . As a consequence we have $dt = GdT$ on $r_- < z < r_+$ where G is a smooth function. Consider the conserved energy for the geodesic, i.e. $\langle \partial_t, u \rangle = -E$ where u is the tangent vector. In the region between r_- and r_+ , in order for the geodesic to enter from the left portion of the null hypersurface $\bar{z} = r_+$ and leave across the left portion of the hypersurface $\bar{z} = r_-$, the geodesic must become somewhere tangent to a hypersurface $T = \text{const}$. At this point we have $-E = dt(u) = GdT(u) = 0$. But $E = 0$ is impossible for a geodesic starting on the left-most region where ∂_t is timelike. A similar argument applies to geodesics starting at the right-most quadrant.

5.3 PHASE SPACE AND DYNAMIC EQUATIONS

Now that we know how to distinguish geodesics in the spacetime and we understand how the causal structure of the spacetime works and which kind of flows can be expected, we are ready to obtain the dynamic equations that describe the phase space of the spatial part of the geodesics in the axis of symmetry of the Kerr metric. From theorem 6 we have that the spatial part of the geodesic flow is carried by the Hamiltonian

$$\hat{H} = T + V(z) = \frac{1}{2}\hat{p}_z^2 - \frac{\lambda\mu Mz}{a^2 + z^2}. \quad (157)$$

where $H = \epsilon = \frac{1}{2}(E^2 - \mu)$. The Hamilton equations for this Hamiltonian are

$$z'(s) = p_z \quad (158)$$

$$p'_z(s) = -\lambda((M(-a^2 + z^2))/(a^2 + z^2)^2) \quad (159)$$

5.3.1 Null geodesics

If we set $\mu = 0$ (null geodesics), the dynamic equations of eqs. (158) and (159) take the form

$$z'(s) = p_z \quad (160)$$

$$p'_z(s) = 0 \quad (161)$$

and therefore the solution of the system is

$$z(s) = z_0 + p_{z0}s \quad (162)$$

$$p_z(s) = p_{z0} \quad (163)$$

where $z(0) = z_0$ and $p_z(0) = p_{z0}$. Hence, the null geodesic along the symmetry axis of the Kerr spacetime move with constant velocity unaffected by any gravitational force. This is quite interesting because this geodesics can travel through the inner disk ($z = 0$) and go from one copy of \mathbb{R}_\pm to another at constant velocity p_{z0} . For the null geodesics there is no fixed points and no excluded regions. In the phase portrait of fig. 19 it can be appreciated that for $p_z = z' > 0$ all geodesics are in the **KS** patch with $\sigma = 1$ because between the horizons $r_- < \lambda z < r_+$ only particles with $z' > 0$ are allowed and for $p_z = z' < 0$ all geodesics are in the **KS** patch with $\sigma = -1$ because between the horizons $r_- < \lambda z < r_+$ only particles with $z' > 0$ are allowed.

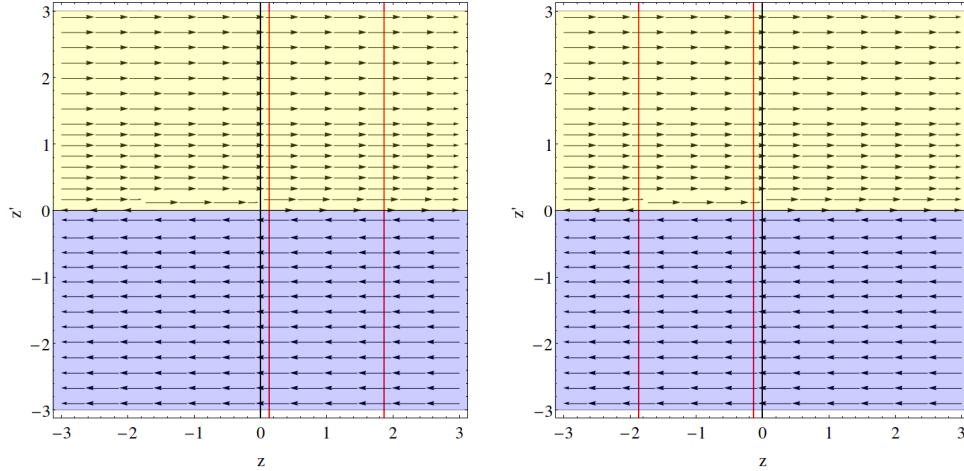


Figure 19: Phase portraits for the null geodesic in the axes of symmetry. The picture on the left shows the phase space for \mathcal{Z}_1 while the picture on the right shows the phase space for \mathcal{Z}_2 . The black thick lines represent the axis ($\{z = 0, z' = 0\}$), the red thick lines represent the horizons at $r = r_\pm$ (notice that $0 < r_- < r_+$ for \mathcal{Z}_1 as $r = z$ and $0 > r_- > r_+ >$ for \mathcal{Z}_2 as $r = -z$). The yellow region indicates the region with $\sigma = 1$ and the blue region indicates the region with $\sigma = -1$

5.3.2 Timelike geodesics

Despite the behavior for null geodesics is quite simple, the behavior for timelike geodesics is not simple at all. In fact, there are now excluded regions provided by corollary 10 that cannot be accessible to the flow of the timelike geodesics in the phase space. The shape of this excluded regions change with the value of the parameter a (as the Kerr black hole spins faster) and must be studied independently to fully understand the dynamic system and the phase portrait that will be displayed along the analysis of the timelike geodesics.

5.3.2.1 Excluded regions

As was noticed before, the allowed variation range is traduced into the existence of excluded regions in the phase space. The existence of this excluded regions is very important because provided the necessary topology to the phase space in order to describe all the geodesic flow for timelike particles in the **MAE** of the symmetry axis of the Kerr spacetime. If the phase space would have trivial homotopy class it could be impossible to “project” the geodesic flow across the **MAE** of the symmetry axis of the Kerr spacetime in one bi-dimensional space phase because all the trajectories that cross the horizons and change between the infinite **KS** patches could not be displayed.

By the use of corollary 10 we find that the expression for the excluded regions of timelike particles are written as

$$\frac{1}{2}\hat{p}_z^2 - \frac{\lambda M z}{a^2 + z^2} < \frac{1}{2} \quad (164)$$

As we see in fig. 20 the excluded regions are like “bubbles” that decreases size when $a \rightarrow M$, vanishing when $a = M$ (extreme Kerr spacetime). Also, the “bubbles” are attached to the axis $z = 0$ for $a = 0$ and they detach from this axis while $0 < a < M$ as they travel along the phase space. The excluded regions are always limited for the horizons at $\bar{z} = r_{\pm}$, as the origin of this excluded regions are the limitations into the initial parameters that the time orientation provides. Also, because in \mathbb{R}_- there is no horizons, there are not excluded regions in this region of \mathcal{Z}_1 and \mathcal{Z}_2 , which corresponds to $z < 0$ in \mathcal{Z}_1 and $z > 0$ in \mathcal{Z}_2 . The boundary of the excluded regions belongs to the phase space because the limit case $\frac{1}{2}\hat{p}_z^2 - \frac{\lambda M z}{a^2 + z^2} = \frac{1}{2}$ is a physical trajectory for the geodesic motion and is included in the phase space. Notice also that proposition 8 excludes the possibility of having a geodesic in the point $\bar{z} = a$ the case where $a = M$ (in which there are no excluded regions and the horizons collapse in one unique surface at $\bar{z} = a$) because this is only allowed for null geodesics $\mu = 0$. The reason is that for $a = M$ the horizons are at $\bar{z} = 0$ and because this surfaces are null hypersurfaces, only null tangent vectors can move remain in them, and therefore, timelike particles are not allowed to remain in this point (unless as we will see it is a stable point) despite there are no apparent excluded regions.

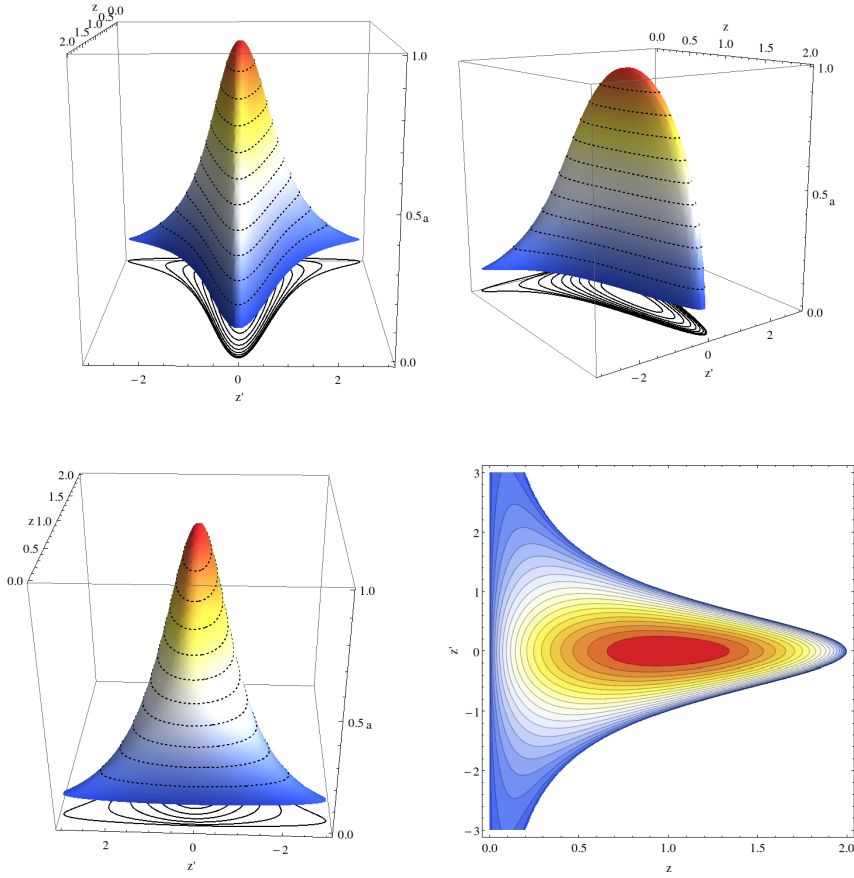


Figure 20: Excluded regions for timelike geodesics and their dependence with the value of the parameter a . The vertical axis represents the value of a (as also the coloring). The other axes represent the values of z and z' . The bottom right picture shows the projection onto the $\{z, z'\}$ plane, which is the phase portrait (the colors serve to help the visualization of the variation with the parameter a). As we can see in the images, the "area" of the excluded regions decreases when the parameter a increases and the excluded region vanishes for $a = M$. Also, the excluded regions move across the $\{z, z'\}$ plane as the parameter a increases. For simplicity $M = 1$ and $\lambda = 1$ is chosen.

5.3.2.2 Phase space

If we set $\mu = 1$ (timelike geodesics), the dynamic equations of eqs. (158) and (159) take the form

$$z'(s) = p_z, \quad (165)$$

$$p'_z(s) = -\lambda \frac{M(z^2 - a^2)}{(a^2 + z^2)^2}. \quad (166)$$

Remember that because the Hamiltonian itself is a first integral with value $\epsilon = \frac{1}{2}(E^2 - 1) = \frac{1}{2}\hat{p}_z^2 - \frac{\lambda\mu M z}{a^2 + z^2}$. The dynamic system for timelike geodesic present

very interesting features that can be observed in fig. 21. The fixed points of the system are given by the equations

$$z'(s) = 0 \implies p_z = 0, \quad (167)$$

$$p'_z(s) = 0 \implies -\lambda \frac{M(z^2 - a^2)}{(a^2 + z^2)^2} = 0. \quad (168)$$

The solution of this system is

$$z_{\pm} = \pm a \quad \text{and} \quad p_z = 0 \quad (169)$$

The nature of the fixed points is obtained linearising the system around them. The linearization is given by

$$\begin{pmatrix} \delta z'(s) \\ \delta p'_z(s) \end{pmatrix} = J|_{z=z_{\pm}, p_z=0} \begin{pmatrix} \delta z(s) \\ \delta p_z(s) \end{pmatrix}. \quad (170)$$

where the Jacobian matrix (J) is given by

$$J = \begin{pmatrix} \frac{\partial z'(z, p_z)}{\partial z} & \frac{\partial z'(z, p_z)}{\partial p_z} \\ \frac{\partial p'_z(z, p_z)}{\partial z} & \frac{\partial p'_z(z, p_z)}{\partial p_z} \end{pmatrix} = \begin{pmatrix} 0 & 1 \\ -\frac{M\gamma\lambda}{2a^3} & 0 \end{pmatrix}, \quad (171)$$

where the sign $\gamma = \pm 1$ corresponds to $z = \gamma a$. The eigenvalues of the Jacobian matrix are

$$\lambda_1 = -\frac{\sqrt{-\lambda\gamma M}}{\sqrt{2a^3}}, \quad (172)$$

$$\lambda_2 = \frac{\sqrt{-\lambda\gamma M}}{\sqrt{2a^3}}. \quad (173)$$

The eigenvalues are real iff $\lambda\gamma = -1$, which corresponds to $z = -a$ in \mathcal{Z}_1 and $z = a$ in \mathcal{Z}_2 . When the eigenvalues are real, they have also opposite signs, and therefore $z = -a$ in \mathcal{Z}_1 and $z = a$ in \mathcal{Z}_2 are unstable saddle points. When $\lambda\gamma = +1$ the eigenvalues are purely imaginary and corresponds to $z = a$ in \mathcal{Z}_1 and $z = -a$ in \mathcal{Z}_2 . As the eigenvalues in this case are complex conjugate they corresponds to a stable point that happens to be a center. Notice that this eigenvalues are always inside the excluded region and therefore no timelike geodesic can rest in the stable center point. The only movement allowed is oscillating around the stable point outside the excluded regions (where the limit case $-\frac{1}{2} = \frac{1}{2}\hat{p}_z^2 - \frac{\lambda\mu M z}{a^2 + z^2}$ is the boundary of the excluded region). In order to treat both spaces (\mathcal{Z}_1 and \mathcal{Z}_2) at once we will use the coordinate $\bar{z} = \lambda z$ when we discuss the different behaviors.

Is important to attend at the fact that the excluded regions are always in between the horizons and hence, the closed curves (green zones in fig. 21) are always crossing the horizons and as we noticed before, these curves are traveling upwards in the PC diagram changing from one KS patch to another as they cross $\bar{z} = r_+$ twice as was noticed and study in section 5.2. The closed curves in the diagram may seem strange at first because they correspond to the physical situation of having a particle that is oscillating around a point in the z -axis.

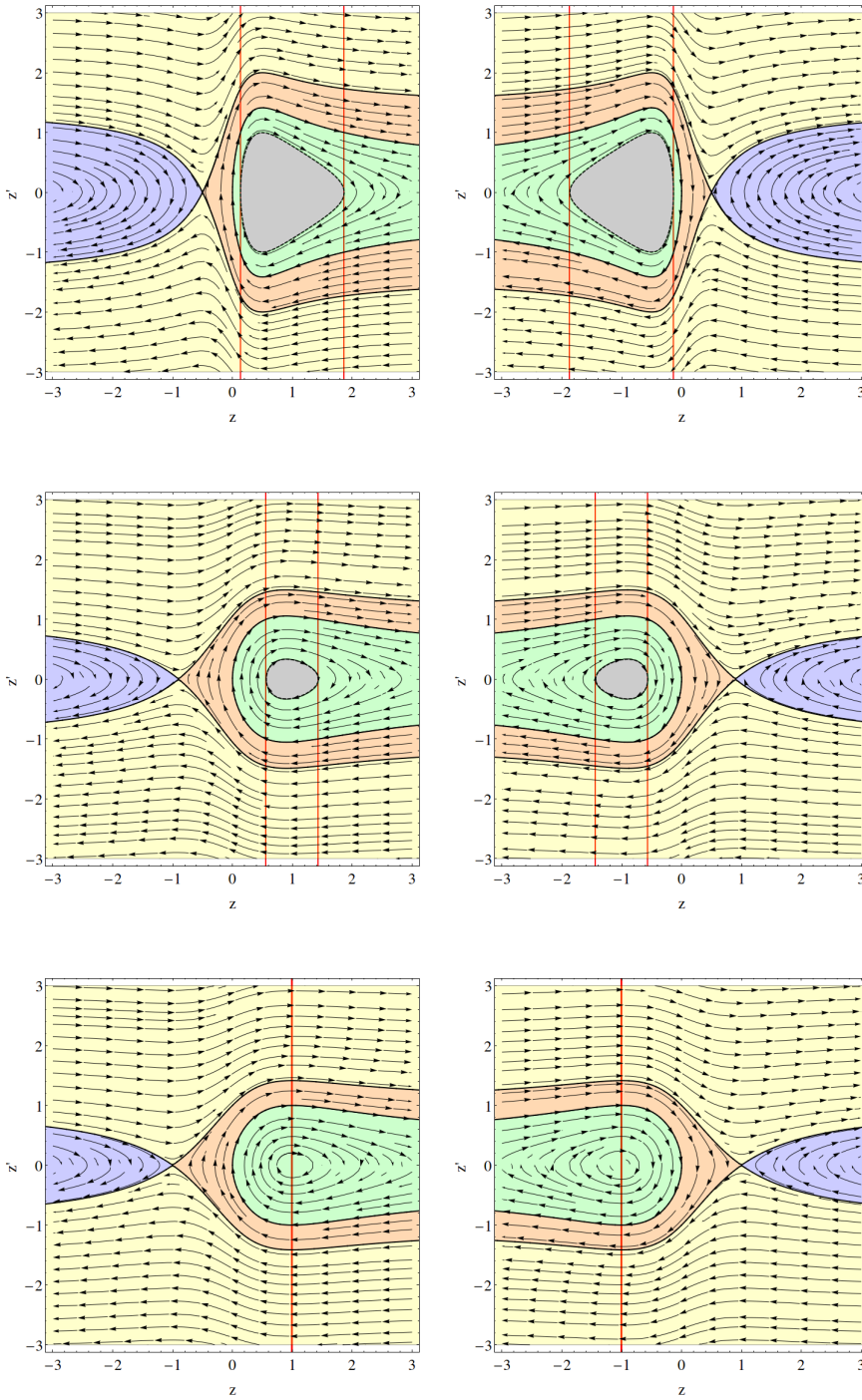


Figure 21: The phase spaces for timelike geodesic are displayed. The left column shows to the phase space for Z_1 and the right column for Z_2 . In each column the phase portraits for the values $a = \{0.8M, 0.9M, M\}$ are displayed (top to bottom). The red lines corresponds to the horizons at $\bar{z} = r_{\pm}$. The red region corresponds to the excluded region, the yellow region represent the curves in the phase space that connects $\bar{z} = \infty$ with $\bar{z} = -\infty$, the blue area represent the curves that start in $\bar{z} = -\infty$ and return to $\bar{z} = -\infty$, the orange zones represent the curves that start in $\bar{z} = \infty$ and end in $\bar{z} = \infty$. The closed curves are in the green area and the limit orbit is the black dashed line surrounding the excluded region. $M = 1$ is settled for simplicity.

But this particle is traveling between different "spaces" as it changes from [KS](#) patches and for a observer, the particle vanishes from his region when it crosses $\bar{z} =_r +$. A complete representation of the fixed points and the horizon structure for different values of a is displayed in fig. [22](#). In this figure one can see that the allowed amplitude of the oscillating movement is always greater than the distance to the horizons and therefore this kind of movement is always traveling upwards in the [PC](#) diagram. As we can see in the phase portraits of figs. [21](#) and [22](#) the region $\bar{z} < 0$ that corresponds on both cases to \mathbb{R}_- has some kind of repulsive behavior. Indeed, the critical points in this region are always unstable saddle points, that behaves "repelling" the geodesic flow. Consider for example a geodesic that start in $\bar{z}_0 = -\infty$ with $\dot{\bar{z}}'_0 > 0$. This geodesic will try to approach \mathbb{R}_+ but if the value of $\dot{\bar{z}}'_0$ is not enough, the geodesic will be repealed by the singular point in $\bar{z} = -a$ and will end in $\bar{z} = -\infty$ again. If the geodesic has enough energy (enough value of $\dot{\bar{z}}'_0$) it will defeat the repulsive behavior of the critical point at $\bar{z} = -a$ and it will end in \mathbb{R}_+ at $\bar{z} = \infty$. The minimum value of $\dot{\bar{z}}'_0$ that allows a geodesic to travel from \mathbb{R}_- to \mathbb{R}_+ is

$$p_{\bar{z}_{\text{critic}}}^2 - \frac{2M\bar{z}_0}{a^2 + \bar{z}_0^2} = \epsilon(p_{\bar{z}} = 0, \bar{z} = -a) \implies p_{\bar{z}_{\text{critic}}} = \dot{\bar{z}}'_{\text{critic}} = \pm \frac{\sqrt{M}(a + \bar{z}_0)}{\sqrt{a}\sqrt{a^2 + \bar{z}_0^2}} \quad (174)$$

where $\bar{z}_0 = \bar{z}(0)$. Note that $\epsilon(p_{\bar{z}} = 0, \bar{z} = -a) = \frac{M}{a}$ which is the fraction of "maximality" of the black hole (remember that the black hole is said to be extremal when $M^2 = a^2$). This can be visualize much more clearly in fig. [23](#) where we can easily realize that the geodesics with $\dot{\bar{z}}'_0 < \dot{\bar{z}}'_{\text{critic}}$ does not have enough energy to get over the potential barrier and only the geodesics with $|\dot{\bar{z}}'_0| \geq |\dot{\bar{z}}'_{\text{critic}}|$ can pass through. In the space \mathbb{R}_+ the situation is the same, i.e. only geodesics with $|\dot{\bar{z}}'_0| > |\dot{\bar{z}}'_{\text{critic}}|$ will reach \mathbb{R}_- . Geodesics with a lower value of $|\dot{\bar{z}}'_0|$ can oscillate around the critical point at $\bar{z} = a$ or reach a return point at end in $\bar{z} = \infty$. The geodesics that will reach a return point satisfies that

$$\epsilon(p_{\bar{z}} = 0, \bar{z} = -a) > \epsilon(p_{\bar{z}_0}, \bar{z}_0) \geq 0 \implies -|\dot{\bar{z}}'_{\text{critic}}| < p_{\bar{z}_0} = \dot{\bar{z}}'_0 \leq -\frac{\sqrt{2M\bar{z}_0}}{\sqrt{a^2 + \bar{z}_0^2}} \quad (175)$$

where $\bar{z}_0 = \bar{z}(0)$. The return point is given by

$$-\frac{2M\bar{z}_{\text{return}}}{a^2 + \bar{z}_{\text{return}}^2} = \epsilon(p_{\bar{z}_0}, \bar{z}_0) \implies \bar{z}_{\text{return}} = \frac{\sqrt{M^2 - a^2 \left(p_{\bar{z}_0}^2 - \frac{2M\bar{z}_0}{a^2 + \bar{z}_0^2} \right)^2} - M}{p_{\bar{z}_0}^2 - \frac{2M\bar{z}_0}{a^2 + \bar{z}_0^2}} \quad (176)$$

where $\frac{\sqrt{2M\bar{z}_0}}{\sqrt{a^2 + \bar{z}_0^2}} < |p_{\bar{z}_0}| < |\dot{\bar{z}}'_{\text{critic}}|$ and $\bar{z} > 0$. Therefore values of $|p_{\bar{z}_0}| < \frac{\sqrt{2M\bar{z}_0}}{\sqrt{a^2 + \bar{z}_0^2}}$ with $\bar{z} > 0$ correspond to geodesic that oscillate around $\bar{z} = a$. As we have commented before, this geodesic are traveling upwards in the [PC](#) diagram changing from one patch to another. The return points of the oscillating movement given

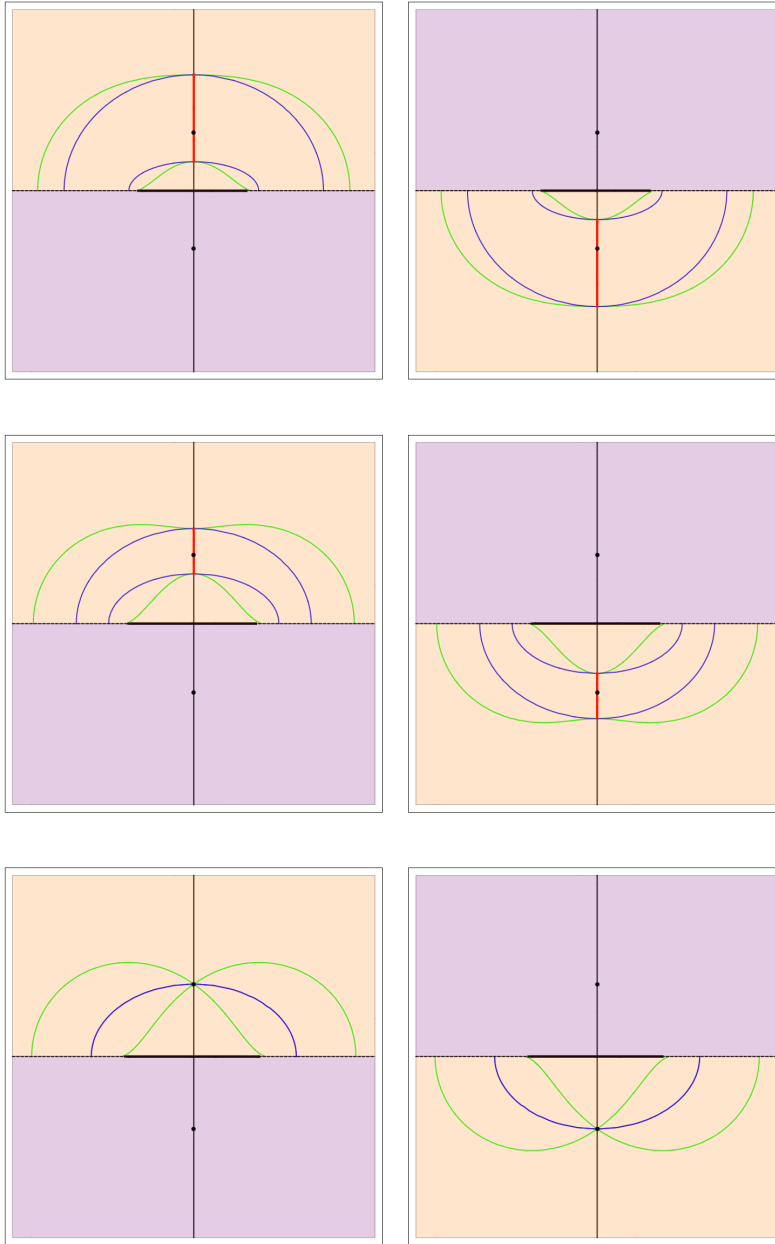


Figure 22: Side view of the Kerr spacetime. The left column corresponds to Z_1 and the right column for Z_2 . The yellow areas represent \mathbb{R}_+ and the pink ones represent \mathbb{R}_- . The green surfaces are the outer and inner ergospheres and the blue one are the outer and inner horizon. The red thick lines are the excluded regions in the z -axis and the black dots are the fixed points of the dynamic system. Notice that the inner and outer horizon coincide with the inner and outer ergosphere for the z -axis and all them collapse for $a = 0$. The thick black line is the singular ring. Notice that as \mathbb{R}_- has no horizons, the pink regions has no curves, only the critical point at $\bar{z} = -a$. $M = 1$ is settled for simplicity.

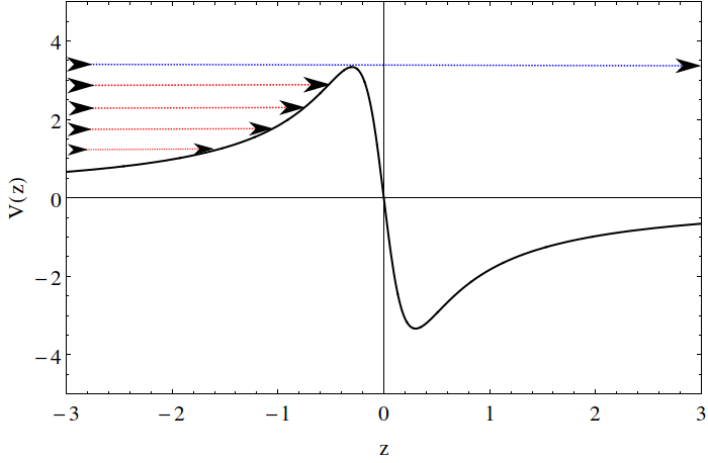


Figure 23: Potential $V(\bar{z})$ and some trajectories that try to go from \mathbb{R}_- to \mathbb{R}_+ . The red trajectories correspond to values of $|z'_0| < |z'_{\text{critic}}|$ and the blue trajectory correspond to values of $z'_0 = z'_{\text{critic}}$. $M = 1$ is settled for simplicity.

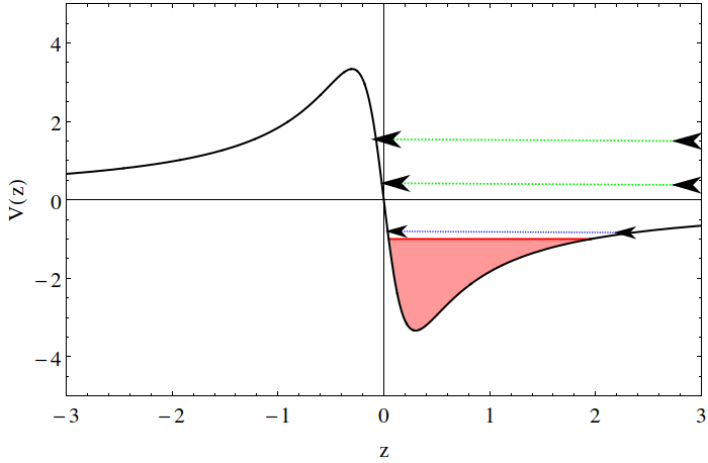


Figure 24: Potential $V(\bar{z})$ and some trajectories that try to go from \mathbb{R}_+ to \mathbb{R}_- but does not reach the top of the potential. The green trajectories correspond to geodesics that end in $\bar{z} = \infty$ and the blue trajectory correspond to geodesics that oscillate around $\bar{z} = a$. The red region represents the excluded region, where no timelike particles are allowed. $M = 1$ is settled for simplicity.

$\bar{z}_0 = \bar{z}(0)$ and $p_{\bar{z}_0} = \bar{p}_z(0)$ are given by

$$\bar{z}_{\text{return}\pm} = \frac{-M \pm \sqrt{M^2 - a^2 \left(p_{\bar{z}_0}^2 - \frac{2M\bar{z}_0}{a^2 + \bar{z}_0^2} \right)^2}}{p_{\bar{z}_0}^2 - \frac{2M\bar{z}_0}{a^2 + \bar{z}_0^2}} \quad (177)$$

where $|p_{\bar{z}_0}| < \frac{\sqrt{2M\bar{z}_0}}{\sqrt{a^2 + \bar{z}_0^2}}$ and $\bar{z} > 0$.

5.3.2.3 The SW limit

The **SW** limit of the dynamic system correspond when $a \rightarrow 0$. In this limit the potential becomes $V(\bar{z}) = \frac{1}{\bar{z}}$, which coincide with the potential for a timelike test particle moving with $L = 0$ (where L is the angular momentum) in the **SW** geometry (see [8]). This potential also coincide with the Newtonian motion of a test particle moving in radial trajectories as the **SW** potential for timelike test particles coincide with the Newtonian potential iff $L = 0$. But in this case more information is provided by the dynamical system. Only the region \mathbb{R}_+ coincide with the radial movement for timelike particles in the **SW** geometry, while the movement in the \mathbb{R}_- space coincide with the radial geodesics in the **SW** geometry with negative mass. As we can see in the phase portrait of the fig. 25, the two regions \mathbb{R}_- and \mathbb{R}_+ are now disconnected and no geodesic can go from one to another. This is the only case in which this disconnection of the regions \mathbb{R}_- and \mathbb{R}_+ occurs. This fact can be understand as the ring singularity became a single point because the singular ring collapses and the inner disk with it, leaving the two cited regions disconnected. Now, the two z -axis of the Kerr geometry exist separately in the sense that for each axis, now the part with $\bar{z} > 0$ and $\bar{z} < 0$ is in the same spacetime (remember that the existence of the inner disk separate the **MAE** in the regions \mathcal{Z}_1 and \mathcal{Z}_2). The fact that \mathbb{R}_- (which corresponds to the space where $r(x, y, z) < 0$) has a repulsive behavior leads in the fact that the Kerr metric has an isometry given by

$$M \rightarrow -M \tag{178}$$

$$r \rightarrow -r \tag{179}$$

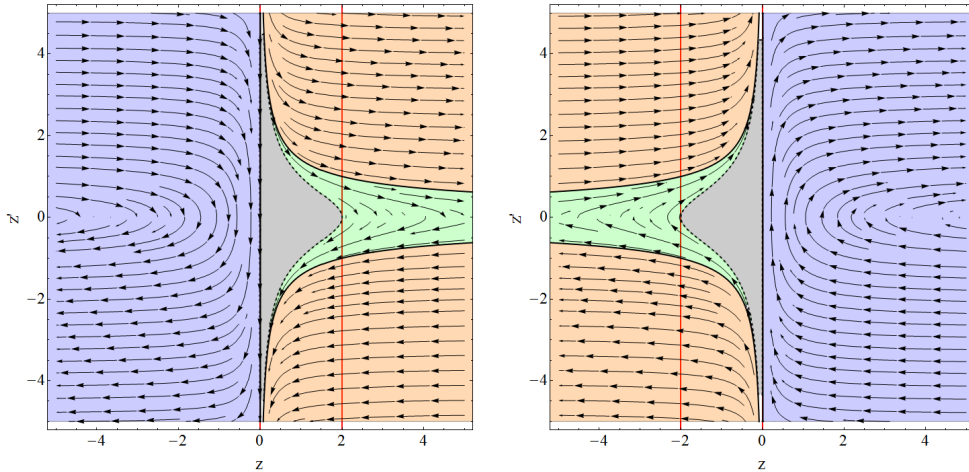


Figure 25: Schwarzschild limit of the dynamic system. The red lines corresponds to the horizons at $\bar{z} = 2M$. The red region corresponds to the excluded region, the blue area represent the curves that start in $\bar{z} = -\infty$ and return to $\bar{z} = -\infty$, the orange zones represent the curves that start in $\bar{z} = \infty$ and end in $\bar{z} = \infty$. The closed curves are in the green area and the limit orbit is the black dashed line surrounding the excluded region. $M = 1$ is settled for simplicity.

being checked more easily when the metric is in **BL** coordinates (see eq. (34)). The **SW** limit has geodesics that can reach the asymptotically flat region at $\bar{z} = \infty$ and geodesics that get trapped by the black hole. The escape velocity is easily computed as

$$\frac{1}{\bar{z}_0} + p_{\bar{z}_0}^2 = 0 \implies p_{\bar{z}_0} = \pm \frac{\sqrt{2M}}{\sqrt{\bar{z}}}. \quad (180)$$

Notice that in the horizon $\bar{z} = 2M$ the escape velocity is $p_{\bar{z}_0} = \bar{z}'_0 = \pm 1$, which in regular units correspond to $\bar{z}'_0 = c$, where c is the speed of light. For points $\bar{z} < 2M$ the escape velocity is $\bar{z}'_0 > c$ and no timelike particles can escape. Obviously, this is in perfect match with the results given in section 5.2, where we obtained that once crossed $\bar{z} = r_+ = 2M$ (for $a = 0$) no timelike particle can go back, and as now $\bar{z} = r_- = 0$ (which coincides with the singularity) the particle cannot change to another **KS** patch because it will fall into the singularity.

5.3.2.4 Oscillation frequencies in extreme Kerr

We have seen that the existence of the excluded regions is translated in the fact that no timelike particles can be in the stable point at $\bar{z} = a$. But as we have studied in section 5.3.2.1, the excluded regions for $a = M$ vanishes. However, as we also saw in section 5.3.2.1, only null geodesic can remain in this critical point, but timelike particles are able to oscillate around this point. In the extreme Kerr ($a = M$) we can linearize the potential $V(\bar{z})$ around the critical point in order to obtain the oscillating frequency. We can linearize the potential to its second

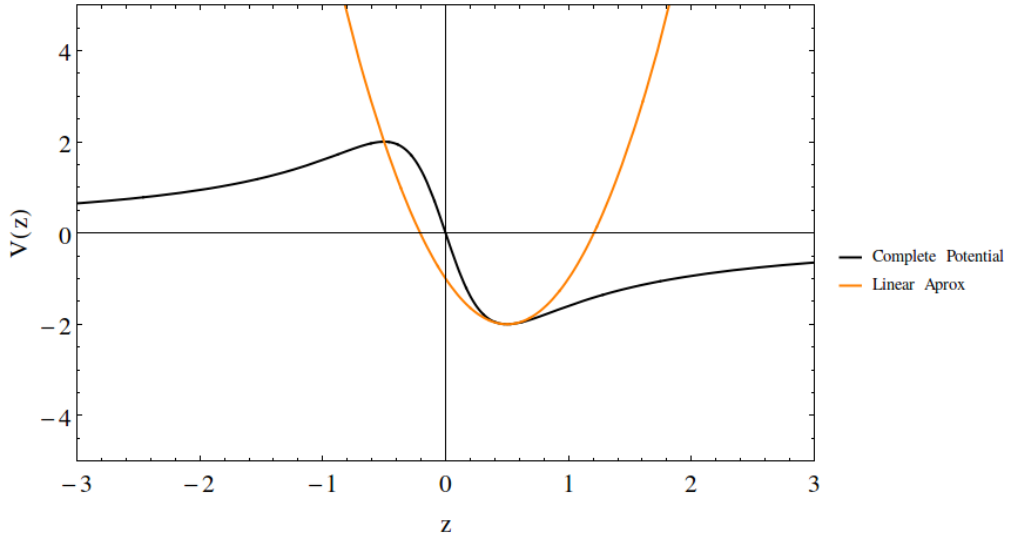


Figure 26: Linearization of the potential $V(\bar{z})$ around the critical point at $\bar{z} = a$. The black line represent the complete potential and the green line correspond to the second order linearization, which transforms the problem into a harmonic oscillator.

order as (remember that we can only do this for the extreme Kerr in which $a = M$)

$$V(\bar{z}) - V(a = M) = \frac{(z - M)^2}{2M^2} + O(\bar{z} - M)^3 \quad (181)$$

The linearization of the potential can be visualized in fig. 26. The dynamic equations are

$$\bar{z}'(s) = p_{\bar{z}}, \quad (182)$$

$$p'_{\bar{z}}(s) = -\partial_{\bar{z}}V(\bar{z}) = -\frac{(z - M)}{M^2}. \quad (183)$$

The solution to this system with initial values $\bar{z}(0) = \bar{z}_0$ and $p_{\bar{z}}(0) = p_{\bar{z}_0}$ is

$$\bar{z}(s) = p_{\bar{z}_0} \cos\left(\frac{s}{M}\right) + \frac{(M - \bar{z}_0) \sin\left(\frac{s}{M}\right)}{M}, \quad (184)$$

$$p_{\bar{z}}(s) = Mp_{\bar{z}_0} \sin\left(\frac{s}{M}\right) + (\bar{z}_0 - M) \cos\left(\frac{s}{M}\right) + M. \quad (185)$$

The oscillating frequency is

$$\nu = \frac{1}{M}. \quad (186)$$

We conclude that when the Kerr black hole is more massive the particle oscillate slower. This is quite surprising because a greater value of the mass of the black hole acts "bounding" the particle to $\bar{z} = a = M$.

5.3.2.5 Stability of the critical point

We are now interested in the Stability of the z -axis itself. This is because unless we have seen that there exist critical points in the axis, we want to know what would happen to this critical points if a little perturbation in every direction is done. This can have two possible consequences, that the particle return to the z -axis or go away. This will give us useful information about if the symmetry axis is stable or unstable. To analyze this we will need the full Hamiltonian to perform the perturbation. The Kerr metric in **KS** coordinates is

$$g = \eta + hK \otimes K, \quad (187)$$

where η is the Minkowsky metric and

$$f = \frac{2Mr^3}{r^4 + a^2z^2},$$

$$K = -\sigma dt + \frac{r(xdx + ydy)}{r^2 + a^2} + \frac{a(xdy - ydx)}{r^2 + a^2} + \frac{zdz}{r}.$$

We have now to repeat all the steps that we performed on section 5.1 to obtain a full Hamiltonian to the general Kerr geodesic. As we use before, affinely parametrized geodesics are the solutions of the Hamilton equations of the Hamiltonian

$$H = \frac{1}{2}(g^{-1})^{\alpha\beta}p_{\alpha}p_{\beta} \quad (188)$$

defined on the cotangent bundle of \mathcal{M} . the Hamilton equations fix $\mathbf{p} = g(u, \cdot)$ where u is the tangent vector to the geodesic. Using the explicit expression (187) for the metric, this Hamiltonian takes the form

$$H = \frac{1}{2} \left(\eta^{\alpha\beta} p_\alpha p_\beta - h(K^\alpha p_\alpha)^2 \right). \quad (189)$$

Given that ∂_t is a Killing vector, the quantity $E := -\mathbf{p}(\partial_t)$ is conserved along geodesics. Note also that, with this definition,

$$K^\alpha p_\alpha = -E\hat{K} + \vec{K} \cdot \vec{p}, \quad (190)$$

where we have written $\mathbf{p} = \{\hat{p}, \vec{p}\}$ and dot means scalar product with δ_{ij} .

The Hamiltonian itself is a conserved quantity with the value of $H = -\frac{1}{2}\mu$ where $\mu = 0, \pm 1$ depending on whether the geodesic is timelike ($\mu = 1$), spacelike ($\mu = -1$) or null ($\mu = 0$). Inserting (133) and the conserved quantity E into (132) the following Hamiltonian arises naturally

$$H' := H + \frac{1}{2}E^2 = \frac{1}{2} \left(\vec{p}^2 - h \left(\vec{K} \cdot \vec{p} - E\hat{K} \right)^2 \right), \quad (191)$$

which is now defined on the cotangent bundle of $\mathbb{R}^3 \setminus \mathcal{C}$, where \mathcal{C} represent the singular ring.

We will perform the perturbations for \mathcal{Z}_1 because the perturbations for \mathcal{Z}_2 have the same behavior but changing the sign of z . The point $z = -a$ result appropriate to analyze because timelike particles are allowed to be at rest for every value of a . Suppose that the particle is at rest in $z = a$. As a rest particle in the z axis has $\dot{z} = 0$, we can use eqs. (138) and (139) to solve for p_z in the rest point of $z = -a$ to get that $p_z(z = -a, \dot{z} = 0) = \frac{EM}{a+M}$. As the particle start at rest in the rest of the variables $p_x = p_y = p_z = x = y = 0$ are settled and then a perturbation is performed as

$$x \rightarrow \delta x, \quad (192)$$

$$y \rightarrow \delta y, \quad (193)$$

$$z \rightarrow -a + \delta z, \quad (194)$$

$$p_x \rightarrow \delta p_x, \quad (195)$$

$$p_y \rightarrow \delta p_y, \quad (196)$$

$$p_z \rightarrow \frac{EM}{a+M} + \delta p_z. \quad (197)$$

$$(198)$$

The Hamilton equations linearized at it first order in the Hamiltonian variables product of the perturbation $\{\delta x, \delta y, \delta z, \delta p_x, \delta p_y, \delta p_z\}$ can be written as

$$\vec{\xi}'(s) = \vec{\xi}_0 \delta E + \mathcal{A} \vec{\xi}(s) \quad (199)$$

where $\vec{\xi}_0 = \vec{\xi}_0(M, a)$ is a non-homogeneous term, the perturbation variables are collected in the vector $\vec{\xi}(s) = \{\delta x(s), \delta y(s), \delta z(s), \delta p_x(s), \delta p_y(s), \delta p_z(s)\}$ and the matrix \mathcal{A} is given by

$$\mathcal{A} = \begin{pmatrix} \frac{ME}{2a^2+2Ma} & -\frac{ME}{2a(a+M)} & 0 & 1 & 0 & 0 \\ \frac{ME}{2a^2+2Ma} & -\frac{ME}{2a(a+M)} & 0 & 1 & 0 & 0 \\ 0 & 0 & 0 & 0 & 0 & \frac{a+M}{a} \\ -\frac{M(a+2M)E^2}{4a^2(a+M)^2} & 0 & 0 & -\frac{ME}{2a(a+M)} & -\frac{ME}{2a(a+M)} & 0 \\ 0 & -\frac{M(a+2M)E^2}{4a^2(a+M)^2} & 0 & \frac{ME}{2a^2+2Ma} & -\frac{ME}{2a(a+M)} & 0 \\ 0 & 0 & \frac{ME^2}{2a(a+M)^2} & 0 & 0 & 0 \end{pmatrix}. \quad (200)$$

where $E = \frac{\sqrt{a+M}}{\sqrt{a}}$ is the energy of the rest particle at $z = -a$. The eigenvalues of this matrix are

$$\begin{aligned} \lambda_1 &= -\sqrt{\frac{M}{2a^3}} & \lambda_2 &= \sqrt{\frac{M}{2a^3}} & \lambda_3 &= -\frac{1}{2}i\sqrt{\frac{M(2(\sqrt{M(a+M)}+M)+a)}{a^3(a+M)}} \\ \lambda_4 &= \frac{1}{2}i\sqrt{\frac{M(2(\sqrt{M(a+M)}+M)+a)}{a^3(a+M)}} & \lambda_5 &= -\frac{1}{2}i\sqrt{\frac{M(-2\sqrt{M(a+M)}+a+2M)}{a^3(a+M)}} \\ \lambda_6 &= \frac{1}{2}i\sqrt{\frac{M(-2\sqrt{M(a+M)}+a+2M)}{a^3(a+M)}} \end{aligned} \quad (201)$$

The two first eigenvalues are associated with z and p_z . This is more clear if we rewrite the matrix \mathcal{A} in the base $\{\delta x(s), \delta p_x(s), \delta y(s), \delta p_y(s), \delta z, \delta p_z(s)\}$ because in this base the matrix decompose in two Jordan boxes as

$$\mathcal{A}' = \begin{pmatrix} \frac{ME}{2a^2+2Ma} & 1 & -\frac{ME}{2a(a+M)} & 0 & 0 & 0 \\ -\frac{M(a+2M)E^2}{4a^2(a+M)^2} & -\frac{ME}{2a(a+M)} & 0 & -\frac{ME}{2a(a+M)} & 0 & 0 \\ \frac{ME}{2a^2+2Ma} & 0 & \frac{ME}{2a^2+2Ma} & 1 & 0 & 0 \\ 0 & \frac{ME}{2a^2+2Ma} & -\frac{M(a+2M)E^2}{4a^2(a+M)^2} & -\frac{ME}{2a(a+M)} & 0 & 0 \\ 0 & 0 & 0 & 0 & 0 & \frac{a+M}{a} \\ 0 & 0 & 0 & 0 & \frac{ME^2}{2a(a+M)^2} & 0 \end{pmatrix}. \quad (202)$$

and now it is clear that the eigenvalues of z and p_z are $\lambda_{\pm} = \pm\sqrt{\frac{ME^2}{2a(a+M)^2}\frac{a+M}{a}} = \pm\sqrt{\frac{M}{2a^3}}$. As $M > a$ the eigenvalues $\lambda_3, \lambda_4, \lambda_5, \lambda_6$ are purely imaginary and therefore the point $z = -a$ happens to be a saddle point along the z axis (as we already know) and a center along the $\{x, y\}$ plane. So if a perturbation that takes away the geodesic from the axis is performed, the particle oscillates around $z = -a$ unless $\delta p_z \neq 0$, in which case the particle moves spirally along the z axis upwards if $\delta p_z > 0$ and downwards if $\delta p_z < 0$. This is of course the composition of the movement in the z axis with a center-like movement in the $\{x, y\}$ plane. The real movement (not only the first order) of the perturbed geodesic can be found through numerical integration in the last image of the chapter 7.

Now that we know the behavior of the unstable point at $z = -a$ we could think of analyzing the stable point at $z = a$ but as we prevent previously, this

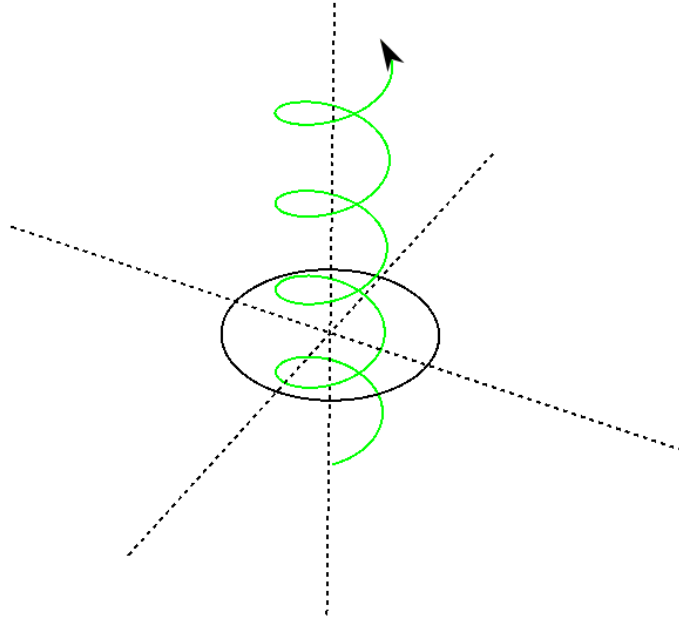


Figure 27: Representation of the movement at its first order after the perturbation in the unstable saddle point $z = -a$. In this image $\delta p_z > 0$ and therefore, the geodesic moves upwards. The thick dashed lines represent the Cartesian axes, the green thick line is the geodesic movement and the black thick ring represents the singular ring.

point is not allowed to timelike particles because of the excluded region. Even when $a \rightarrow M$, the point is still inaccessible to timelike particles as we saw in section 5.2. Either way, the stability behavior of the whole axis is expected to be the same as when we linearize the Hamiltonian equations around an arbitrary value of z_0 and p_{z_0} the matrix that we obtain already have the same structure as the one that we obtain when we linearize the axis, but with much more complicated terms that are not very enlightening to display here.

5.4 LOWER ENERGY ORBIT

We are now interested in the lower energy orbit. As we notice in section 5.3.2.1 this orbits are the boundary of the excluded regions and the last orbit that is allowed as we approach the forbidden region. We can compute the proper time (τ) that this geodesic (that as we have seen before, is a closed curve in the phase portrait and therefore corresponds to a periodic orbit) needs to complete a full turn around the forbidden region. Also, we know that the forbidden region for every value of the parameter a is always between in the interval $[r_-, r_+]$. To compute the period of this movement we must use the energy equation. In virtue of corollary 10 we know that the lower energy orbit satisfies

$$(z')^2 - \frac{2Mz}{a^2 + z^2} = 2\epsilon = -1. \quad (203)$$

We can now solve for z' as

$$z' = \pm \frac{\sqrt{z(2M - z) - a^2}}{\sqrt{a^2 + z^2}}. \quad (204)$$

Using this relation we can write

$$\int_0^T dt = \int_{r_-}^{r_+} \frac{1}{\sqrt{2Mz - (a^2 + z^2)}} dz \quad (205)$$

This integral has a very complicated expression for a general value of $a \in [0, M]$ that can be visualized in fig. 28, but for $a = 0$ we can compute this integral analytically as

$$2 \int_0^{2M} \frac{z}{\sqrt{z(2M - z)}} dz = \\ -2 \left(\sqrt{z(2M - z)} \left(\frac{2M \log(\sqrt{z - 2M} + \sqrt{z})}{\sqrt{z^2 - 2Mz}} + 1 \right) \right) \Big|_0^{2M} = 2\pi M$$

which coincides with two times the maximum time of a timelike particle to fall from the even horizon into the singularity in the SW geometry. Notice that this period is the maximum time that a timelike geodesic expends traveling from r_- to r_+ . This can be checked analyzing the behavior of the bounded orbits ($\epsilon \in [-\frac{1}{2}, 0]$) as is displayed in fig. 29. In this figure we can see that the travel time is always $\tau < \tau(\epsilon = -\frac{1}{2})$.

This analysis reveal interesting features. First of all, notice that the time for $a = 1$ is $\tau = 0$ because in this limit $r_- = r_+$. But what is really unexpected is

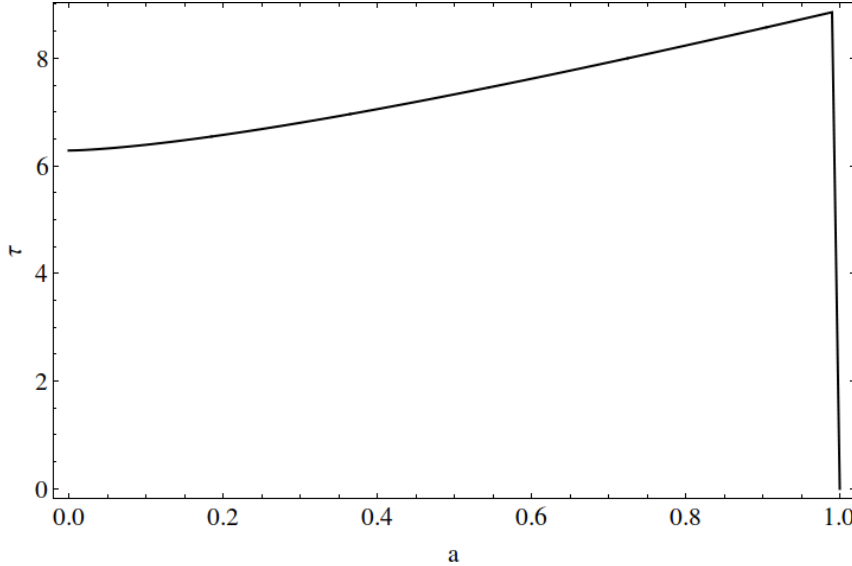


Figure 28: Period of the lower energy orbit as a function of the parameter a . For simplicity $M = 1$ is chosen.

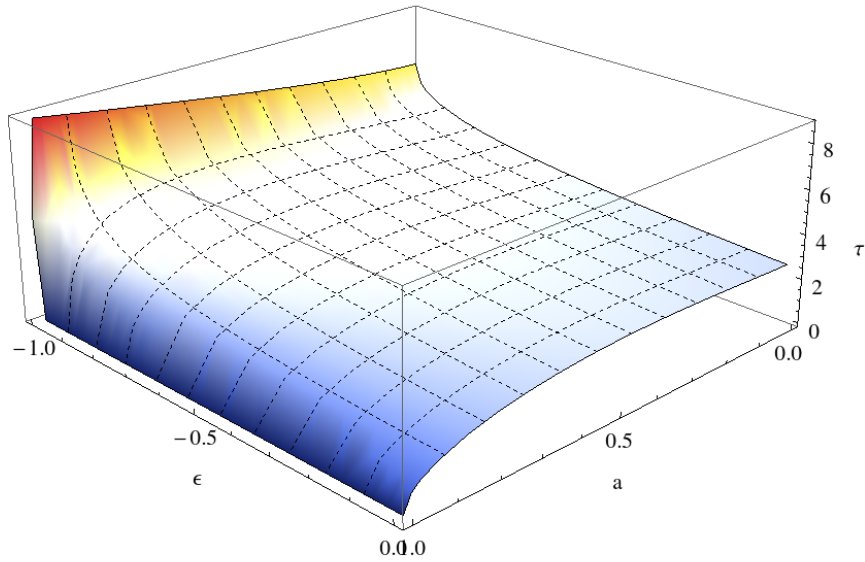


Figure 29: Period of the bounded orbit as a function of the parameter a and the Newtonian energy ϵ . For simplicity $M = 1$ is chosen.

the fact that the period of the lower energy orbit is greater as the parameter a increases. This is very strange because the area of the excluded regions decreases as the parameter a increases as we saw in section 5.3.2.1, and therefore the boundary of the excluded regions (which is the lower energy orbit) decreases as well.

6

THE EQUATORIAL PLANE: THE INNER DISK

Now that we understand the behavior of the geodesic movement along the axis of symmetry we will center our efforts in the movement restricted to the equatorial plane. The movement in the equatorial plane outside the horizons is well known in [BL](#) coordinates. The fact that the metric is singular at the horizons prevent the geodesics to be extended across the horizons in this coordinate system. A complete analysis of the geodesic movement in the equatorial plane can be found in chapter 4 of [\[11\]](#). The geodesic flow in the inner disk cannot be analyzed easily in [BL](#) coordinates as the spacetime singularity is located at $r = 0$ in this coordinates and therefore the “ring” shape cannot be analyzed in this coordinate system. The [KS](#) coordinates are regular across all the horizons and in this system, the inner disk is well located at $x^2 + y^2 < a^2$ with $z = 0$. Remember that this inner disk is the identification region between \mathbb{R}_+ and \mathbb{R}_- as was previously noticed in chapter 4. As the geodesic behavior in the [KS](#) coordinates in the equatorial plane is rather complicated and exceeds this work and because in the other hand, has been previously analyzed in more suitable coordinates, we are going to center our efforts in the inner disk.

6.1 HAMILTONIAN EQUATIONS OF THE GEODESICS

We are going to discuss the geodesic equations inside the inner disk. Remember that this region is defined as $x^2 + y^2 < a^2$ with $z = 0$. The complete understanding of the geodesic flow involves not only the knowledge of the geodesic equations but also the conditions that lead to future directed solutions. In this section we are going to derive the geodesic equations in the inner disk.

Theorem 11. *The geodesic equations for the Kerr metric restricted to the inner disk in [KS](#) coordinates are the solution of the Hamilton equations derived from the Hamiltonian*

$$H' = \frac{1}{2}\vec{p}^2 \tag{206}$$

where $H = \frac{1}{2}(E^2 - \mu)$ with $\mu = 0$ for null geodesics, $\mu = 1$ for timelike geodesics.

Proof. Unless it is specified otherwise, $x^2 + y^2 < a^2$ is assumed. In the previous chapter, we derived a Hamiltonian (see eq. [\(191\)](#)) that describes the geodesic flow in the hole Kerr spacetime. We can adapt this Hamiltonian to the equatorial plane taking the limit $z \rightarrow 0$. This limit has to be computed carefully as we have terms involving $r(x, y, z)$ and z . The Hamiltonian is written as

$$H' = \frac{1}{2}(E^2 - \mu) \frac{1}{2} \left(\vec{p}^2 - \lim_{z \rightarrow 0} (h) (\vec{K} \cdot \vec{p} - E\hat{K})^2 \right), \tag{207}$$

which is defined on the cotangent bundle of $\mathbb{R}^3 \setminus \mathcal{C}$, where \mathcal{C} represent the singular ring, $p = (p_x, p_y, 0)$ $\vec{K} = \lim_{z \rightarrow 0} \left(\frac{xx(x,y,z)+ay}{r(x,y,z)^2+a^2}, \frac{yr(x,y,z)-ax}{r(x,y,z)^2+a^2}, \frac{z}{r(x,y,z)} \right)$ and $\hat{K} = \sigma$.

As we have studied before in chapter 4, the function $r(x, y, z)$ can be written near the inner disk as

$$r(x, y, z) = z\sqrt{f(x, y, \bar{z})}, \quad (208)$$

where $f(x, y, \bar{z})$ is a nonzero positive smooth function. Then, the limits can be written as

$$\lim_{z \rightarrow 0} h = \lim_{z \rightarrow 0} \frac{2Mr^3}{r^4 + a^2z^2} = \lim_{z \rightarrow 0} \frac{2M(z\sqrt{f(x, y, \bar{z})})^3}{(z\sqrt{f(x, y, \bar{z})})^4 + a^2z^2} \quad (209)$$

$$= \lim_{z \rightarrow 0} \frac{2Mz f(x, y, \bar{z})^{\frac{3}{2}}}{z^2 f(x, y, \bar{z})^2 + a^2} = 0, \quad (210)$$

$$\lim_{z \rightarrow 0} h = \frac{z}{r} = \frac{1}{\sqrt{f(x, y, \bar{z})}} \quad (211)$$

The Hamiltonian becomes

$$H' = \frac{1}{2}\vec{p}^2 \quad (212)$$

so the solutions to the geodesic equations are

$$x(s) = z_0 + p_{x0}s \quad (213)$$

$$y(s) = z_0 + p_{y0}s \quad (214)$$

$$p_x(s) = p_{x0} \quad (215)$$

$$p_y(s) = p_{y0} \quad (216)$$

where s is the proper time $z(0) = z_0$ and $p_z(0) = p_{z0}$. With no difference if the geodesics are null or timelike. \blacksquare

This result is very interesting because it tell us that the geodesic in the inner disk behaves as if the spacetime inside the singular ring were Minkowsky. This is analogous to the case in which a thin spherically symmetric shell is set as the source of the gravitational field. In this scenario and in virtue of Birkhoff's theorem [2] we will have the SW metric outside the shell and the Minkowsky metric inside the shell. This also resembles the behavior of the electromagnetic field generated by a electrically charged thin shell, as in this case there is no field inside the shell and the field outside the shell behaves as the field generated by a punctual charge located at the center of the shell.

6.2 VARIATION RANGES AND CAUSAL STRUCTURE

As we did in the previous chapter, we must now analyze the conditions that lead to future-oriented geodesics. This case is rather simple because the function $h_{z \rightarrow 0} = 0$ for points inside the inner disk.

Lemma 12. *If the time orientation of (\mathcal{M}, g) is chosen so that the null vector $K^\alpha = \left(-\sigma, \frac{y}{a}, -\frac{x}{a}, \frac{\sqrt{a^2 - x^2 - y^2}}{a}\right)$ is future directed, then a geodesic with $\mu = 0, 1$ starting at a point (t_0, x_0, y_0) with $x_0^2 + y_0^2 < a^2$ is future causal if and only if Carter's constant is positive for timelike geodesics and zero for null geodesics.*

Proof. As the function $h_{z \rightarrow 0} = 0$ the metric in the inner disk becomes

$$g = \eta \quad (217)$$

where η is the Minkowsky metric. The 1-form K of the Kerr metric becomes (after taking the limit $z \rightarrow 0$) $K = \left(-\sigma, \frac{y}{a}, -\frac{x}{a}, \frac{\sqrt{a^2 - x^2 - y^2}}{a} \right)$ as $\lim_{z \rightarrow 0} r(x, y, z) = 0$ when $x^2 + y^2 < a^2$ and $\lim_{z \rightarrow 0} \frac{z}{r(x, y, z)} = \frac{1}{\sqrt{f(x, y, \bar{z})}} = \frac{\sqrt{a^2 - x^2 - y^2}}{a}$. Before we can compute the conditions for future oriented geodesics notice that

$$p_x = dx(u) = \dot{x}, \quad (218)$$

$$p_y = dy(u) = \dot{y}, \quad (219)$$

$$-E = dt(u) = -\dot{t}, \quad (220)$$

$$L_z = p_y x - p_x y = \dot{y}x - x\dot{y}, \quad (221)$$

where $u = (t, \dot{x}, \dot{y}, 0)$ is the tangent vector to the geodesics. The conditions that leads to future oriented casual (timelike and null) geodesics are $g(u_0, \sigma K|_{s=0}) < 0$ or $g(u_0, \sigma K|_{s=0}) = 0$ which implies $u_0 = b\sigma K|_{s=0}$, with $b \geq 0$. This conditions reads

$$K_\alpha u^\alpha|_{s=0} = -a\dot{t}_0 + \sigma(\dot{y}_0 x_0 - y_0 \dot{x}_0) \leq 0 \quad (222)$$

where the equality is only when $u_0 = b\sigma K|_{s=0}$. There is still another relation that allows us to distinguish between null an timelike geodesics given by

$$-\mu = u_\alpha u^\alpha = -\dot{t}^2 + \dot{x}^2 + \dot{y}^2. \quad (223)$$

As K^α is a null vector, i.e $K^\alpha K_\alpha = 0$, the condition $u_0 = b\sigma K|_{s=0}$ implies that $u_\alpha u^\alpha = \mu = 0$. Using the eqs. (220) and (221) we can rewrite this conditions as

$$K_\alpha u^\alpha|_{s=0} \leq 0 \rightarrow -\sigma L_z + aE = \mathcal{C}^{\frac{1}{2}} \geq 0 \quad (224)$$

$$\frac{1}{2} (E^2 - \mu) = \frac{1}{2} (\dot{x}^2 + \dot{y}^2) \quad (225)$$

where C is the Carter's constant restricted to the equatorial plane that we have seen in eq. (97) on page 33 and the condition $\mathcal{C}^{\frac{1}{2}} = 0$ occurs if $\mu = 0$. Notice that the third equation is a direct consequence of theorem 11 because this equation can be written using eqs. (207), (218) and (219) as

$$\frac{1}{2} (E^2 - \mu) = H' = \frac{1}{2} (\dot{x}^2 + \dot{y}^2) = \frac{1}{2} \vec{p}^2 \quad (226)$$

So, the only independent condition that lead to future casual geodesics is $\mathcal{C} > 0$ ($\mu=1$) or $\mathcal{C} > 0 = 0$ ($\mu = 0$) as claimed. \blacksquare

As we are going to see in the next section, causal geodesic with starting point at x_0, y_0 with $z_0 = 0$ and $x_0^2 + y_0^2 < a^2$ cannot remain in the inner disk.

6.3 STABILITY OF THE INNER DISK

Although the geodesic behavior of the inner disk is interesting, we are going to show that a geodesic that starts in the inner disk cannot remain in it. A heuristic argument that leads to this conclusion is that when we studied the axis of symmetry ($x = y = 0$) the point $z = 0$ was not a stable point, indeed, the geodesic flow go upwards the axis if $\dot{z}_0 = 0$ (remember that $\ddot{z} = \lambda z$, where $\lambda = \pm 1$). Now, we are going to extend this behavior to all geodesic that starts with $p_{\bar{z}} = 0$ and $x_0^2 + y_0^2 < a^2$, $z = 0$.

Proposition 13. *Only null geodesic that starts starts in the inner disk ($x_0^2 + y_0^2 < a^2$ and $\bar{z} = 0$) with $\dot{z} = 0$ can remain in this region while timelike geodesics leaves the disk with $\ddot{z} > 0$.*

Proof. Lets consider the general Hamiltonian that describes the geodesic flow in [KS](#) coordinates along all the spacetime derived in eq. (132) on page 46 that writes

$$H' = \frac{1}{2} \left(\vec{p}^2 - h \left(\vec{K} \cdot \vec{p} - E \hat{K} \right)^2 \right), \quad (227)$$

defined on the cotangent bundle of $\mathbb{R}^3 \setminus \mathcal{C}$, where \mathcal{C} represent the singular ring. Here $\hat{K} = \sigma$, $\vec{p} = (p_x, p_y, p_{\bar{z}})$ and $K = -\sigma dt + \frac{r(xdx+ydy)}{r^2+a^2} + \frac{a(xdy-ydx)}{r^2+a^2} + \frac{zdz}{r}$. The function $r(x, y, z)$ is defined for points near the inner disk as

$$r(x, y, \bar{z}) = \bar{z} \sqrt{f(x, y, \bar{z})} \quad (228)$$

where $f(x, y, \bar{z})$ is a nonzero positive smooth function. Let's start by checking what value of $p_{\bar{z}_0}$ satisfies $\dot{z}_0 = 0$. The Hamilton equation for \dot{z} evaluated at $t = 0 \rightarrow \bar{z}_0 = 0$ implies that

$$\dot{\bar{z}}_0 = \frac{\partial H}{\partial p_{\bar{z}}} \Big|_{t=0 \rightarrow z=0} = p_{\bar{z}_0}. \quad (229)$$

So $\dot{\bar{z}}_0 = 0 \rightarrow p_{\bar{z}_0} = 0$. We need to calculate now $\ddot{\bar{z}}_0 > 0$. To achieve this we are going to calculate \dot{z} and derive this equation. Then, using the Hamilton equations for \dot{p}_x , \dot{p}_y and $\dot{p}_{\bar{z}}$ we can obtain the equation for \ddot{z} as a function of z, p_z, x, y, p_x y p_y . As we will need the derivatives of $f(x, y, \bar{z})$ we can compute these from the equation that defines $r(x, y, z)$ that is

$$r^2 |\vec{x}|^2 = \bar{z}^2 |\vec{x}|^2 + r^2 (x^2 + y^2). \quad (230)$$

After substituting $r = \bar{z} \sqrt{f(x, y, \bar{z})}$ and derive we can obtain

$$\partial_x f(x, y, \bar{z}) = -\frac{2xf(x, y, \bar{z})}{-2\bar{z}^2 f(x, y, \bar{z}) - a^2 + x^2 + y^2 + \bar{z}^2}, \quad (231)$$

$$\partial_y f(x, y, \bar{z}) = -\frac{2yf(x, y, \bar{z})}{-2\bar{z}^2 f(x, y, \bar{z}) - a^2 + x^2 + y^2 + \bar{z}^2}, \quad (232)$$

$$\partial_{\bar{z}} f(x, y, \bar{z}) = \frac{2\bar{z}(f(x, y, \bar{z}) - 1)f(x, y, \bar{z})}{-2\bar{z}^2 f(x, y, \bar{z}) - a^2 + x^2 + y^2 + \bar{z}^2}. \quad (233)$$

The Hamilton equation $\dot{z} = \frac{\partial H}{\partial p_z}$ reads

$$\dot{z} = \left(p_{\bar{z}} - \frac{4f(x, y, \bar{z})\bar{z}^3 \left(\frac{p_x(ay + \sqrt{f(x, y, \bar{z})x}\bar{z})}{a^2 + f(x, y, \bar{z})\bar{z}^2} + \frac{p_y(\sqrt{f(x, y, \bar{z})y}\bar{z} - ax)}{a^2 + f(x, y, \bar{z})\bar{z}^2} - E + \frac{p_{\bar{z}}}{\sqrt{f(x, y, \bar{z})}} \right)}{2(a^2\bar{z}^2 + f(x, y, \bar{z})^2\bar{z}^4)} \right) \quad (234)$$

The general form of the rest Hamilton equations is quite complicated and not very enlightening to display, and therefore we are going to display the final result. After computing \ddot{z} by deriving eq. (234), substituting the Hamilton equation for \dot{p}_x , \dot{p}_y and $\dot{p}_{\bar{z}}$, and evaluating the result at $t = 0$ (which implies that $x = x_0$, $y = y_0$, $\bar{z} = 0$, $p_x = p_{x_0}$, $p_y = p_{y_0}$, $p_{\bar{z}} = 0$) we obtain that

$$\ddot{x}_0 = 0 \quad (235)$$

$$\ddot{y}_0 = 0 \quad (236)$$

$$\ddot{z}_0 = \frac{f(x, y, \bar{z})^{3/2}(aE - \sigma L_z)^2}{a^4} = \frac{f(x, y, \bar{z})^{3/2}\mathcal{C}}{a^4} \quad (237)$$

$$(238)$$

As from section 6.2 timelike geodesics starting at the inner disk must have $\mathcal{C} > 0$ and therefore $\ddot{z}_0 > 0$ while null geodesics can have $\mathcal{C} = 0$ and remain in the inner disk as claimed. ■

This shows that as the acceleration of the particle must be positive at the points in the inner disk, then the particle will start moving upwards \bar{z} as is shows in fig. 30. Of course, this is in perfect agreement with the results derived in chapter 5, implying that a particle starting in $\bar{z} = 0$ with $\dot{z} = 0$ will move in the direction that \bar{z} increases (what we have called *upwards*).

6.4 A GLIMPSE AT THE GEODESICS OUTSIDE THE INNER DISK

As we said above, the geodesic flow outside the inner disk in the equatorial plane is hard to analyze, mostly because the causal structure is very complicated. In this section we are going to derive a energy-like equation for the geodesics in the Equatorial plane, that we are not going to analyze because it exceeds this work. The main difference between outside the ring and inside the ring is that outside the ring the function $r(x, y, z)$ is defined as

$$\lim_{z \rightarrow 0} r(x, y, z)|_{x^2 + y^2 > a^2} = \sqrt{x^2 + y^2 - a^2}. \quad (239)$$

and therefore the Hamiltonian eq. (207) becomes in this case

$$H' = \frac{1}{2} (E^2 - \mu) \frac{1}{2} (\vec{p}^2 - h (\vec{K} \cdot \vec{p} - E \hat{K})^2), \quad (240)$$

which is defined on the cotangent bundle of $\mathbb{R}^3 \setminus \mathcal{C}$, where \mathcal{C} represent the singular ring, $p = (p_x, p_y, 0)$, $\vec{K} = \left(\frac{xr(x, y, z) + ay}{r(x, y, z)^2 + a^2}, \frac{yr(x, y, z) - ax}{r(x, y, z)^2 + a^2}, 0 \right)$ and $\hat{K} = \sigma$. The next theorem proofs that there exist a Energy-like equation for the geodesic movement in the equatorial plane.

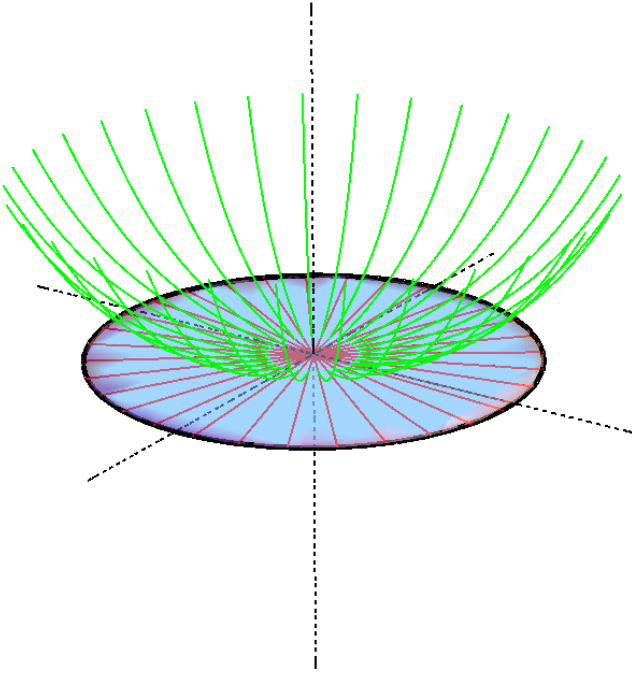


Figure 30: The behavior of causal geodesics that start in the inner disk is depicted in this figure. The black dashed lines are the Cartesian axes, the green curves represent the causal geodesic at its first order of approximation, the red curves represent the background geodesic in the inner disk (the behavior that the geodesic would have if $\mathcal{C} = 0$). The blue region represent the inner disk and the black ring represent the singular ring.

Theorem 14. *The geodesic equations for the Kerr metric restricted to the equatorial plane outside the inner disk in [KS](#) coordinates are the solution of the Energy-like equation*

$$\frac{1}{2} (E^2 - \mu) = \frac{1}{2} \left(\rho'^2 + \frac{L_z^2}{\rho^2} \right) - \frac{MC}{(\rho^2 - a^2)^{\frac{1}{2}} \rho^2} - \frac{\mu M (\rho^2 - a^2)^{\frac{1}{2}}}{\rho^2}. \quad (241)$$

where C is the Carter's constant, L_z is the axial angular momentum, $\mu = 1$ for timelike geodesics and $\mu = 0$ for null geodesics and $\rho^2 = r^2 + a^2$.

Proof. The Hamiltonian [240](#) reads

$$\frac{1}{2} (E^2 - \mu) = H' = \frac{1}{2} \left(\vec{p}^2 - \frac{h (E|\vec{x}|^2 + a(p_y x - p_x y) - r(p_x x + p_y y))^2}{(|\vec{x}|^2)^2} \right) \quad (242)$$

where $\vec{x} = (x, y)$. The angular momentum equation can be written from its definition ($L_z = p_y x - p_x y$) as $\vec{L}_z^2 = (\vec{x} \times \vec{p})^2 = \vec{x}^2 \vec{p}^2 - (\vec{x} \cdot \vec{p})^2$. We can use this relation to write the Hamiltonian as

$$H' = \frac{1}{2} \left(\frac{L_z^2 + (\vec{x} \cdot \vec{p})^2}{|\vec{x}|^2} - \frac{h (E|\vec{x}|^2 + aL_z - r\vec{x} \cdot \vec{p})^2}{|\vec{x}|^4} \right). \quad (243)$$

As from eq. (239) one can derive that $r\dot{r} = \vec{x} \cdot \dot{\vec{x}}$, multiplying the Hamilton equation $\dot{\vec{x}} = \frac{\partial H}{\partial \vec{p}}$ by \vec{x} we obtain that

$$\vec{x} \cdot \dot{\vec{x}} = r\dot{r} = \frac{2M(E|\vec{x}|^2 + aL_z) + \vec{x} \cdot \vec{p}(|\vec{x}|^2 - 2Mr)}{|\vec{x}|^2}, \quad (244)$$

from where we can solve for $\vec{x} \cdot \vec{p}$ and then, substituting this into the Hamiltonian of the eq. (243), which becomes

$$H' = \frac{2L_z^2 M |\vec{x}|^2 + |\vec{x}|^2 (4aEL_z M + 2E^2 M |\vec{x}|^2 - L_z^2 r - r^3 r'^2)}{2r|\vec{x}|^2 (2Mr - |\vec{x}|^2)}. \quad (245)$$

As $H' = \frac{1}{2}(E^2 - \mu)$ we can write

$$\frac{1}{2}(E^2 - \mu) = \frac{2L_z^2 M |\vec{x}|^2 + |\vec{x}|^2 (4aEL_z M + 2E^2 M |\vec{x}|^2 - L_z^2 r - r^3 r'^2)}{2r|\vec{x}|^2 (2Mr - |\vec{x}|^2)}. \quad (246)$$

Rearranging this equation and substituting $|\vec{x}|^2 = r^2 + a^2$ can obtain

$$E^2 - \mu = r'^2 + \frac{L_z^2}{r^2} - \frac{a^2(E^2 - \mu)}{r^2} - \frac{2MC}{r^3} - \frac{2\mu M}{r} \quad (247)$$

which is not a Energy equation because it has $E^2 - \mu = 2\epsilon$ (where ϵ is the Newtonian energy) in both sides. We can obtain get a new equation with the term $E^2 - \mu$ only in one side of the equation taking common factor in this term as

$$(E^2 - \mu) \left(1 + \frac{a^2}{r^2}\right) = r'^2 + \frac{L_z^2}{r^2} - \frac{2MC}{r^3} - \frac{2\mu M}{r}. \quad (248)$$

Leaving alone this term in the left side the equation reads

$$E^2 - \mu = \left(\frac{r^2}{r^2 + a^2}\right) r'^2 + \frac{L_z^2}{r^2 + a^2} - \frac{2MC}{r(r^2 + a^2)} - \frac{2\mu Mr}{r^2 + a^2}. \quad (249)$$

which is not still a Energy-like equation because the term that goes with r'^2 is not a Kinetic-Energy term because it has the factor $\frac{r^2}{r^2 + a^2}$. To finally obtain a Energy-like equation we can perform the transformation

$$\rho^2 = a^2 + r^2 \quad (250)$$

as $\rho\rho' = rr'$, then the section 6.4 becomes

$$\frac{1}{2}(E^2 - \mu) = \frac{1}{2} \left(\rho'^2 + \frac{L_z^2}{\rho^2}\right) - \frac{MC}{(\rho^2 - a^2)^{\frac{1}{2}}\rho^2} - \frac{\mu M(\rho^2 - a^2)^{\frac{1}{2}}}{\rho^2}. \quad (251)$$

■

First of all, notice that as the ring singularity is located at $x^2 + y^2 = r^2 - a^2 = a^2$ this implies that $r \in (0, \infty)$ and therefore $\rho \in (a, \infty)$. So the terms with ρ^{-n} ($n > 0$) are not divergence-terms because they are bounded by $\frac{1}{a^n} \leq \frac{1}{\rho^n}$. The

true divergence-term is $(\rho^2 - a^2)^{-\frac{1}{2}}$. We say that this is a Energy-like equation because it can be decomposed as

$$\epsilon = (E^2 - \mu) = T + V \quad (252)$$

where $T = \frac{1}{2} \left(\rho'^2 + \frac{L_z^2}{\rho^2} \right)$ is the kinetic energy in spherical-like coordinates and $V = V(\rho) = - \left(\frac{MC}{(\rho^2 - a^2)^{\frac{1}{2}} \rho^2} + \frac{\mu M (\rho^2 - a^2)^{\frac{1}{2}}}{\rho^2} \right)$ is the potential. Notice that as the Carter's constant depends on the Energy as $\mathcal{C} = (aE - \sigma L_z)^2$ this is not a true Energy equation, but can be analyzed like that if we impose this relation for the Carter's constant. Notice also that in the limit $a \rightarrow 0$ the equation becomes

$$\frac{1}{2} (E^2 - \mu) = \frac{1}{2} \left(\rho'^2 + \frac{L_z^2}{\rho^2} \right) - \frac{ML_z^2}{\rho^3} - \frac{\mu M}{\rho}. \quad (253)$$

that is the Energy equation for [SW](#) geometry in [KS](#) coordinates (see [7] for more information). To analyze the general Kerr Energy-like equation, we must obtain first the conditions that lead to future directed causal geodesics, but this task is quite complicated and exceeds the present work. As the ring singularity in some way regularizes the terms that diverge as $\frac{1}{\rho^n}$ (when we see the Kerr equation as an extension from the [SW](#) equation), we must deal only with the $(\rho^2 - a^2)^{-\frac{1}{2}}$ divergence term. As was analyzed in [7], once we have solved the conditions that lead to future directed causal geodesics, a interesting analysis of this equation would be based on apply the McGehee method to the phase space which derives from this equation. The Mcgehee method is a procedure that allows us to analyze the behavior of divergence dynamic systems near the singular points (and also *in* the singular points). Although this is very interesting and novel, we left it for future work.

7

NUMERICAL RESOLUTION OF THE GEODESICS

In order to understand more the general behavior of the geodesic flow in the Kerr spacetime, a numerical integration of the geodesic has been performed. The numeric code that has been used has been developed in *C++* using a modified Runge-Kuta 11 method, which avoids convergence problems in different horizons. The input for this program consists in a set of initial conditions $(a, r_0, L_z, \theta_0, p_{\theta_0})$ where a is the rotation parameter of the Kerr black hole, $(r_0, \theta_0, p_{\theta_0})$ are the initial values of the [BL](#) coordinates at the starting point of the geodesic and L_z is the value of the axial angular momentum. The output of this program consist in a *.txt* file with the values of (τ_i, x_i, y_i, z_i) (where the index i denotes the step of the numerical integration). In order to represent the trajectories the *.txt* file has been import into *Wolfram Mathematica*, where we have used the representation capabilities of this program to make the final plots. The legend in each plot is

- The black sphere represent the outer horizon $r = r_+$. As a geodesic that cross this point cannot be seen beyond the horizon, the behavior of the geodesic flow beyond this point is not in the figures, as we want to show how a test particle will be seen from *outside*.
- The green transparent sphere represent the outer ergosphere.
- The blue curve represent the geodesic path over the integration.
- The dashed black lines represent the (x, y, z) axes.

The values of each initial condition set is included in the caption of each figure, with a brief explanation of the corresponding orbit.

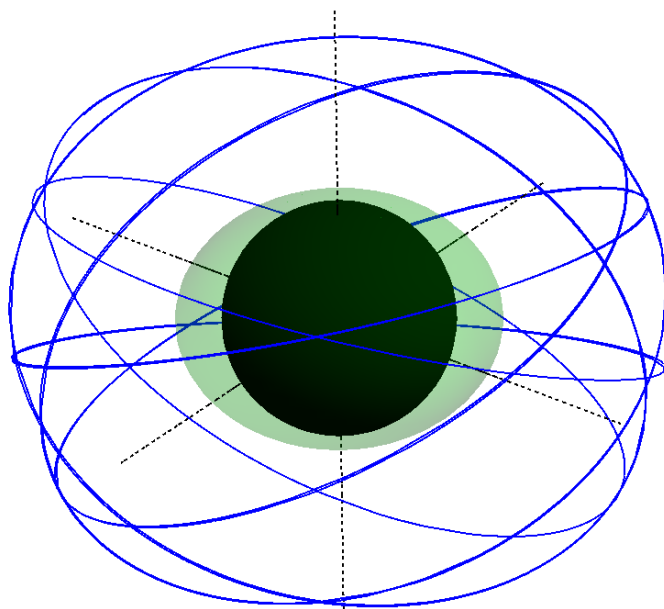


Figure 31: The figure shows a closed geodesic outside the outer horizon in the Kerr geometry. As is well known, closed geodesics are a very important class of orbits that provide very useful information of the spacetime and the geodesic taxonomy. In this figure, the closed orbit is not restricted to any plane and runs across all the spacetime.

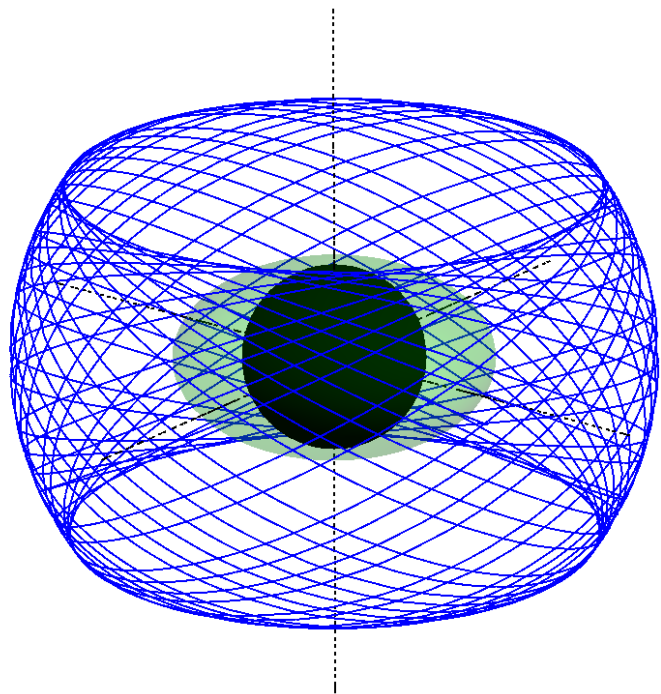


Figure 32: The figure shows a geodesic with constant value of the coordinate r (in BL coordinates). This kind of motion is not as interesting as the closed orbit motion, but also provides useful information because, as we can see in the figure, this kind of geodesics are bounded between two limit circles whose height depend on the initial value of the Carter's constant.

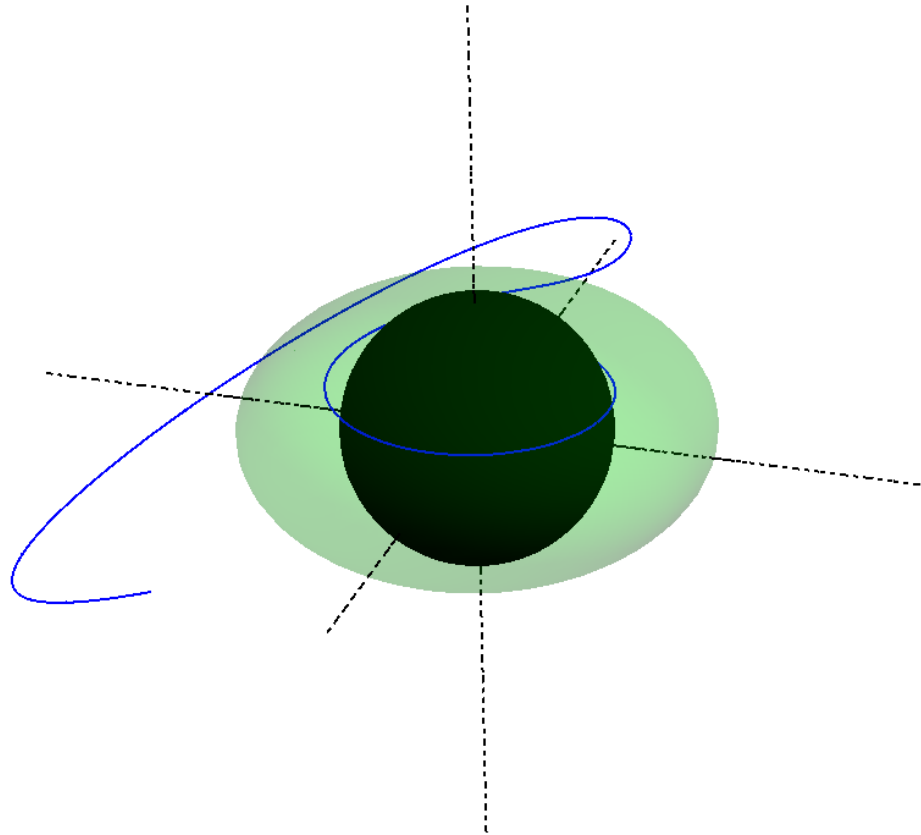


Figure 33: The figure shows what is known as the *Ergosphere capture*, that is a process in which the geodesic tries to enter the ergosphere counterclockwise to the Kerr black hole rotation (in this case with its angular momentum pointing upwards) and as the properties of the Kerr geometry avoid that kind of movement, the geodesic is bend inwards and enters the ergosphere co-rotating with the Kerr black hole. Then, the geodesic is trapped in a circular co-rotating motion that ends in the outer horizon. This ergosphere capture is bounded to the equatorial plane.

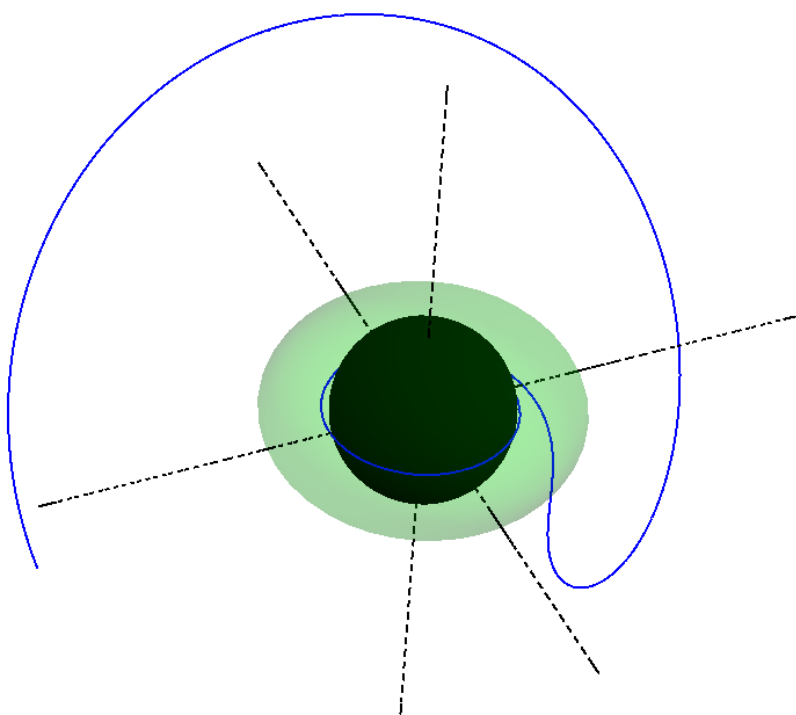


Figure 34: The figure shows another ergosphere capture but this time, the process is not bounded to a plane. As we can see in this image, the process is quite similar to the previous one, but this time the geodesic travels from the top to bottom after entering being captured by the ergosphere and bended inwards to be finally capture in a co-rotating movement that ends in the outer horizon.

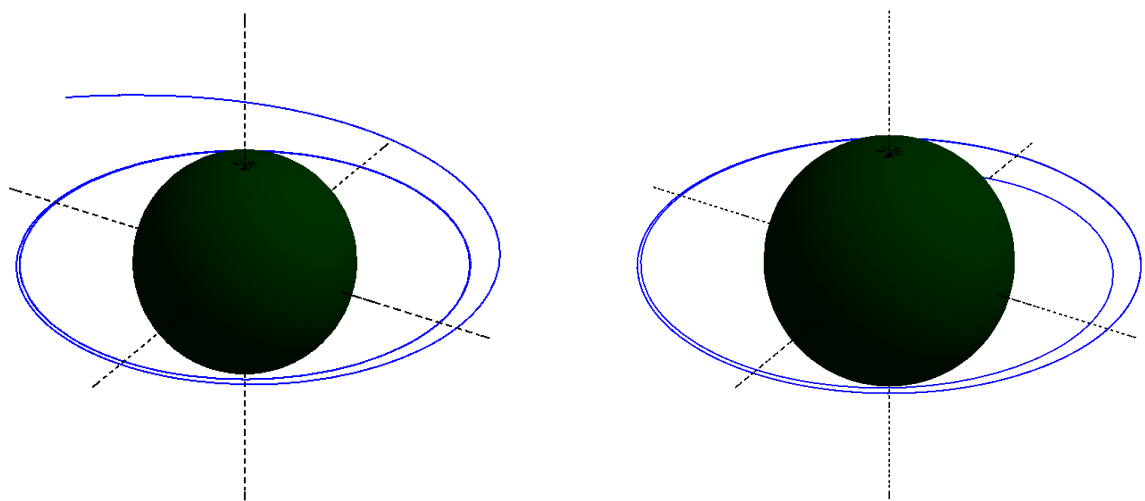


Figure 35: The two figures shows the behavior of the Innermost stable circular orbits (ISCOs). In the figure on the left, a geodesic that comes from the asymptotically flat region falls into the ISCO and remains there, while in the figure on the right, a particle that is initially at the ISCO is perturbed and trapped by the gravitational field of the black hole.

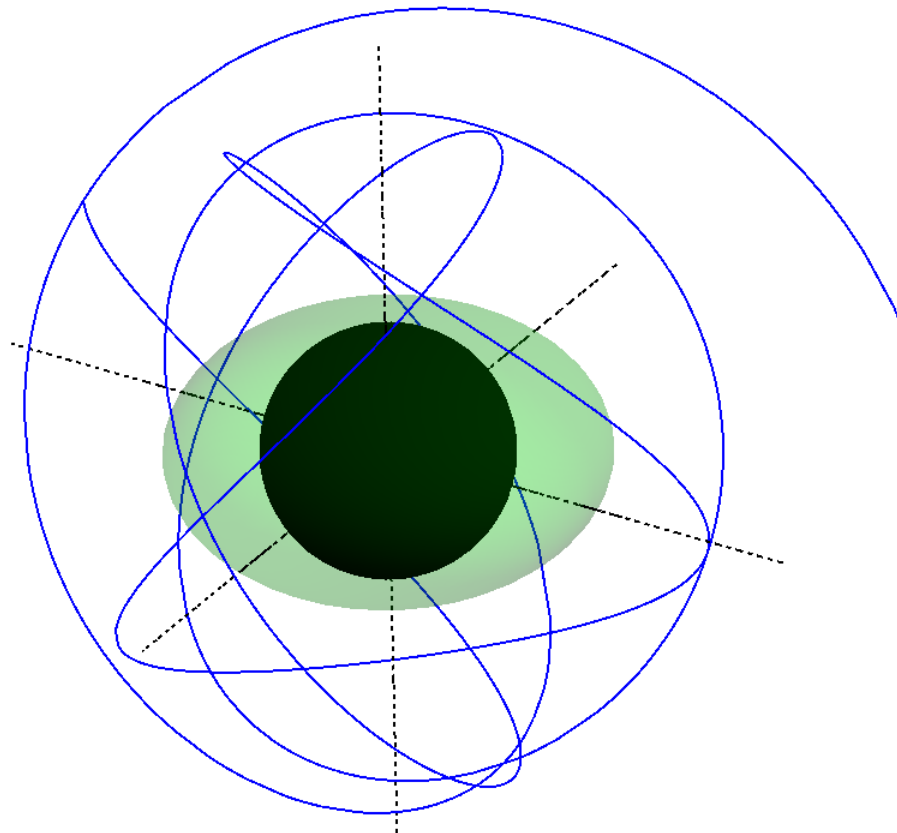


Figure 36: The figure shows what is known as the Whirl orbit. This kind of orbits may seem chaotic (and indeed they are) but they helped to understand and study the geodesic taxonomy based on the values of the Carter's constant. In this figure, the principal Whirl orbit is depicted. This kind of orbits are bounded asymptotically by the coordinate r (in BL coordinates) once they get near the ergosphere but they are not bounded by the coordinates θ and ϕ , which gives the geodesic its characteristic behavior.

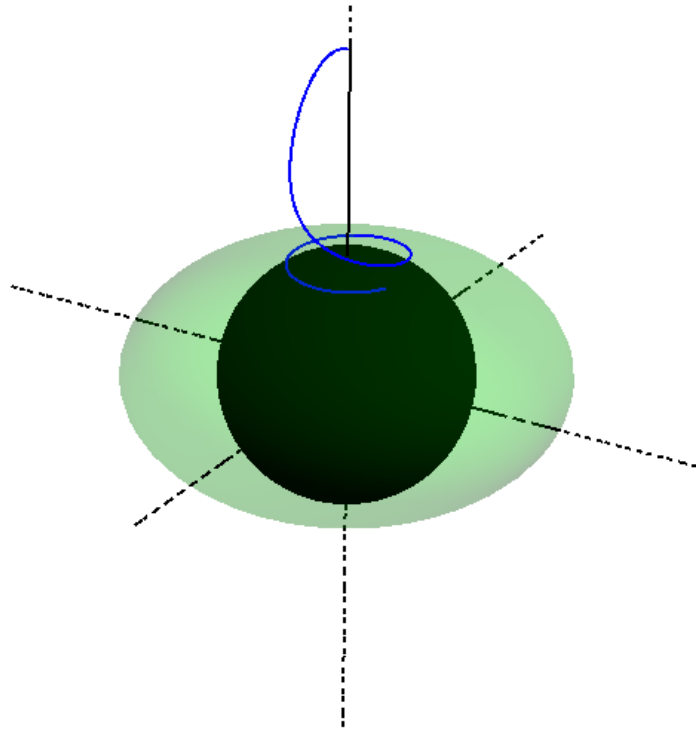


Figure 37: The figure shows the real behavior of a geodesic trajectory that is perturbed away from the axis of symmetry. The geodesic go away from the axis and when reaches the ergosphere, the frame dragging effect starts and force the geodesic to spin co-rotating with the black hole to finally being captured by the outer horizon.

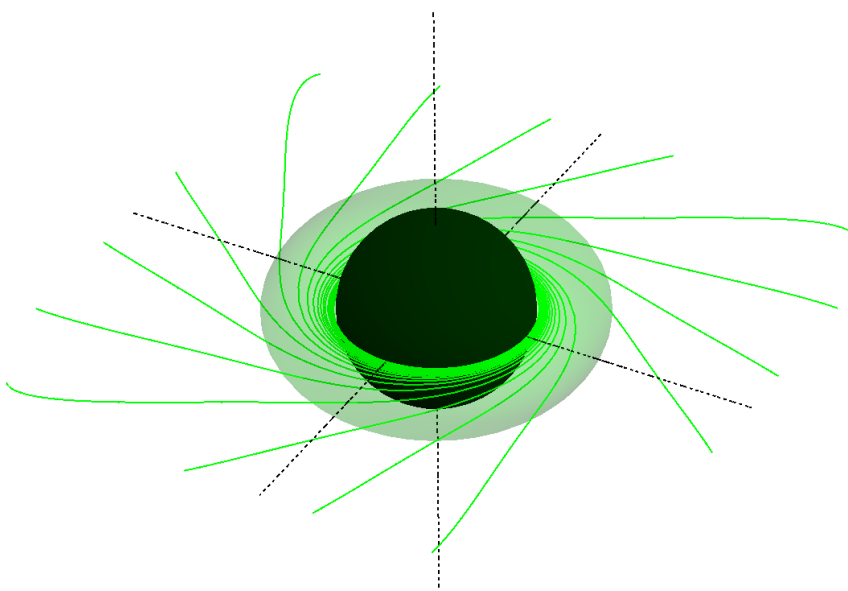


Figure 38: The figure shows the trajectories with zero angular momentum in the Kerr spacetime. Notice how in the first stages of the movement, the trajectories are straight lines and as the geodesics approaches the black hole, they are dragged by the ergosphere and acquire the **ZAMO** angular velocity before cross the outer horizon.

Part III
CONCLUSIONS AND COMMENTS

8

CONCLUSIONS

The main result of this work is a detailed understanding of the motion of particles in free fall in the Kerr geometry, both for massless and massive particles. We have focused on the analysis of the axis of symmetry, the equatorial plane, and, in particular, the disk inside the singular ring of the Kerr black hole. Some of the most remarkable aspects in this work are, for example, the importance of the excluded regions, which provide the necessary topology to the physical region of the phase space to cover the whole structure of the Penrose-Carter diagram in a single two-dimensional phase space. We have obtained completely new results on the geodesic flow in the axis of symmetry and in the inner disk from the point of view of dynamical systems, which as discussed above, is a novel approach to the problem. Some of these results are the existence of two critical points in the geodesic flow for timelike particles in the axis of symmetry, the fact that the axis of symmetry is stable, the result about the period of the lower energy orbit (which unexpectedly increases as the rotation increases) or the fact that only null geodesics that starts in the inner disk can remain in it. We have also found that the spacetime inside the singular ring behaves as the Minkowsky spacetime, analogous to the behavior of a thin, electrically charged shell, in which there is no electrical field. In the study of the movement along the axis of symmetry we have made a complete taxonomy of all kinds of movements as well as returning points and critical values of the kinetic parameters. Also, we have found some strange features as that the maximum time expended in travel along the Penrose diagram increases with the value of the rotation parameter a . To complete the understanding of the geodesic flow in the axis of symmetry and the equatorial plane we have obtained the necessary conditions that lead to future causal geodesic, which allow us to interpretate uniquely all curves in the phase portraits. The description of all geodesic flow along the maximal extension of the Kerr spacetime in terms of one two-dimensional phase space thanks to the future geodesic conditions is a great simplification to the geodesic analysis and is a very novel approach to this problem. Finally, we have derived an Energy-like equation for the exterior geodesic flow in the equatorial plane, which has a lot of advantages respect to the classical formulation of the geodesic equations.

Part IV
APPENDIX

A

KILLING VECTORS AND KILLING TENSORS

To obtain a simple form of the geodesic equations of a spacetime, a useful tool are Killing vectors. In a simple way, the Killing vectors are objects that inform us of symmetries of the spacetime and its metric. Using their properties we can obtain first integrals of the geodesic equations. Therefore, understanding the Killing vectors of a space time is an important step to obtain more simple equations for the geodesic flow.

A.1 PROPERTIES OF KILLING VECTORS

Formally Killing vectors are defined as:

$$\mathcal{L}_\xi g = 0, \quad (254)$$

where \mathcal{L}_ξ is the Lie derivative along the vector field ξ . If the manifold has a torsion-free metric connection ∇ , this expression becomes:

$$\begin{aligned} \mathcal{L}_\xi g_{ab} &= \xi^c \nabla_c g_{ab} + g_{ac} \nabla_b \xi^c + g_{cb} \nabla_a \xi^c \\ &= \nabla_b \xi_a + \nabla_a \xi_b = 0, \end{aligned} \quad (255)$$

where $g_{\alpha\beta}$ is the spacetime metric and the indices will be raised and lowered with g .

A.2 KILLING VECTORS AND LAGRANGIAN SYMMETRIES

We will see that Lagrangian symmetries correspond to the Killing vectors of the spacetime. For this purpose consider:

$$v \in T_p M \quad (256)$$

$$L(v, p) = \frac{1}{2} g|_p(v|_p, v|_p) \quad (257)$$

Considering a generic vector $Y \in T_p M$, we will move \mathcal{L} along the one-parameter group ϕ_t generated by Y . If we name ϕ_t the tangent application ϕ we will have that:

$$Y(L(v|_p, p)) = \frac{d}{dt}|_{t=0} (L(\phi_{*t}(v), \phi_t(p))) \quad (258)$$

$$= \frac{d}{dt}|_{t=0} \left(\frac{1}{2} g|_{\phi_t(p)}(\phi_{*t}(v), \phi_{*t}(v)) \right) \quad (259)$$

In geometric terms all you are doing is moving the vector v by the group of diffeomorphisms ϕ_t and contracting it with the metric evaluated at $\phi_t(p)$. This process is the same as applying the pull-back to the metric evaluated at $\phi_t(p)$

and contract it in p with the vector being evaluated at p . That is, given $\omega \in T_p^*M$, $v \in T_p M$ and ϕ_t a diffeomorphism, they fulfill:

$$\phi_t^*(\omega|_{\phi_t(p)})|_p(v|_p) = \omega(\phi_{*t}(v|_p))|_{\phi_t(p)} \quad (260)$$

Therefore, from eq. (259) it follows that:

$$\frac{1}{2} \frac{d}{dt}|_{t=0} \phi_t^*(g|_{\phi_t(p)})|_p(v|_p, v|_p) \quad (261)$$

$$= -\frac{1}{2} \lim_{t \rightarrow 0} \frac{\phi_0^*(g|_{\phi_t(p)}) - \phi_t^*(g|_{\phi_t(p)})|_p}{t}(v|_p, v|_p) = -\frac{1}{2} \mathcal{L}_Y(g)(v|_p, v|_p) \quad (262)$$

If $\mathcal{L}_Y(g) = 0$ then Y is a Killing field and is also a symmetry of the Lagrangian.

A.3 KILLING VECTORS AND FIRST INTEGRALS

Killing vectors are useful among many other reasons for defining conserved quantities. The definition of the conserved quantities is simply the dot product of the Killing vector for the tangent vector of the geodesic:

$$u^\beta \nabla_\beta (\xi_\alpha u^\alpha) = u^\beta \xi_\alpha \nabla_\beta u^\alpha + u^\beta u^\alpha \nabla_\beta \xi_\alpha \quad (263)$$

$$= u^\beta u^\alpha \nabla_\beta \xi_\alpha = u^\alpha u^\beta \nabla_\beta \xi_\alpha \quad (264)$$

$$= \frac{1}{2} (u^\alpha u^\beta \nabla_\beta \xi_\alpha + u^\alpha u^\beta \nabla_\alpha \xi_\beta) = 0 \quad (265)$$

and hence we obtain that, along the geodesic:

$$g(u, \xi) = cte \quad (266)$$

A.4 NOETHER CURRENTS AND KILLING VECTORS

It is convenient to relate the Noether currents defining the symmetries of a Lagrangian and the Killing vectors of the metric. Noether currents of a Lagrangian satisfied that:

$$\dot{q}^\alpha \nabla_\alpha J + \ddot{q}^\alpha \nabla_\alpha J = 0 \quad (267)$$

where q^α and \dot{q}^α are the natural coordinates on the tangent bundle J is defined, in case that the Lagrangian remains invariant under a symmetry generated by ξ , as:

$$J = \frac{\partial \mathcal{L}}{\partial(\dot{q}^\alpha)} \xi^\alpha \quad (268)$$

At infinitesimal level, the transformation whose generator is ξ takes the form:

$$q^\alpha \rightarrow q^\alpha + \xi^\alpha \quad (269)$$

In the case of the Lagrangian of eq. (256):

$$J = \frac{\partial \frac{1}{2} g_{\alpha\beta} \dot{q}^\alpha \dot{q}^\beta}{\partial(\dot{q}^\gamma)} \xi^\gamma = \frac{1}{2} (g_{\gamma\beta} \dot{q}^\beta + g_{\alpha\gamma} \dot{q}^\alpha) \xi^\gamma \quad (270)$$

$$= g_{\gamma\beta} \dot{q}^\beta \xi^\gamma = g(\dot{q}, \xi) \quad (271)$$

And we get that for Killing vectors, the Noether currents are exactly the conserved geometric quantities associated Killing vector ξ .

A.5 KILLING TENSORS

A generalization of the Killing vector equation can be achieved generalizing the eq. (255) for tensors:

$$\nabla_{(\alpha} T_{\beta\gamma)} = 0 \quad (272)$$

Thus, the following conserved quantities (using eq. (265)) will hold:

$$T_{\alpha\beta} u^\alpha u^\beta = cte \quad (273)$$

There are Killing tensors that comes from tensor products of Killing vectors, and therefore does not provide independent conserved quantities. In other words, the Killing tensors:

$$T_{ij} = \xi_i \otimes \xi_j \quad (274)$$

generate the conserved quantities:

$$T_{ij} u^i u^j = c_i c_j \quad (275)$$

where $c_i = g(u, \xi_i)$.

A.6 KILLING ALGEBRA

An useful property is that, given two Killing vectors ξ_1 y ξ_2 :

$$\xi_3 = [\xi_1, \xi_2] \quad (276)$$

Is also a Killing vector because:

$$\mathcal{L}_{[\xi_1, \xi_2]} g = [\mathcal{L}_{\xi_1}, \mathcal{L}_{\xi_2}] g = 0 \quad (277)$$

It is well-known that the set of all the complete vector fields on a manifold constitute also a Lie algebra which is naturally identifiable to the Lie algebra of the isometry group of the (semi-Riemannian) manifold. When completeness is dropped, analogous considerations hold locally.

BIBLIOGRAPHY

- [1] Belbruno, E. and Pretorius, F. (2011). A dynamical system's approach to Schwarzschild null geodesics. *Classical and Quantum Gravity*, 28(19):195007.
- [2] Birkhoff, G. D. (1923). Relativity and modern physics. *Cambridge, Mass.*
- [3] Boyer, R. H. and Lindquist, R. W. (2004). Maximal analytic extension of the kerr metric. *Journal of mathematical physics*, 8(2):265–281.
- [4] Carter, B. (1968). Global structure of the kerr family of gravitational fields. *Physical Review*, 174(5):1559.
- [5] Carter, B. (1987). Separability of the killing–maxwell system underlying the generalized angular momentum constant in the kerr–newman black hole metrics. *Journal of mathematical physics*, 28(7):1535–1538.
- [6] Faridi, A. M. (1986). Precession of angular momentum vector in a slowly rotating kerr metric. *General relativity and gravitation*, 18(3):271–286.
- [7] Galindo, P. and Mars, M. (2014). Mcgehee regularization of general so (3)-invariant potentials and applications to stationary and spherically symmetric spacetimes. *arXiv preprint arXiv:1405.7627*.
- [8] Hawking, S. W. (1973). *The large scale structure of space-time*, volume 1. Cambridge university press.
- [9] Kerr, R. P. and Schild, A. (1965). A new class of vacuum solutions of the Einstein field equations. *Atti del Congregno Sulla Relativita Generale: Galileo Centenario*.
- [10] Marck, J.-A. (1996). Short-cut method of solution of geodesic equations for Schwarzschild black hole. *Classical and Quantum Gravity*, 13(3):393.
- [11] O’Neill, B. and Stewart, J. (1995). *The geometry of Kerr black holes*. AK Peters Wellesley, MA.
- [12] Stoica, C. and Mioc, V. (1997). The Schwarzschild problem in astrophysics. *Astrophysics and Space Science*, 249(1):161–173.